SUGAR CANE JUICE CONCENTRATION USING GAS HYDRATE TECHNOLOGY

Parisa Doubra
BSc. Eng. Urmia University of Technology (Iran)
MSc. Eng. University of Science and Technology of Mazandaran (Iran)

Submitted in fulfilment of the Academic Requirements for the Awards of

the Doctor of Philosophy Degree in Engineering at the School of

Engineering,

University of KwaZulu-Natal.

March 2020

Supervisor: Prof Paramespri Naidoo

Co-supervisors: Prof Deresh Ramjugernath and Dr Wayne M Nelson

As the candidate's supervisor, I agree to the submission of this thesis:

_____ _____

Prof. Paramespri Naidoo Date

Declaration

I, <u>Parisa Doubra</u>, student number <u>216072592</u> declare that:

(i) The research reported in this dissertation, except where otherwise indicated or acknowledged, is my original work.

(ii) This dissertation has not been submitted in full or in part for any degree or examination to any other university.

(iii) This dissertation does not contain other persons' data, pictures, graphs or other information unless specifically acknowledged as being sourced from other persons.

(iv) This dissertation does not contain other persons' writing unless specifically acknowledged as being sourced from other researchers. Where other written sources have been quoted, then:

    a) Their words have been rewritten but the general information attributed to them has been referenced.

    b) Where their exact words have been used, their writing has been placed inside quotation marks, and referenced.

(v) This dissertation is primarily a collection of material, prepared by myself, published as journal articles or presented as a poster and oral presentations at conferences. In some cases, additional material has been included.

Signed: _____ Date: _____

Acknowledgements

Abstract

Concentration technologies such as evaporation, freezing, and membrane processes, are used for juice production, with the most common method being evaporation. However, the high energy demand for the evaporation process as well as the reduction of the quality of temperature-sensitive materials is among the disadvantages of this technology. Furthermore, at high-temperature, sucrose inversion causes a significant loss of revenue together with caramelisation. Scale deposition resulting from sulphate ions present in the sugarcane juice solution leads to a significant reduction of the heat transfer coefficient of the evaporators. For temperature-sensitive materials, membrane and freezing techniques appear to be desirable; however, each of these methods has its unique disadvantages. Hydrate technology is an interesting application used for the capture of greenhouse gases, oil and gas transmissions, and also recommended for food concentration. Due to the low latent heat of fusion compared to evaporation, as well as better preservation of sucrose solution at low temperature as salt deposition is avoided during hydrate formation, hydrate technology can be considered as an attractive concentration technology solution to evaporation.

In this research study, gas hydrate technology is investigated for the concentration of sugar cane juice from a feed concentration of 12 °Brix sucrose solution. Concentration experiments were conducted on a newly commissioned 750 ml hydrate reactor to assess the final concentration of the product. The novel feature of the apparatus is a sampling mechanism to remove the concentrated liquid once the hydrate had formed. A significant portion of this study was dedicated to the assembling and commissioning of the experimental apparatus, which included two polycarbonate windows, a sampling mechanism and enhanced mixing mechanism. Parallel tasks were performed to meet the objectives which included thermodynamic model developments and phase equilibrium measurements with a previously tested experimental apparatus to establish the hydrate phase boundaries.

Once the experimental technique was validated on the new setup using a test system measured within the acceptable uncertainty range, novel phase equilibrium data were generated for the CO_2 + sucrose solutions (35 and 40 °Brix) and CO_2 + fructose solution (15 °Brix). Several thermodynamic model combinations were used to obtain the best correlation for the systems measured. Both the direct and combined methods were used for modelling. New model algorithms were developed in which the empirical parameters for the activity coefficient models of the non-random two liquid (NRTL) and universal quasi chemical (UNIQUAC) were tuned for the systems studied. The best combination of models was reported for each system using the statistical

analysis. Excellent consistency between experimental data and data fit results were obtained with average absolute relative deviation (AARD) errors smaller than 1 %.

The experimental procedure was developed for the kinetic studies with sample withdrawal of the concentrated solutions. The sample withdrawal procedure was developed in a way such that the kinetic parameters such as induction time could be evaluated for each test. Novel kinetic measurements were performed on aqueous feed solutions up to 35 °Brix sucrose solution with the aim to investigate the temperature and pressure effect. Several experiments were performed on the new experimental apparatus to assess the concentration and number of stages required for the sucrose solutions and sugar cane juice, and whether it was possible to achieve the desired 60 °Brix sucrose solution as compared to conventional methods in the sugar cane factories. The effect of parameters such as temperature, pressure, time, mixer speed, and mesh size on the concentration of the sugar solution were investigated.

Experimental measurements were performed for sucrose solutions at the concentrations up to 60 °Brix using three hydrate stages with optimum conditions for temperature, pressure, mesh size, and mixer speed of 1.5 ° C, 3.70 MPa, 26 μm, and 130 rpm, respectively. Thereafter, measurements were performed using cane juice solution at the same conditions. The hydrate concentration results showed that from an initial concentration of 12 °Brix (cane juice), approximately 55-60 °Brix can be achieved in a four-stage process, with operating conditions at 37 bar, temperatures of 1.5 ° C and a stirring speed of 130 rpm. Promising results from this study reveal a significant concentration from 12 to approximately 30 °Brix over the first stage at the stated conditions within 4 hours. By contrast, three stages are required in a typical multi-effect evaporation train to obtain 28 °Brix cane juice.

In summary, this study assessed the viability of sugar cane juice concentration via hydrate formation in comparison to the multi-effect evaporation process. A preliminary assessment of the energy usage for the hydrate process was performed for benchmarking purposes on a simplified basis, and the feasibility of this technology was evaluated. The preliminary calculations showed an estimated 20 % decrease in energy usage with hydrate technology compared to that of evaporation for the concentration of sugar cane juice up to 30 °Brix.

Nomenclature

English letters

Symbol	Description	Unit
Å	Angström unit	--
AARD	Average Absolute Relative Deviation	--
a_{ij}	Cross parameters for the terms a_m	Pa.(m^3.mol^{-1})^2
a_m	EOS parameter for the mixture	Pa.(m^3.mol^{-1})^2
a_w	Activity of water	--
b_{ij}	Cross parameters for the terms b_m	m^3.mol^{-1}
°*Brix*	Sugar content by mass expressed as a percentage	--
b_m	EOS parameter for the mixture	m^3.mol^{-1}
C	Langmuir constant	Pa^{-1}
C	Celsius	--
C_{ml}	Langmuir constant for component l in cavity m	--
Cp	Heat capacity	J.mol^{-1}.K^{-1}
CSTR	Continuous Stirred-Tank Reactor	--
DO	Direct Osmosis	--
EOS	Equation of State	--
f	Fugacity	Pa
FCS	Freeze Concentration System	--
FO	Forward Osmosis	--
HFR	Hydrate formation rate	mol$_{gas}$.mol$_{wate}$$^{-1}$.min^{-1}
K	Kelvin	--
k_{app}	Apparent rate constant	mol$_{gas}$.mol$_{wate}$$^{-1}$.min^{-1}. Pa^{-1}
k_{ij}	Binary interaction parameters	--
L_w	The liquid phase	--
M	Hydration number, Molecular weight	--, kg/kmol, respectively
m	Meter	--
MD	Membrane Distillation	--
N	Number of experimental data	--
n	Number of moles	mole
NF	Nano Filtration	--
NRTL	Non-Random Two-Liquid model	--
n_{w0}	Initial number of moles of water in the liquid phase	mole
OE	Osmotic Evaporation	--
P	Pressure	MPa
PR	Peng Robinson	--
r	Radial coordinate	m
R	Universal gas constant	m^3.Pa.mol^{-1}.K^{-1}
r(t)	Rate at time equal t	mol.min^{-1}
RO	Reverse Osmosis	--
s	Structure of gas hydrate	--
SC	Storage capacity	v/v
V_{S0}	Initial volume	m^3
SMRI	Sugar Milling Research Institute	--
SRK	Soave-Redlich-Kwong	--
T	temperature	K
t	Time	s
TRU	Thermodynamics Research Unit	--
UF	Ultra-Filtration	--
UNIQUAC	UNIversal QUAsi Chemical	--
UNIFAC	UNIQUAC Functional-group Activity Coefficients	--

English letters continued.

Symbol	Description	Unit
V_{cell}	Cell volume	m^3
VdW	Van der Waals	--
V_{Ht}	Volume of the hydrate at time = t	m^3
V_{Rwt}	Volume of reacted water	m^3
x	Mole fraction in the liquid phase	--
y	Mole fraction in the vapour phase	--
Z	Compressibility factor	--

Greek Letters

Symbol	Description	Unit
α	NRTL dimensionless parameter	--
γ	Activity coefficient	--
δ	Kihara potential parameter	--
ε	Characteristic energy	$J.mol^{-1}$
θ	Surface area parameter UNIQUAC, hydrate cage type	--
μ	Chemical potential	$J.mol^{-1}$
σ	Collision diameter	m
τ	Binary parameters, UNIQUAC model	--
$\bar{\nu}$	Number of cavities of each hydrate structure	--
ω	Eccentric factor	--
Δ	Gradient	--
$\emptyset$	Fugacity coefficient	--

Superscripts

Symbol	Description
C	Combinational
E	Excess
H	Hydrate
I	Ice
L	Liquid
MT	Empty hydrate lattice
R	Residual
sat	Saturated
V	Vapour
W	Water

Subscripts

Symbol	Description
app	Apparent
c	Critical
calib	Calibration
cell	Hydrate cell
equilib	Equilibrium
g	Gas
H	Hydrate
i	Species i
I	Ice

Subscripts continued.

Symbol	Description
j	Species j
k	Species k
L	Liquid
mix	Mixture
RW	Reacted Water
S_0	Initial volume of the water in the cell
STD	Standard
STP	Standard Temperature Pressure
t	Respective time
W	Water

Table of Contents

List of Figures

List of Tables

Chapter 1: Introduction

The method of sugar manufacturing has stayed traditionally the same for many years, with the proven technology of multi-effect evaporation trains being used to concentrate the juice. Several research studies have presented alternative techniques for sugar cane juice concentration; however, the basic principles of the evaporation technology remain intact. In this regard, various methods have been tested, including membrane utilisation (Nene et al., 2002) and freezing technology (Rane and Jabade, 2005). The use of processing methods such as evaporation, membrane separation and freezing technology generally has a very high energy demand and, in some cases, a high maintenance cost. There has been no attempt reported in the literature to commercialise the research projects using other technologies. The use of evaporation is the most common and traditional method of sugar production locally, despite the disadvantages such as the loss of the sugar cane juice contents such as sucrose due to juice entrainment, inversion (hydrolysis of sucrose to fructose and glucose) (Chen and Chou, 1993) and polymerisation (e.g. through caramelisation reactions) (Hugot, 2014) on hot surfaces during evaporation. Such process-related constraints pose a significant problem resulting in the production of undesired quality products. On the other hand, relatively high energy costs as well as expense and time are required to clean the heat transfer surfaces, which accumulate scale and need to be mechanically or chemically cleaned every few weeks, (Hu et al., 2006) are among other disadvantages of the evaporation technology.

The major share of the sugar is produced globally from sugar cane juice (80 %), and the rest is produced from beetroot (Punda et al., 2009). Evaporation is the dominant technology to produce sugar globally. The energy required for sugar production is either electrical energy or cogeneration. In South Africa, multi-effect evaporation trains are used to concentrate the sugar cane juice. South Africa is among the top 20 countries in sugar production. Following the statistics (published by the United States Department of Agriculture, USDA) over 2011 to 2016 there is a peak of sugar production in 2013, and with a decline thereafter (Sikuka, 2019). Figure 1-1 shows the sugar production in South Africa from 2011/2012 to 2018/2019. At the time that this research project started, the sugar market was distinguished by a shortage in sugar supply being at the height of the drought. There has been a significant increase in sugar production since then though the South African sugar industry is struggling with low prices and a severe oversupply due to the international sugar market. In the current situation, the overall production cost of sugar is more than the market price. In recent years, South African industries have been facing challenging circumstances with increasing cheaper imports and agricultural land issues. This has impacted on increasing the production costs of sugar (Mchunu, 2019).
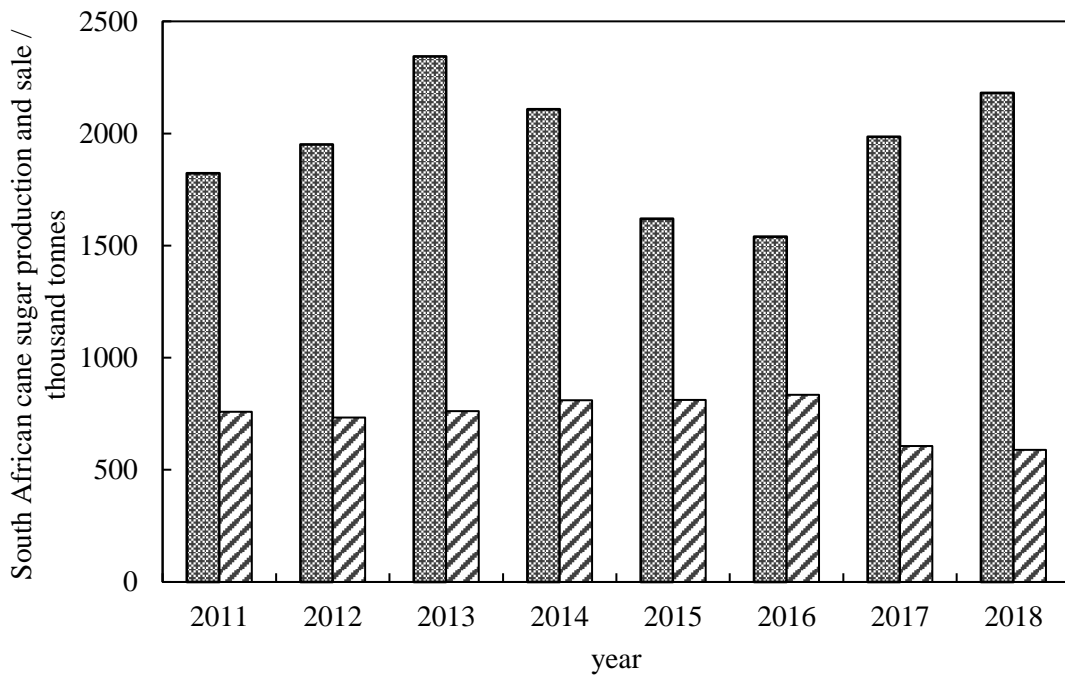
Figure 1-1. South African sugar ▨ production and ▨ sales between 2011 to 2019, extracted from the (SASA, 2019).

This study aims to investigate the use of hydrate technology in sugar cane juice concentration as an alternative to evaporation. For this purpose, the investigation included the commissioning of a new experimental apparatus with a sampling mechanism to remove the concentrated sample from the sugar solution. The hydrate stability zone and the hydrate formation rates were evaluated experimentally to understand the boundary operating and processing conditions. The thermodynamic dissociation data and the hydrate formation kinetics were measured. Thermodynamic modelling of the dissociation and hydrate formation kinetic data were performed. These are useful in understanding and proposing a process design. The experimental concentration tests were performed on sucrose and sugar cane juice solutions, by varying several parameters including pressure, temperature, mixer speed and mesh size. Once these objectives were met, a preliminary assessment of the energy usage was performed comparing the hydrate and evaporation processes.

1.1 Overview of the sugar manufacturing process

Cane juice is concentrated in the multi-effect evaporator which operates under vacuum conditions. For better results, cane juice is pre-heated to the boiling temperature before entering the first evaporation stage. Usually, the concentration of the product in evaporation is 65-70 ºBrix. The ºBrix is a quantity indicating the mass percentage of sugar content in the solution which is named after its funder, Adolf Brix (Hough et al., 2012). The juice is preheated in 2 or 3 stages to

2

above-boiling temperature together with either cold or hot liming, which could be in any stage. The hot, limed juice is then flashed at atmospheric pressure, so that the temperature drops to the boiling temperature (at atmospheric pressure), removing dissolved gases, especially oxygen. The juice is then clarified in a large clarifier to settle out calcium phosphate precipitate which is sometimes followed by some heat loss. Most factories have clear juice heaters, where the clarified juice is heated before evaporation. For those that do not have clear juice heaters, the final heating to the first effect juice temperature occurs inside the evaporator. The multi-effect evaporation uses the vapour generated in each effect as the heating medium for the subsequent effect. This results in significant energy savings compared to single-effect evaporation. Furthermore, in sugar factories, bleed streams are drawn from intermediate vapours as low-grade heating streams for the rest of the factory. This builds significant energy efficiency into the evaporator station design through the use of multiple effect vapour bleeding rather than using exhaust steam in general factory heating duties (Hough et al., 2012, Hugot, 2014, Chen and Chou, 1993). A typical evaporation based sugar factory requires a relatively high amount of energy to maintain the system temperature at the level needed for each step. Novel processing technologies are being investigated to reduce energy requirements.

The significance of this work is that gas hydrate technology needs to be compared against a robust and highly integrated energy design. The justification for attempting this is because the latent heat of melting is much less than that of vapourisation. The other benefits relating to the lower temperature also might provide material benefits to the process, but not if the project economics are not significantly better than an equivalent evaporator station design.

Outline of the thesis:
This thesis is presented in 8 chapters.
Chapter 1 gives an introduction to the thesis.
Chapter 2 discusses the literature review on sugar production techniques.
Chapter 3 gives a review of the modelling approaches used in this work.
Chapter 4 discusses a literature review on sugar concentration via gas hydrate technology.
Chapter 5 provides a discussion on the equipment design as well as the different apparatuses used in this work.
Chapter 6 presents the experimental thermodynamic and kinetic data measured in this work along with the juice sampling results. A preliminary study of a gas hydrate plant is also shown in this chapter.
Chapter 7 presents the concluding remarks in this study.
Chapter 8 provides recommendations for future work.

Chapter 2: Literature review of juice concentration techniques

This chapter compares the various methods used for sugar production, with a focus on the energy demand, the capability of each technique, and the product recovery. The four processing methods, *viz*., evaporation, membrane separation, freezing and gas hydrate are presented with a brief summary provided on each technology, and its capacity.

2.1 Evaporation

This is the traditional and most commonly used method, which is based on evaporating water to concentrate the sugar cane juice with operating temperatures up to 112 $^\circ$C and pressures below 2 mbar. Generally, a product of ~ 65 to 70 $^\circ$Brix is obtained. While there should be no change to the physical and chemical properties of the solution, these components are sensitive to high temperatures, causing the fluid to lose sucrose due to juice entrainment, inversion (hydrolysis of sucrose to fructose and glucose) and polymerisation (e.g. through caramelisation reactions) on hot surfaces, thereby reducing the quality of the material (Kujawski et al., 2008, Madaeni and Zereshki, 2010, Jiao et al., 2004). The valuable compounds of fruit juice are also sensitive to heat. Therefore processing is desirable at low temperatures and over short periods (in average, almost 50 % of the vitamin C content of vegetables is lost in an environment of 60 $^\circ$C (Igwemmar et al., 2013)).

It is important not to combine fruit juice and sugar cane juice. The fruit juice vitamin content and flavour are negatively influenced by heat and the aim is to retain the flavour and vitamins. In sugar juice, the aim is to recover sucrose in as pure form as possible. This involves the elimination of flavours and colour. Heat adds flavour and colour which are subsequently removed in the crystallisation steps. The biggest problem is the loss of sugar, which means loss of saleable product.

The flow diagram of the sugar factory is shown in figure 2-1 (FASTONLINE, 2017). The sugar cane is first crushed and washed with hot water in the cane cutter to extract the juice. The extracted juice is then clarified, preheated and limed to be prepared for the concentration process. Thereafter the juice is introduced to the multi-effect evaporation train to produce syrup. The syrup is then crystallised in a crystalliser. The syrup and crystals formed in the previous stage are sent to the centrifuge to separate molasses from raw sugar.
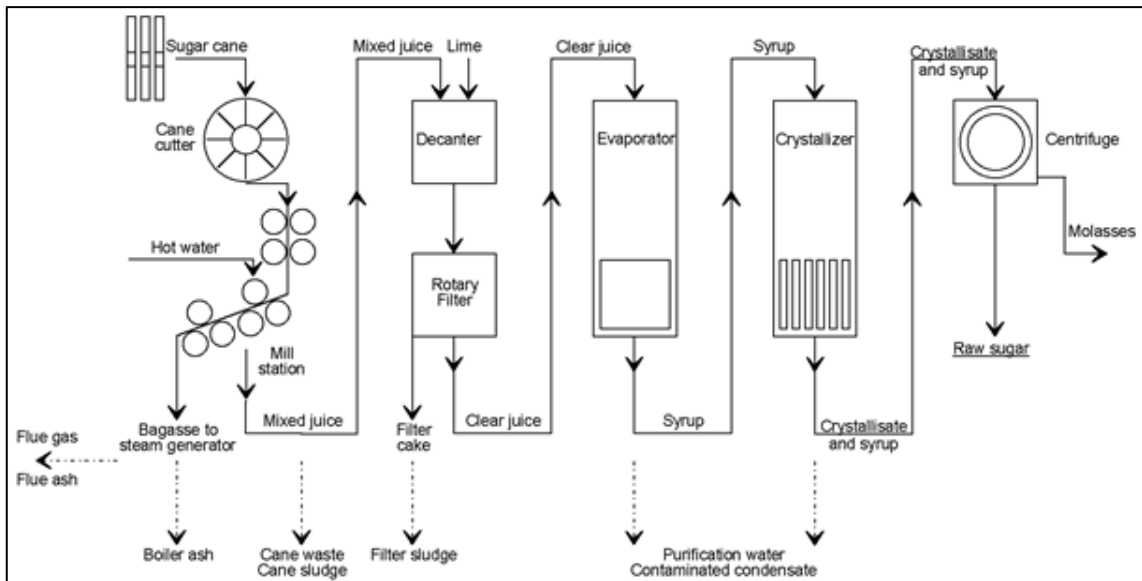
Figure 2-1. Flow chart of the cane sugar manufacturing process (Fastonline, 2017).

Vacuum thermal evaporation is a common approach for juice concentration to reduce the boiling point of the material. Therefore, before the juice enters the evaporation train, it is preheated to raise its temperature to above the boiling point to save energy and cost. A multi-effect evaporation train (4-5 effects) is usually used, working in series to reduce the energy requirements (Poel et al., 1998, Honig, 1963). Some disadvantages are explained as follows:

The *inversion of sucrose* happens when the pH of the juice is below 5, and the temperature is higher than 60 º C. This causes the decomposition of sucrose to glucose and fructose (Honig, 1963).

$$C_{12}H_{22}O_{11} + H_2O \quad \rightarrow \quad C_6H_{12}O_6 + C_6H_{12}O_6 \qquad (R1)$$
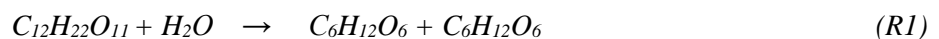
There are several species such as salts, ions, phosphate, mineral and organic material, present in the sugar cane juice. While some components of the juice cane are removed during clarification, the final molasses has some salts, and other components present. The existence of these components during the concentration steps cause the formation of scale on the walls of the unit vessels. Scale deposits reduce the heat transfer coefficient, compromising the evaporation rate which is required (Poel et al., 1998, Honig, 1963).

The significance of this work from the energy point of view is due to the extremely low latent heat of melting compared to its vaporising counterpart. Rather, better preservation of sucrose at a lower temperature could eliminate revenue loss. However, the project economics plays an important role compared to that of an equivalent evaporator station. On the other hand, the vapour

bleed from the evaporation trains is usually used to provide the energy required for other parts of the factory which is a significantly important source to save energy. This is one of the drawbacks in adopting gas hydrate technology in such conditions as there is no access to the extra energy output stream.

2.2 Membrane separation

In recent years, there has been tremendous growth in the use of membranes for water treatment (Madhura et al., 2018), gas separations (Bernardo et al., 2009), and fruit juice concentration (Cassano et al., 2018). Due to their advantages to conventional separation methods, their use in different industries such as chemical, petrochemical, refining, food and medicine is growing (Zambra et al., 2015). Generally, the membrane technology has been used in several forms of reverse osmosis (RO), direct osmosis (DO), osmosis distillation (OD), membrane distillation (MD) and forward osmosis (FO).

Industrially, fruit juice concentrated via evaporation often results in loss of flavour, colour and taste, decreasing the juice quality. Recent reports of membrane applications in the industry show a final product having the sugar content of 25-30 °Brix using RO. Usually, to achieve a higher concentration, a hybrid system is necessary. In such cases, a membrane is used, followed by evaporation (Gul and Harasek, 2012). However, this increases the capital and energy requirement together with maintenance cost (especially membrane). Several authors (Cassano et al., 2003, Koroknai et al., 2008, Onsekizoglu et al., 2010) report the concentration of fruit juices using a combination of hybrid operations.

Figure 2-2 shows a typical flow diagram for osmosis distillation, which operates at room temperature and atmospheric pressure to extract water molecules selectively from the solution using a microporous hydrophobic membrane. Concentrated brine is utilised as the stripping solution downstream of the membrane (Jiao et al., 2004).
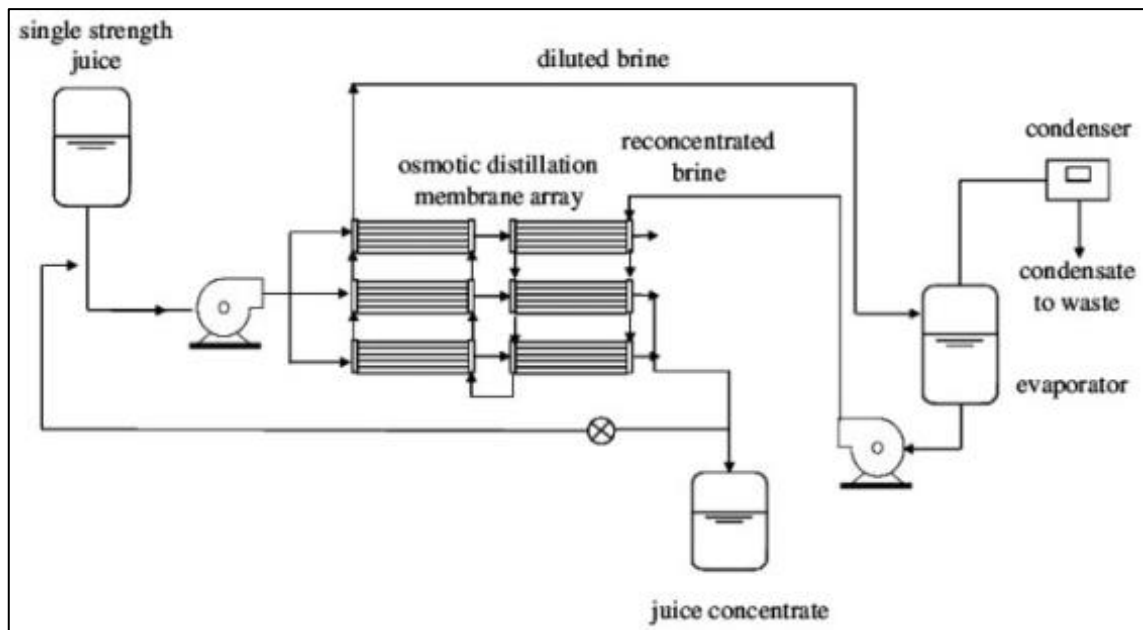
Figure 2-2. Typical osmosis distillation system for juice concentration (Jiao et al., 2004).

Several parameters affecting the membrane concentration methods have been studied in the literature. The difference in temperature affects the vapour pressure which leads to diffusion of water vapour through the membrane. As the difference in temperature increases, the difference of vapour pressure and thus the flux of distillation in membrane rises (Nene et al., 2002). The gradual decrease of the driving force in MD reduces the flux of water, but generally, the driving force does not change the mass transfer coefficient throughout the process (Alves et al., 2004). The results of another study (Warczok et al., 2007) also prove that RO distillation is an efficient method in the treatment of high viscous solutions by dehydration of the solution. The examination of the water flux on the available commercial membranes showed the improved ability of FO in the concentration of sugar solution compared to RO which is attributed to the internal polarisation of the solution. This is defined as the concentration gradient generated at the interface of the membrane and solution due to membrane permselectivity. The temperature can also affect the water flux significantly by increasing the diffusion coefficient (Garcia-Castello et al., 2009). Furthermore, studies on the energy consumption showed that RO requires significantly lower energy to concentrate the sugar solution which is additional to no sugar loss in the membrane concentration process (Madaeni and Zereshki, 2010). Table 2-1 summaries the literature review on such methods.

Table 2-1. Summary of the literature review on fruit juice concentration using membrane technology.

References	Juice	$C_{initial}$/ ºBrix	C_{final}/ ºBrix	Operation[1]	P/ MPa	T/ º C
(Alvarez et al., 1997)	Apple juice	11	27	RO	0.55	17-47
(Petrotos et al., 1998)	Tomato juice	4.3-11.7	24	OD	0.2	25-26
(Bailey et al., 2000)	Grape juice	23	68	OD	0.15	25
(Curcio et al., 2001)	Orange juice		+15 of $C_{initial}$	MD	0.5	25
(Cassano et al., 2003)	Carrot and citrus	15-20	63	UF, RO, OD	7	Up to 45
(Matta et al., 2004)	Acerola juice	7.1	29	RO	0.16	25
(Alves et al., 2004)	Fruit juice	12	60	OE		30
(Warczok et al., 2004)	Pear and Apple juice	10	71	NF	1.2	25-35
(Gunko et al., 2006)	Apple juice	11	50	MD	0.3	10-70
(Rektor et al., 2006)	Grape juice	17	60	MD	14.2	15 and 30
(Jesus et al., 2007)	Orange juice	2.3 - 5.8	36	RO	0.6	25
(Cassano and Drioli, 2007)	Kiwifruit juice	9.4	67	OD	0.04	25
(Cassano et al., 2007)	Cactus pear juice	11	61	OD	0.048	28
(Hongvaleerat et al., 2008)	Pineapple juice	12.5	57	OE	0.2	20-35
(Koroknai et al., 2008)	Chokeberry, redcurrant, cherry	9.6	65	UF-MD	0.16	25 and 30
(Pap et al., 2009)	Black currant	16.5	29	RO	6	25
(Bánvölgyi et al., 2009)	Black currant	10	25	RO	3.5	30
(Valdés et al., 2009)	Onion juice	8	32	OD		30
(Pap et al., 2010)	Black currant	18	25	RO	0.45	30
(Onsekizoglu et al., 2010)	Apple juice	12	70	OD, MD		25 to 30
(Sotoft et al., 2012)	Black currant	12	66	MD	0.015	40
(Echavarría et al., 2012)	Fruit juice	12.2	30.5	RO	4	25-27
(Kujawski et al., 2013)	Grape juice	5	8	OD		35
(Destani et al., 2013)	Orange juice	11	61	OD	0.0375	25
(Zambra et al., 2015)	Cranberry juice	8.6	40	OD		30

[1] reverse osmosis (RO), direct osmosis (DO), osmosis distillation (OD), membrane distillation (MD) and forward osmosis (FO).

2.3 Freezing

This method is used for heat-sensitive juices. In this process, the water becomes ice, thus the amount of solvent is reduced. After the ice is formed the two phases can be separated mechanically (Chen et al., 2015). As an example for apple juice with 11% dry material, the freezing point is between -5 to -8 ℃. After the process is finished, the mixture contains ~81.5% ice crystals, and dry material content is increased by approximately 40% (Miyawaki et al., 2016).

In freezing, the energy required for concentration and freezing per unit of water (80 kcal per kg water) is less than evaporation (approximately 30 % of a three-stage evaporator (Guignon et al., 2012)). Due to the expensive form of energy and the high cost of the facility, the system is more costly compared to evaporation (Guignon et al., 2012). Hence, concentration via freezing is used just for heat-sensitive materials, such as, orange juice, which has limited applications. In this case, the final dry matter content depends on the viscosity, which for fruit juice is about 40-50 °Brix (Guignon et al., 2012). Table 2-2 shows the advantages and disadvantages of freezing technology on orange juice concentration.

Table 2-2. Advantages and disadvantages of using freezing for orange juice concentration (Farnworth et al., 2001, Polydera et al., 2005).

Advantage	Disadvantage
Operates at a low temperature	Refrigeration cost is very high
The volatile aroma remains intact	Capital investment is very high
	The operating cost is very high
	The rate of production is very low

There are several papers published in the literature with highly valuable outcomes in terms of sugar cane juice concentration and separation using freezing technology. A summary of the available methods is presented in table 2-3.

Table 2-3. A brief summary of the literature on freezing technology for vegetables, fruit and sugar cane juice concentration.

Year	Method or aim	Results
(Huige and Thijssen, 1972)	To study the bulk crystallisation and crystal growth	- Increased mean size prediction by feeding smaller crystals - Better crystal growth by increasing the crystal concentration in the feed
(Flesland, 1995)	layer crystallisation of aqueous solutions in falling film configuration	- Less than 0.2 (kg) ice removal in each test
(Kobayashi et al., 1996)	To develop a more straightforward method to produce large ice crystals	- Keep the initial supercooling, and the solution melting point below 0.2 K - Introducing heavier ice crystals
(Liu et al., 1998)	To prevent the accumulation of solution in the solid phase.	- Successful use of the plate with holes to prevent subcooling - 54% higher purity of the solid phase
(Chen et al., 1998)	To investigate the inclusion levels of the solute	- Same inclusion of solute on the horizontal coordinate (width 1-4 cm)
(Chen et al., 1999)	Impact of potato starch on sucrose inclusion	- Sucrose in the ice layer is not sensitive to potato starch - Potato starch in the ice layer is sensitive to sucrose concentration
(Wakisaka et al., 2001)	To examine ice productivity	- Ice production: rejection of 578.6 kg/m^2 h 99% of glucose - The optimum flow velocity of 1 m/s
(Rane and Jabade, 2005)	To study the heat transfer and the power requirement for the bench-scale plant	- Power requirement rose synchronously with the ice fraction
(Kawasaki et al., 2006)	To investigate the efficiency at the fixed rate of freezing	- Effective separation of lighter solutes
(Qin et al., 2006)	To obtain eutectic points	- The properties of eutectic point and heat transfer coefficient has been obtained
(Raventós et al., 2007)	To study the multi-plate cry concentrator outcome	- The maximum concentration of 32.2 ºBrix - shortest process time of 16.6 h
(Chudotvortsev and Yatsenko, 2007)	To obtain eutectic points	- An anomalous behaviour near the eutectic point - Similar component distribution in all of the systems studied
(Sahasrabudhe et al., 2012)	Freeze concentration system (FCS) equipped to a process of layer freezing	- Increasing concentration along the plate length leads to increasing viscosity - Improving the viscosity results in lower velocity
(Lopez-Quiroga et al., 2015)	Determining the quality and safety of product	- highly concentrated systems - A classical Stefan formulation coupling mass and heat transfer was used

2.4 Gas hydrate technology

A hydrate is an ice-like crystal, which forms under specific thermodynamic conditions. It means that water makes a cavity with hydrogen bonding forces and traps gas molecules inside the cavity. Gas hydrates will be discussed extensively in Chapter 4. Few researchers have reported on sugarcane juice concentration using gas hydrate such as (Chun and Lee, 1999, Andersen and Thomsen, 2009, Purwanto et al., 2014, Smith et al., 2016).

Based on the studies performed on the concentration methods of sugar cane juice, the drawbacks and advantages are presented in Table 2-4. This table shows a summary of the available techniques including their qualitative energy consumption and capital investment, the rate of product formation, quality of product and the stage of development for each technology.

With evaporation, the concentration of the initial juice increases from 2.5-6 to 60 °Brix. However, the product quality is not rated high, but the plant can be constructed with modest capital investment. Another positive point is the water elimination rate of 200–300 l/m^{2}h which is highest among other available methods (Jiao et al., 2004). The main drawback of the technique is high energy consumption.

The final concentration of the product in membrane technology depends on the method or approach selected. The final concentration can vary between (55 to 70) °Brix. Due to the lack of high temperatures, the product quality is notable. However, the operational cost is very high, the maintenance of the plant requires a lot of time and energy, but the energy consumption is low. The concentration rate is on average almost 95 % less than evaporation (Madaeni and Zereshki, 2010).

With the freezing approach, looking at the operating temperature which can be down to -20 ° C, it requires the highest energy requirement among the available methods. Depending on the production capacity of the product and because of the low rate of the freezing process, for production of the same amount of product, very high energy is required. With all the drawbacks in terms of energy and capital investment, it has a high-quality product with the concentration of at most 40 °Brix (Sánchez et al., 2009, Lopez-Quiroga et al., 2015).

Gas hydrate is a new technology with the potential to overcome the high energy requirements for evaporation as well as a high-quality product. Table 2.4 presents a comparison among concentration methods available in the literature for sugar cane juice.

Table 2-4. Comparison of the different juice concentration methods including membrane and evaporation (extracted from (Jiao et al., 2004)), freezing and hydrate technology.

Process	Initial concentration (ºBrix)	Final concentration (ºBrix)	Product quality	Evaporation rate or flux (l/m²h)	Operating cost	Capital investment	Energy consumption	Maturity
Evaporation[1]	2.5-6	60	Moderate	200–300	Moderate	Moderate	Very high	Developed
Reverse osmosis[1]	2.3-5.8	25-30	Very good	5–10	High	High	High	Developed
Direct osmosis[1]	4.3-11.7	50	Good	1–5	High	High	Low	Developing
Membrane distillation[1]	5-10	60	Good	1–10	High	High	Low	Developing
Osmotic distillation[1]	9.6-11	60	Very good	1–3	High	High	Low	Developing
Freezing[2]	10-15.5	40	Very good	Low	High	High	High	Developing
Hydrate[2]	10-15	60	To be studied	---	---	---	---	New

[1] Jiao et al. (2004)

[2] This work

In summary

Various treatment methods used in sugar production industry were reviewed in this chapter investigating the pros and cons of each technique. Due to the operating temperature of gas hydrate technology and its potential to overcome the energy required for conventional industrial methods, it can be considered as an attractive option. Furthermore, the operational condition helps the heat-sensitive material remain intact and in excellent product quality, lowering inversion and heat-related losses of sucrose as well as no colour change is anticipated.

Chapter 3: Thermodynamic and kinetic modelling

This chapter discusses the modelling approaches used in this research study. The three phases in co-existence and equilibrium are hydrate, liquid, and vapour (SLVE). Each phase is modelled using appropriate thermodynamic relations concerning the measured variables of *P, T*, and *x (sucrose)*. The experimental phase data were treated to find the best fit for the model parameters using either direct method ($\varphi - \varphi$) or combined method ($\gamma - \varphi$). Furthermore, the kinetic modelling of the experimental data was performed to obtain the gas hydrate formation rate, storage capacity, gas consumption, and apparent rate constant. Thereafter, a summary of the available literature data on the kinetics of the CO_2 hydrate and most important parameters are presented.

Since the discovery of the gas hydrate and its potential hazards to the petroleum industry by (Hammerschmidt, 1934) numerous studies on the development of theoretical and empirical-based models have been performed to better understand its behaviour. Different guest molecules are encapsulated in various types of cavities namely structures sI, sII and sH which differ in cavity size, geometric arrangements, number of cavity per unit cell, average cavity radius and number of water molecules participating in the formation of the cavity (Sloan and Koh, 2008, Carroll, 2014). CO_2 gas hydrate crystals has the structure type I (Sloan and Koh, 2008). The reader is referred to the selected texts for further reading.

3.1 Thermodynamic modelling for gas hydrate

In this study, the equilibrium state of the hydrate phase is modelled using the (Parrish and Prausnitz, 1972) approach. The method proposed is based on solving the equality of the fugacity of water in the liquid phase f_w^L and hydrate phase f_w^H:

$$(f_w^H = f_w^L)$$
3.1

f_w^L is calculated using either the UNIFAC group-contribution model, UNIQUAC or NRTL models, while the fugacity of water in the hydrate phase is calculated using the solid solution theory of (Van Der Waals and Platteeuw, 1959) based on statistical thermodynamics.

3.1.1 Data regression for the equilibrium of vapour-liquid

There are two methods used to regress phase equilibrium data; the phi-phi ($\emptyset - \emptyset$) or direct method, and the gamma-phi ($\gamma - \emptyset$) or the combined method. In the combined method, the fugacity coefficient is used to describe the vapour phase non-ideality while the activity coefficient

is used to describe the liquid phase non-ideality. However, in the direct method, the fugacity coefficient is used to calculate both vapour and the liquid phase non-ideality.

Thermodynamic models are developed to estimate the fugacity of components in different phases. These include equations of state models (EOS) with mixing rules, as well as activity coefficient models. A summary of EOS models developed for better estimation of non-ideality in the mixtures is presented in table 3-1. (Tohidi et al., 1995) compares the results of hydrate modelling using the Valderrama EOS, with the non-density-related mixing rules and the Peng-Robinson EOS (Peng and Robinson, 1976), with the classical mixing rules of Van der Waals for single and mixed electrolyte-solutions. Both models can be used to model vapour and liquid phases for a non-electrolytic mixture in which the gas solubility is low.

Table 3-1. Equations of states used in the hydrate phase equilibrium calculations (Smith, 2015).

EOS	Used in hydrate studies	Mixing Rule
Soave-Redlich-Kwong (Soave, 1972)	(Chun and Lee, 1998)	Modified Huron-Vidal (Dahl and Michelsen, 1990)
	(Sugahara et al., 2005)	Classical
	(Delahaye et al., 2006)	Modified Huron-Vidal
	(Mooijer-van den Heuvel et al., 2006)	N/S
(Peng and Robinson, 1976)	(Tohidi et al., 1995)	Classical
	(Javanmardi et al., 2004)	N/S
PRSV (Stryjek and Vera, 1986)	(Klauda and Sandler, 2000)	N/S
	(Khosravani et al., 2013)	Non-density-dependent
(Patel and Teja, 1982)	(Chen and Guo, 1996)	N/S
	(Ma et al., 2003)	(Kurihara et al., 1987)
(Trebble and Bishnoi, 1988)	(Englezos and Bishnoi, 1991)	N/S
	(Englezos, 1994)	Quadratic
(Valderrama, 1990)	(Mohammadi et al., 2003)	Non-density-dependent
	(Javanmardi et al., 2012)	Non-density-dependent

N/S – Not specified

Conventional methods for calculating the hydrate phase equilibria (Chun and Lee, 1998, Cao et al., 2001, Klauda and Sandler, 2000) use various thermodynamic models to calculate the fugacity of water in the liquid phase.

Based on the factors mentioned, the Peng-Robinson EOS was used in conjunction with the Van der Waals mixing rules for vapour phase modelling in this study for systems with carbon dioxide. This EOS was selected because it is commonly used in the industry, and requires less detailed and quantitative inputs for gas system prediction than Soave-Redlich-Kwong EOS (Smith et al., 2005). To model the liquid phase, the UNIFAC model was selected because of the use of the functional group according to the approach by (Chun and Lee, 1999).

3.2 Fugacity of water in liquid and gas phases

The Peng Robinson (PR EOS) (Peng and Robinson, 1976) is used to calculate the fugacity of water in the vapour phase. Equation 3.2 represents the EOS with the parameters a and b are given in equations 3.3 and 3.6.

$$P = \frac{RT}{v - b} - \frac{a(T)}{v(v + b) + v(V - b)} \tag{3.2}$$

$$a(T) = \frac{0.45724(RT_c)^2}{P_c} a(T_c) \tag{3.3}$$

$$a(T_c) = \left\{ 1 + \alpha \left[1 - \left(\frac{T}{T_c} \right)^{0.5} \right] \right\}^2 \tag{3.4}$$

$$\alpha = 0.37464 + 1.5422\omega - 0.2699\omega^2 \tag{3.5}$$

$$b = 0.0778 \left(\frac{RT_c}{P_c} \right) \tag{3.6}$$

a denotes the attractive volume parameter and b is the excluded volume parameter. T_c is critical temperature, ω is acentric factor and P_c is critical pressure, which are listed in table 3-2.

Table 3-2. Properties of the pure component for EOS (Frenkel et al., 2005).

Component	P_c (MPa)	T_c (K)	ω
Water	22.064	647.14	0.344
CO_2	7.3830	304.21	0.224

The fugacity coefficient can be calculated as follows (Peng and Robinson, 1976):

$$Z^3 - (1 - B)Z^2 + (A - 3B - 2B)A - (AB - B^2 - B^3) = 0 \tag{3.7}$$

$$A = \frac{Pa(T)}{(RT)^2} \tag{3.8}$$

$$B = \frac{Pb}{RT} \tag{3.9}$$

$$\widehat{\emptyset}_i^{EoS} \tag{3.10}$$
$$= exp \left\{ (Z - 1) \frac{B}{b_{mix}} - Ln(Z - b_{mix}) - \frac{A_i}{2\sqrt{2}B_i} \left(\frac{2 \sum_j a_{ij}}{a_{mix}} - \frac{b_i}{b_{mix}} \right) Ln \left[\frac{Z + (1 + \sqrt{2})b_{mix}}{Z + (1 - \sqrt{2})b_{mix}} \right] \right\}$$

The following equations were used to calculate the fugacity of water in vapour and liquid phase:

$$\hat{f}_w^V = \widehat{\emptyset}_w^V y_w P \tag{3.11}$$

$$\hat{f}_w^L = \widehat{\emptyset}_w^L x_w P \tag{3.12}$$

The fugacity of water in the liquid phase is calculated as follows:

$$\hat{f}_w^L = a_w P_w^{sat} \qquad\qquad 3.13$$

Where:

$$a_w = \gamma_w x_w \qquad\qquad 3.14$$

The saturation pressure is obtained as follows (where subscripts w and I are indicators of water and ice) (Dharmawardhana et al., 1980):

$$P_w^{sat} = 10^{-6} exp\left(73.649 - \frac{7258.2}{T} - 7.3037\ln(T) + 4.1653 \times 10^{-6}T^2\right) \qquad 3.15$$

$$P_I^{sat} \qquad\qquad\qquad 3.16$$

$$= \frac{10exp\left(-\frac{1032.558}{T} + 51.0561\log(T) - \frac{0.0977}{T} + 0.70357 \times 10^{-5}T^2 - 98.512\right)}{7600}$$

3.3 Activity Coefficient

In this study, the Gibbs excess energy models were used to calculate fugacity or activity coefficients. The models used are UNIFAC, UNIQUAC and NRTL.

3.3.1 UNIQUAC functional-group activity coefficients (UNIFAC) model

For calculation of the activity coefficient using the UNIQUAC functional-group activity coefficients (UNIFAC) method the following equations were used (Fredenslund et al., 1975):

$$ln\gamma_i = ln\gamma_i^C + ln\gamma_i^R \qquad\qquad 3.17$$

$$ln\gamma_i^C = 1 - J_i + lnJ_i - 5q_i\left(1 - \frac{J_i}{L_i} + ln\frac{J_i}{L_i}\right) \qquad\qquad 3.18$$

$$ln\gamma_i^R = q_i\left[1 - \sum_k\left(\theta_k\frac{\beta_{ik}}{s_k} - e_{ki}ln\frac{\beta_{ik}}{s_k}\right)\right] \qquad\qquad 3.19$$

$$q_i = \sum_k v_k^{(i)}Q_k \qquad\qquad 3.20$$

$$\theta_k = \frac{\sum_i x_i q_i e_{ki}}{\sum_j x_j q_j} \qquad\qquad 3.21$$

Subgroup and interaction parameters are listed in tables 3-3 and 3-4 for sucrose, fructose and glucose (Magnussen et al., 1981). The use of the UNIFAC group contribution method showed good correlation of the data for modelling gas hydrate inhibitors such as alcohol-alkane systems (Kontogeorgis et al., 2007), electrolytes (Moradi et al., 2013) and organic additives to natural gas systems (Gnanendran and Amin, 2004).

Table 3-3. Subgroup parameters for fructose, sucrose and glucose (Magnussen et al., 1981).

subgroup	[a]k	[b]R_k	[c]Q_k
CH_2	2	0.6744	0.540
CH	3	0.4469	0.228
OH	5	1	1.2
CHO	10	0.9980	0.948
COO	41	1.3800	1.2
H_2O	7	0.92	1.4
CO	8	0.7713	0.640

[a] Subgroup number
[b] Van der Waals volume subgroup
[c] Van der Waals surface subgroup

Table 3-4. Interaction parameters for sucrose, fructose and glucose (Magnussen et al., 1981).

	CH_2	CH	OH	CHO	COO	H_2O	CO
CH_2	0	0	986.5	677	387.1	1318	1565
CH	0	0	986.5	677	387.1	1318	1565
OH	156.4	156.4	0	-203.6	190.3	353.50	462.3
CHO	505.70	505.70	529	0	-275.5	480.80	------
COO	529	529	88.63	577.5	0	284.4	------
H_2O	300	300	-229.1	-116.1	-197.5	0	287.5
CO	3000	3000	-106.5	-------	-------	-532.6	0

3.3.2 UNIQUAC model

The second method used for the calculation of activity coefficient is UNIversal QUAsi Chemical model (UNIQUAC) (Abrams and Prausnitz, 1975):

$$ln\gamma_i = 1 - \emptyset_i + ln\emptyset_i - 5q_i(1 - \frac{\emptyset_i}{\theta_i} + ln\frac{\emptyset_i}{\theta_i}) + q_i(1 - lnS_i - \sum_j \frac{x_j\theta_j\tau_{i,j}}{S_j}) \qquad 3.22$$

Where S is dependent on the binary parameters of $\tau_{i,j}$. $\emptyset$ and θ are the volume and surface area parameters which are dependent on r_i and q_i, respectively. The parameters are listed in table 3-5 which are adopted from (Poling et al., 2001).

Table 3-5. UNIQUAC parameters of r_i and q_i (Poling et al., 2001).

	M (g/mol)	r_i	q_i
Water	18.01528	0.92	1.4
Sucrose	342.30	14.5586	13.764
Fructose	180.16	8.1589	8.004
Glucose	180.16	8.1558	7.92

$$\tau_{i,j} = \exp(-\frac{A_{ij}}{T}) \qquad 3.23$$

Where, $A_{ii} = A_{jj} = 0$ and $A_{ij} \neq A_{ji}$. The values of the parameter A_{ij} are presented in table 3-6 (Poling et al., 2001).

Table 3-6. Parameters for the binary interaction energy (A_{ij} (K)) for UNIQUAC (Poling et al., 2001).

	Water	Sucrose	Fructose	Glucose
Water	0	-127.48	65.91	-124.81
Sucrose	410	0	-	-
Fructose	48.58	-	0	-
Glucose	380.87	-	-	0

UNIQUAC model is capable of good predictions of the hydrate phase data in the pressure and temperature ranges of (0 – 10) MPa and (273.15 – 373.15) K. It has been used in gas hydrate studies for phase behaviour prediction of the systems such as carbon capture studies (Darde et al., 2010), organic inhibitors (Delavar and Haghtalab, 2015) and alcohols (Kondori et al., 2018).

3.3.3 NRTL model

The third method used in this study for calculation of liquid fugacity is the non-random two-liquid (NRTL) activity coefficient model of (Renon and Prausnitz, 1968):

$$\frac{g^E}{RT} = x_1 x_2 \left[\frac{G_{21}\tau_{21}}{x_1 + x_2 G_{21}} + \frac{G_{12}\tau_{12}}{x_2 + x_1 G_{12}} \right] \tag{3.24}$$

$$ln\gamma_1^L = x_2^2 \left[\tau_{21} \left(\frac{G_{21}}{x_1 + x_2 G_{21}} \right)^2 + \frac{G_{12}\tau_{12}}{x_2 + x_1 G_{12}} \right] \tag{3.25}$$

$$ln\gamma_2^L = x_1^2 \left[\tau_{12} \left(\frac{G_{12}}{x_2 + x_1 G_{12}} \right)^2 + \frac{G_{21}\tau_{21}}{x_1 + x_2 G_{21}} \right] \tag{3.26}$$

$$G_{12} = exp(-\alpha\tau_{12}) \qquad G_{21} = exp(-\alpha\tau_{21}) \tag{3.27}$$

$$\tau_{12} = \frac{b_{12}}{RT} \qquad \tau_{21} = \frac{b_{21}}{RT} \tag{3.28}$$

Where α, b_{21} and b_{12} are the dimensionless parameters of the model which are assumed to be independent of composition and temperature. These parameters are presented in table 3-7 (Nowak et al., 2009). In order to calculate the activity coefficient for a mixture of several compounds, the NRTL equation can be expanded as follows:

$$ln\gamma_i = \frac{\sum_{j=1}^n \tau_{ji} G_{ji} x_j}{\sum_{l=1}^n G_{li} x_l} + \sum_{j=1}^n \frac{x_j G_{ij}}{\sum_{l=1}^n G_{lj} x_l} \left[\tau_{ij} - \frac{\sum_{r=1}^n x_r \tau_{rj} G_{rj}}{\sum_{l=1}^n G_{lj} x_l} \right] \tag{3.29}$$

Table 3-7. NRTL parameters for different sugar and water systems (Nowak et al., 2009).

	Sucrose-water	Glucose- Water	Fructose-Water
b_{12}	6710	3550	4300
α	0.384	0.409	0.420
b_{21}	7860	6700	6920

Several research studies used the NRTL model which showed satisfactory results in the phase behaviour of thermodynamic inhibitors. These include the study of hydrate formation in ionic liquids (Keshavarz et al., 2013) electrolytes and inhibitors (Osfouri et al., 2015, Dehaghani and Badizad, 2016).

3.4 Fugacity of water in the hydrate phase

In this study, two different methods were used for calculating the fugacity of water in the hydrate phase, including the pressure of water in the empty hydrate lattice and chemical potential. Each model follows a theoretical and empirical basis which is listed below:

$$f_w^H = f_w^{MT} \exp\left(\frac{\Delta\mu^{H-MT}}{RT}\right) \qquad 3.30$$

$$f_w^H = p_w^{MT}\left[(1 + C_{small}P)^{-v'_{small}} + \left(1 + C_{large}P\right)^{v'_{large}}\right] \qquad 3.31$$

R and T are the Universal gas constant and temperature, respectively. $\Delta\mu^{H-MT}$ represents the difference between the chemical potential of water in the hydrate phase and the empty hydrate lattice. The empty hydrate lattice is presented by f_w^{MT}. f_w^{MT} and $\Delta\mu^{H-MT}$ are calculated as follows:

$$f_w^{MT} = f_w^L \exp\left(\frac{\Delta\mu^{MT-L}}{RT}\right) \qquad 3.32$$

$$\Delta\mu_w^{H-MT} = \mu_w^H - \mu_w^{MT} = RT\sum_m \bar{v}_m ln\left[1 + \sum_j C_{jm}f_j\right] \qquad 3.33$$

In the above equations C_{jm}, f_j, $\bar{v}_m$, and f_w^L show the Langmuir constant, fugacity of the gas component, number of cavities of each structure per molecule of water in the one hydrate cell (shown in table 3-8) inferring the interaction of gas-water in the cavity, and fugacity of pure water in liquid phase respectively (Eslamimanesh et al., 2011).

Table 3-8. Cavity number of each structure per molecule of water in each hydrate cell (Eslamimanesh et al., 2011).

Property	Value	
	Structure I	Structure II
$\bar{v}_{small}$	1/23	2/17
$\bar{v}_{large}$	3/23	1/17

Three approaches were followed to calculate the Langmuir constant to find the most suitable method. The cell potential approach, the empirical equations of Parrish and Prausnitz (Parrish and Prausnitz, 1972) and Munck and Rasmussen (Munck et al., 1988) are the basic models that were tested with different models in the comparative study. The calculation of the Langmuir constant is shown in the following section.

3.4.1 The cell potential approach

The cell potential approach was used to calculate the Langmuir constant numerically by employing a model for considering the interaction between water and gas molecules inside the cavities.

$$C_{mj}(T) = \frac{4\pi}{KT} \int_0^{\bar{R}/2} exp\left[-\frac{w(r)}{KT}\right] r^2 dr \qquad 3.34$$

Where $w(r)$, K, r and R represent the potential function of the spherically symmetric cell and Boltzmann's constant, cell radius, and distance from the centre of the cavity, respectively. The Kihara potential (Kihara, 1953) was taken into account in the calculation of w(r). It is calculated as follows:

$$w_r = 2z\varepsilon\left[\frac{\sigma^{12}}{R^{11}r}\left(\delta^{10} + \frac{a}{R}\delta^{11}\right) - \frac{\sigma^6}{R^5 r}\left(\delta^4 + \frac{a}{R}\delta^5\right)\right] \qquad 3.35$$

Where:

$$\delta^{\bar{N}} = \frac{1}{N}\left[1 - \frac{r}{R} - \frac{a}{R}\right]^{-\bar{N}} - \left[1 + \frac{r}{R} - \frac{a}{R}\right]^{-\bar{N}} \qquad 3.36$$

In the equations presented above, z, a, ε, σ and N denote the coordinate number, the radius of the spherical molecular core, characteristic energy, collision diameter and an integer (of either 4, 5,10 or 11) respectively. Parameters for the Kihara potential are shown in table 3-9. The parameter optimisations of this work for different modelling approaches were done using the genetic algorithm procedure in MATLAB® software.

Table 3-9. Parameters of Kihara potential for CO_2.

Components	$a\ (A^0)$	$\delta\ (A^0)$	ε/K (K)
CO_2 (optimized)	6.81	2.98	168.77

3.4.2 Empirical equation approach

3.4.2.1 Empirical equation of (Parrish and Prausnitz, 1972)

The second approach which used to calculate the Langmuir constant is the empirical equation of (Parrish and Prausnitz, 1972):

$$C_{ml}(T) = \left(\frac{A_{ml}}{T}\right)\exp(\frac{B_{ml}}{T})$$

3.37

B_{ml} and A_{ml} are parameters which are shown in table 3-10.

Table 3-10. Langmuir constants is presented for various material (Parrish and Prausnitz, 1972).

Former	Value (K)							
	Structure I				Structure II			
	Small		Large		Small		Large	
	A_{ml}	B_{ml}	A_{ml}	B_{ml}	A_{ml}	B_{ml}	A_{ml}	B_{ml}
CO_2	1.2×10^{-3}	2860.5	0.8507×10^{-2}	3277.90	0.0	0.0	0.0	0.0

3.4.2.2 Empirical equation of (Munck et al., 1988)

The third approach is the empirical equation of (Munck et al., 1988). The parameters for A_{ml} and B_{ml} are shown in table 3-11.

Table 3-11. Langmuir constant via (Munck et al., 1988)'s parameters.

Former	Value(k)							
	Structure I				Structure II			
	Small		Large		Small		Large	
	A_{ml}	B_{ml}	A_{ml}	B_{ml}	A_{ml}	B_{ml}	A_{ml}	B_{ml}
CO_2	0.2474×10^{-3}	3410	42.46×10^{-3}	2813	0.0	0.0	0.0	0.0

The difference in the chemical potential between the chemical potential of water in the empty hydrate lattice and the liquid phase is calculated via (Holder et al., 1980):

$$\frac{\Delta\mu^{MT-L}}{RT} = \frac{\mu_w^{MT}(T,P)}{RT} - \frac{\mu_w^{L}(T,P)}{RT} = \frac{\Delta\mu_w^0}{RT_0} - \int_{T_0}^{T}\frac{\Delta h_w^{MT-L}}{RT^2}\,dT + \int_0^P \frac{\Delta v_w^{MT-L}}{RT}\,dp$$

3.38

In the above equation μ_w^{MT} denotes the chemical potentials of the empty hydrate cavity, μ_w^{L} shows the chemical potential of pure water in the liquid phase, $\Delta\mu_w^0$ is the chemical potential difference between pure water in the ice phase and water in the empty hydrate cavity at 273.15 K. T_0 and P are the absolute temperature related to the ice point and the equilibrium pressure. Δv_w^{MT-L} represents the differences in volume between liquid water and the empty hydrate cavity. Δh_w^{MT-L} is molar enthalpy difference between liquid water and the empty hydrate cavity. The enthalpy difference is calculated as follows:

$$\Delta h_w^{MT-L} = \Delta h_w^0 + \int_{T_0}^{T} \Delta C_{Pw} dT \tag{3.39}$$

$$\Delta C_{Pw} = -38.12 + 0.141(T - T_0) \tag{3.40}$$

Where, Δh_w^0 is the difference of enthalpy between ice and empty hydrate cavity (at zero pressure and the ice point) and ΔC_{Pw} is the difference of the heat capacity between the pure liquid water and empty hydrate lattice. ΔC_{Pw} has a temperature-dependent relation. The equation below can be used to calculate the water fugacity in the hydrate phase.

$$f_w^H = P_w^{MT} \left[(1 + C_{small}P)^{-\bar{v}_{small}} + \left(1 + C_{large}P\right)^{-\bar{v}_{large}} \right] \tag{3.41}$$

in which, P_w^{MT} refers to the pressure of water in the empty hydrate lattice. It can be calculated for SI and SII structures using the following equations (T is in K):

$$P_w^{MT} = 0.1exp\left(17.440 - \frac{6003.925}{T}\right) \tag{3.42}$$

$$P_w^{MT} = 0.1exp\left(7.332 - \frac{6017.635}{T}\right) \tag{3.43}$$

Table 3-12. Thermodynamic properties of the structure I and II (Parrish and Prausnitz, 1972).

Property	Value		Unit
	Structure I	Structure II	
Δh_w^{MT-L}	-4858	-5201	J. mol^{-1}
$\Delta \mu_w^0$	1264	883	J. mol^{-1}
Δv_w^{MT-L}	4.6	5	cm^3.mol^{-1}

3.5 Kinetic model

The kinetics of hydrate formation is essential in understanding the feasibility of the concentration process. The initial temperature and pressure, stability region, water history and cooling degree are parameters that can affect the hydrate formation kinetics (Vysniauskas and Bishnoi, 1983).

Using kinetic parameters, Vysniauskas and Bishnoi developed a semi-empirical kinetic model showing that water history increases the induction time (Vysniauskas and Bishnoi, 1983). In this study, known kinetic models designed by (Englezos et al., 1987) were utilised to determine the rate constant and hydrate formation rate. (Englezos et al., 1987) used crystalline and mass transfer theory showed that the consumption gas for hydrate formation depends on the rate of crystals growth (Englezos et al., 1987).

The theory of crystallisation (Englezos et al., 1987) is determined from the difference of the fugacity of the gas molecule in the vapour and hydrate phases. The hydrate formation rate depends on the mass transfer between the guest and water molecules and does not relate to the surface area of the solid particles (Englezos et al., 1987) (Skovborg and Rasmussen, 1994). As a result, there is no need to know the distribution of particle size in the process of hydrate formation.

Research on the effects of several additives on hydrate formation kinetics is a different feature of the kinetic study which has been carried out in numerous studies (Mohammadi et al., 2014, Manteghian et al., 2013, Fazlali et al., 2013, Arjang et al., 2013, Partoon and Javanmardi, 2013, Kelland et al., 2013). Investigation of the hydrate formation rate of methane and nitrogen mixture in a one-litre reactor (CSTR) shows that the hydrate formation rate in a CSTR reactor is much higher than those in a closed reactor (Vysniauskas and Bishnoi, 1983). Therefore, the results of a semi-closed reactor may cause problems in the design of a continuous hydrate-forming reactor (Happel et al., 1994).

According to (Englezos et al., 1987), hydrate formation consists of three steps. Steps one and two include the penetration of the gas into the liquid phase and then to the hydrate phase. The physical reaction of water and hydrate molecules in the hydrate phase is the final stage of hydrate formation. Some models consider the three steps collectively (Englezos et al., 1987), while others only consider the first two processes mentioned in (Khokhar et al., 1998, Skovborg and Rasmussen, 1994). The physical reaction between the gas and water for the formation of gas hydrates is defined as follows (Sloan Jr and Koh, 2007):

$$Gas \ + \ MH_2O \rightarrow Gas.MH_2O \qquad\qquad 3.44$$

M in the above equation is the hydration number that is displayed as the ratio of the number of water molecules to the number of gas molecules. In the event of blocking of cages, the only hydration value for sI, sII and sH is 23/4, 17/3 and 17/3. Hydration number, M, for sI is calculated using the equation (Sloan Jr and Koh, 2007):

$$M = \frac{46}{6\theta_L + 2\theta_S} \qquad\qquad 3.45$$

Where θ shows the occupancy of cages and indicators of S and L represents small and large cavities. The parameter θ can be defined:

$$\theta_i = \frac{C_i f_g}{1 + C_i f_g} \qquad \text{3.46}$$

Where f_g is the fugacity of the gas in the vapour phase, and C_i shows the fixed constant of Langmuir as previously defined. The ideal gas law is used to estimate gas consumption through the formation of hydrates (Smith et al., 2005):

$$\Delta n_g = \frac{P_0 V_0}{Z_0 R T_0} - \frac{P_t V_t}{Z_t R T_t} \qquad \text{3.47}$$

Where *P, T,* and *V* represent the pressure, temperature and volume of the gas inside the equilibrium cell. The elements *'0'* and *'t'* define the equilibrium conditions at time *0* and *t*. The compressibility factor is estimated using the PR EOS. The volume of gas inside the cell (V_t) is calculated at the time *t* using the following equation (Mohammadi et al., 2014):

$$V_t = V_{Cell} - V_{S_0} + V_{RW_t} - V_{H_t} \qquad \text{3.48}$$

Where V_{cell} is the cell volume and V_{S_0} represents the initial volume of water injected. In this study, the volume of the cell is approximately 750 cm³, and the initial volume of water entering the cells at the beginning of the test is about 160 cm³. In Equation 3-47, V_{RW_t} and V_{H_t} represent the volume reacted and hydrate volume at time t. The amount of water reacted at any time is calculated using the equation (Mohammadi et al., 2014):

$$V_{RW_t} = M \times \Delta n_g \times v_w^L \qquad \text{3.49}$$

Where v_w^L shows the molar volume of water. The molar volume of the hydrate is calculated as follows (Mohammadi et al., 2014):

$$V_{H_t} = M \times \Delta n_g \times v_w^{MT} \qquad \text{3.50}$$

The amount of gas consumed by gas hydrate formation is calculated according to the following equation (Mohammadi et al., 2014):

$$r(t) = \frac{n_{g,i-1} - n_{g,i+1}}{(t_{i+1} - t_{i-1})n_{w_0}} \qquad \text{3.51}$$

Where n_{w0} denotes the initial number of water molecules in the aqueous phase, which is calculated using the initial volume of water (160 cm^3 in this study) and the molecular volume of water. In equation 3-50, $n_{g,i-1}$ and $n_{g,i+1}$ define the number of gas molecules in the vapour phase at the time t_{i-1} and t_{i+1}. Another parameter described in the model is k_{app} (the constant of the reaction rate when hydrate formation), using the equation below (Englezos et al., 1987):

$$K_{app} = \frac{r(t)}{f_g - f_{equib}} \qquad 3.52$$

In Equation 3-51, $f_{equib.}$ is described as the gas fugacity at the hydration pressure ($P_{equib.}$) and the initial temperature conditions. $f_{equib.}$ can be calculated using the thermodynamic model to calculate the gas equilibrium conditions described in the previous sections. Storage capacity (SC) refers to the amount of gas stored in each hydrate volume at standard conditions which can be explained as follows:

$$SC = \frac{V_{STP}}{V_H} = \frac{\Delta n_g R T_{STP}/P_{STP}}{V_H} \qquad 3.53$$

Where STP stands for the standard temperature pressure conditions. The kinetic measurements in this study were performed on {CO$_2$ + water} and {CO$_2$ + sucrose + water} solutions. The parameters such as the rate constant, hydrate formation rate, induction time, gas consumption and storage capacity were determined for the systems {CO$_2$ + water} and {CO$_2$ + sucrose + water} using the abovementioned models.

The induction time indicates the time required for the hydrate crystal to create a stable nucleus and grow to a significant size (Sloan Jr and Koh, 2007). The induction time is a function of surface level, cell volume, mixer speed, pressure and temperature, mass and heat transfer rates and gas consumption (Sloan Jr and Koh, 2007).

During the formation of CO$_2$ hydrates, three distinct stages can be determined. The first stage is the dissolution stage. During this period, some of the gas in the vapour phase is discharged at the gas-liquid level and dissolved in the water phase. During the induction period, carbon hydrate crystals are formed and decomposed until a nucleus is created and grows to a detectable size. The cloud point is the beginning of the growth stage, which corresponds to the last period. At the growth stage, CO$_2$ molecules are encapsulated into the hydrate holes, and the system pressure is significantly reduced to a constant value.

The hydrate formation rate determined using equation 3.50. It is an indicator of the time required for the cavity to form and encapsulate the gas under the desired condition for the hydrate formation per initial mole of water.

Equation 3.65 proposed by (Englezos et al., 1987) was used to estimate the intake of gas molecules during hydrate formation under different conditions of initial pressure and temperature. A summary of works done by various scholars on kinetic of CO_2 + pure water system is provided in table 3-13. Induction time is a value that changes from equipment to equipment, and it is a function of several factors including cell volume, pressure, temperature, mixer speed and memory of the used water. The kinetic data of the literature are in the temperatures between (273.65 and 283) K and pressures up to 4.50 MPa.

Table 3-13. Summary of studies done on the kinetics of CO_2 + water system.

Cell volume (ml)	Pressure (MPa)	Temperature (K)	Induction time (min)	Mixer speed (rpm)	Reference
23.6	4.50	275.4	2600	No agitation	(Zhang et al., 2004)
150	2.06	275.6	75	500	(Sabil et al., 2010)
	3.25	278.2	40		
500	3.55	274	- NA -	- NA -	(Kumar et al., 2013)
35	5.00	279.3	60	- NA -	(Lirio et al., 2013)
450	3.44	283	<5	120	(Farhang et al., 2014b)
450	3.44	283	<5	120	(Farhang et al., 2014a)
460	2.05	273.65	1	500	(Mohammadi et al., 2014)
169	3.80	278.15	73	10	(Mohammadi et al., 2018)

The hydrate forms on the gas-liquid interface and the larger surface area improve the nucleation. Furthermore, the hydrate formation is profoundly affected by the driving force and kinetic constant. In the event of no stirring, the gas-liquid interface remains intact. By contrast, stirring the gas-liquid mixture increases the gas-liquid interface dramatically, which consequently increases the rate of hydrate formation on the interface (Tajima, 2011). The literature data show that no agitation results in a long induction time (Zhang et al., 2004).

Increases in the pressure causes a rise in the driving force of the system, and an improved tendency of the system to encapsulate the gas increases the rate of hydrate formation (Mohammadi et al., 2014). The temperature rise shifts the hydrate boundary to a higher temperature zone, decreasing the driving force of the system (Sloan and Koh, 2008). From the factors affecting the kinetics of hydrate, the mixer speed is the most influential. The driving force is the second most crucial factor

affecting the induction time. As the cell volume increases, the solution volume is also increased in the same proportion which is the least important factor among the others.

Chapter 4: Review of experimental gas hydrate methods

This chapter presents a literature review on the concentration of food juice using gas hydrate technology. The data published in the literature for the gas hydrate phase equilibria of sugar species include thermodynamic data with various formers and refrigerants. The equipment used for these measurements as well as other investigations of hydrate concentration of food solutions is provided.

4.1 Overview

The experimental methods for phase boundary measurements are divided into the dynamic methods which are distinguished by recirculation of phases and static methods with the closed equilibrium cells being their distinguishing feature (Richon, 1996, Richon and Loos, 2005). Another classification method divides the experimental techniques into the two major groups of visual, with the possibility to observe the experimental procedure (Hammerschmidt, 1934) and non-visual, which mainly depend on the measurements of thermo-physical properties of the systems studied (Makogon et al., 1996). The reader is referred to (Sloan and Koh, 2008) for further information on these classifications along with their pros and cons.

The experimental apparatuses are designed and commissioned based on the experimental technique that has been implemented to measure the phase boundary. These include isothermal, isobaric and isochoric apparatuses. With the isothermal measurements, the hydrate dissociation condition is obtained via trial and error around the formation and dissociation points (Makogon et al., 1996). With the isobaric method, the temperature of the system is decreased at the constant pressure condition until the hydrate is formed. Thereafter, the temperature is increased to dissociate the crystals. The condition at which the last crystal has dissociated is considered as the hydrate dissociation point (Kobayashi and Katz, 1949). With the isochoric pressure search method, the volume of the cell is kept constant while the temperature is decreased. A sharp drop in the pressure of the system indicates that hydrate formation has started. The pressure drop is continued until the pressure is stable and no hydrate is formed. Thereafter, the temperature is increased until the last crystal has dissociated (Javanmardi et al., 2012).

Due to the automatic measurement of the entire hydrate formation process and the possibility of performing the measurement overnight, the isochoric pressure search method (IPSM) apparatuses are preferred. The following research works report the successful use of this method (Belandria et al., 2011, Chun and Lee, 1998, Andersen and Thomsen, 2009, Smith, 2015, Li et al., 2014, Javanmardi

et al., 2005). They were able to ensure good entrainment of gas within the hydrate. Furthermore, it does not require observation for hydrate formation which eliminates a source of uncertainty (Sloan Jr and Koh, 2007). The usual approach to measure phase equilibrium data is to use an indirect method which monitors pressure using the isochoric pressure-search method. The static apparatus for this method is classified as the high pressure "blind" autoclave cell. This type of hydrate apparatus is capable of measuring the hydrate phase equilibria and kinetic measurements at high pressures (Sloan and Koh, 2008). The basic apparatus for the static type of the hydrate equipment was commissioned by Deaton and Frost (Deaton and Frost, 1937). Several improvements have been performed on the hydrate equipment based on the IPSM. Some of these apparatuses include the withdrawal of samples from either the hydrate phase or the slurry (solution residue) (Purwanto et al., 2014, Park et al., 2011). The reader is referred to (Sloan and Koh, 2008) for detailed information on different apparatus and methods for hydrate phase studies.

4.2 Fruit juice concentration via gas hydrate technology

Studies on the effects of parameters such as the mixer speed and the formation of hydrate for a wide range of fruit juices (including apple, and orange juice), proteins and lipids show that carbohydrates, proteins and lipids are capable of forming gas hydrates. The use of trichlorofluoromethane (CCl_3F) as the hydrate former showed that the hydrate is formed better at lower concentrations of the juice. By contrast, hydrate formation is scarce at higher concentrations (Huang et al., 1965).

The results of high-pressure measurements (2.10 to 4.43 MPa) for the concentration of orange juice with ethylene gas show the ability of the technology in dehydration ratios of up to 99 % indicating the capacity of hydrate technology to concentrate juice (Li et al., 2014). Experiments on gas hydrate phase equilibria of tomato juice show its promotion effect on CO_2 gas hydrate. Furthermore, CO_2 gas hydrate is capable of concentrating tomato juice up to 63.2 % dehydration of the initial juice at pressures up to 4.0 MPa (Li et al., 2014). The improved concentration of the orange juice is achieved at higher pressures. It is proven that carbon dioxide gas hydrate can dehydrate orange juice by 57 % of initial juice at pressures up to 4.1 MPa (Li et al., 2015). Results from measurements of ethylene gas hydrate show the improved orange juice dehydration ratio of 92 % compared to that of carbon dioxide hydrate. This is because of the greater entrapment of gas molecules due to volume difference between ethylene and CO_2 leading to more water molecules taking part in the formation of the hydrates (Li et al., 2017).

It was found that the use of xenon as the former gas has the potential to form and grow hydrate in coffee solutions. Additionally, performing experiments at lower pressures and higher temperatures can develop relatively larger crystals. The results indicate the requirement of relatively higher pressures for elevated concentrations of coffee solutions. This is due to the increased bubble point of the mixture as a result of more soluble solids in the highly concentrated mixture. The equipment used in the reported work was a static-view cell (Ya et al., 1998). The concentration of coffee juice up to 14.7 wt. % via xenon gas hydrate in the temperature range of 275.15 to 283.15 K and a pressure range of 0.2 to 1.0 MPa showed that the induction time is affected directly by the concentration of the juice. The hydrate crystal size of the xenon gas is more prone to larger crystals at high temperatures and low pressures (Purwanto et al., 2001).

In another study from this group, the design of a new high-pressure apparatus provided the ability to withdraw a sample of coffee solution at low concentrations. The 700 ml high-pressure cell was made of stainless steel housing a U-shaped polycarbonate mixing blade (Purwanto et al., 2014). It was also equipped with two viewing windows to monitor the reaction inside the cell. The coffee juice sampling studies were performed at the temperature and pressure of 282.13 K and 0.90 MPa, respectively. The experimental apparatus was fitted with three interconnected valves with a steel screen to withdraw the sample from coffee juice and filter the hydrate crystals at the same time. The feature of having three valves enabled sampling in three steps with improved separation of the hydrate crystals from coffee solution. The mass of the withdrawn sample was recorded once after withdrawal from the cell and once it was oven-dried to calculate the concentration. Meshes with the sizes of 53, 75, and 150 μm were tested. The results showed that the use of a smaller mesh is by far the most efficient in achieving better concentration results. This is due to the prevention of the small crystals from passing through the holes of the screen. Greater concentration efficiency is also achieved using a lower mixing rate. The three mixer speeds were tested, with of 100, 200, and 400 rpm. As the speed of the mixer increases, the crystal forms rapidly with a small size distribution, which decreases the separation. The same behaviour applies to a higher temperature with the ability to create larger crystals. However, due to the shift in the phase boundary to higher pressures, the driving force required increases in the case of high pressures. This method could only concentrate the juice by a negligible amount of 0.04 ºBrix (Purwanto et al., 2014). Figure 4-1 shows the schematic of the equipment used by (Purwanto et al., 2014). To the best of the author's knowledge, no further work on this apparatus has been reported to date.
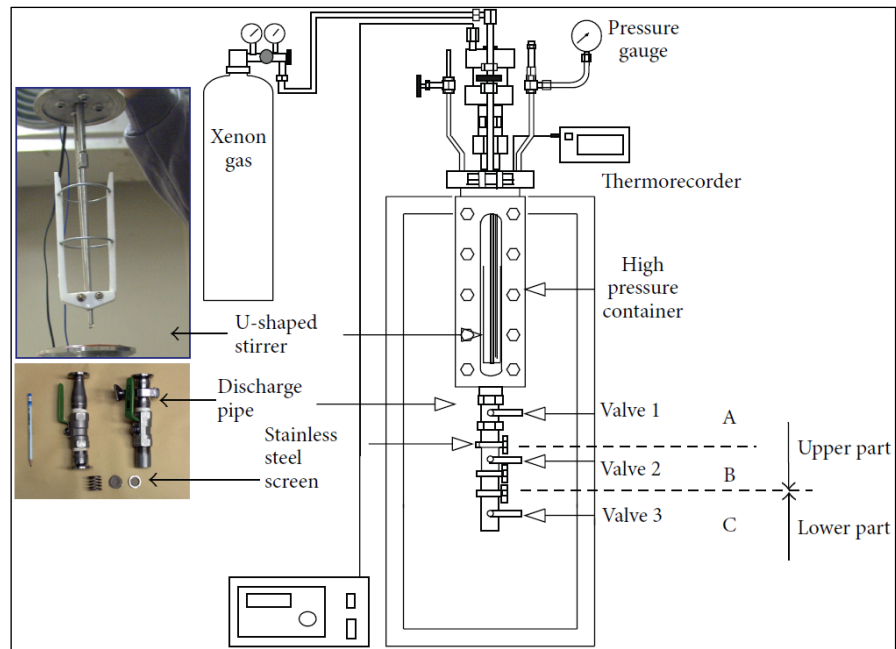
Figure 4-1. Schematic diagram of the apparatus used by (Purwanto et al., 2014).

A summary of the experimental studies on fruit juice concentration using various hydrate formers is presented in table 4-1. It lists some information about the apparatuses used, operational conditions, the material of construction, and volume of the reactor. The mixer speed is also included in the case of availability. The experimental data mentioned in the literature were measured following the isochoric pressure method.

Evaporation technology is a very well developed technique for industrial applications as opposed to hydrate technology. For process designs using traditional technologies economic feasibility studies and energy considerations can be performed quite straightforward. However, much more research is required to understand the technical constraints in gas hydrate separation, equipment design and scale-up.

Table 4-1. Review of the food juice concentration by gas hydrate technology following the isochoric pressure method.

Reference	Food juice	Former gas	T (K)	P (MPa)	$C_{initial}$ (ºBrix)	V_{cell} (ml)	Mixer speed (rpm)	Aim
(Huang et al., 1965)	Apple Orange Sucrose D-glucose	CCl_3F	273.15 – 281.85	-NA-	10 - 40 10 - 36 5 - 50 5 - 30	700	3000 - 3500	Formation and dissociation
(Ya et al., 1998)	Coffee	Xe	275.00 – 283.00	Up to 1.00	5.1 & 14.7	4.5	-NA-	Crystal size distribution
(Purwanto et al., 2001)	Coffee	Xe	275.13 – 283.15	0.2 - 1.00	1.5 - 14.7	4.5	-NA-	Crystal size distribution
(Purwanto et al., 2014)	Coffee	Xe	282.15 – 287.95	0.38 – 1.09	4.75	700	100 - 400	Sampling the juice
(Li et al., 2014)	Orange	C_2H_4	275.95 – 276.75	2.10 – 4.43	-NA-	300	500	Kinetic measurement
(Li et al., 2014)	Tomato	CO_2	275.80	1.81 - 3.95	-NA-	300	500	Kinetic measurement
(Li et al., 2015)	Orange	CO_2	274.80 - 279.80	1.96 - 4.10	-NA-	300	500	Kinetic measurement
(Li et al., 2017)	Orange	CO_2, C_2H_4, C_2H_6	274.80 - 283.30	0.68 - 4.40	-NA-	300	500	Kinetic measurement

4.3 Hydrate studies on carbohydrate solutions

Experimental studies show the inhibition behaviour of the carbohydrates of dextrose and sucrose on hydrogen sulphide gas hydrate. The presence of sugar content can decrease the maximum temperature at which H_2S hydrate can form by 0.8 K (Bond and Russell, 1949). The comparative studies on the inhibition effects of the sucrose, glucose and lactic acid solutions on R22 gas hydrate show that the most significant inhibition effect results in the lactic acid solution. The experimental pressures were in the low-pressure range of 0.15 to 0.9 MPa (Chun and Lee, 1998). A similar inhibition effect of the sucrose, glucose, and fructose solutions were observed on the CO_2 gas hydrate in a higher range of operating pressure compared to R22. It is also proven that the inhibition effect of the sugar species is equivalent to alcohols (Chun and Lee, 1999). The use of gases such as toxic refrigerants and hydrogen sulphide with food products should be avoided as some residue could remain in the food product. Therefore, while it is necessary to investigate the behaviour of the hydrate formation and dissociation conditions with alternate gases, the use of toxic gases is not recommended for food or fruit juice concentration studies.

A limited number of studies focused on the potential of gas hydrate technology on the concentration of sugar cane juice. Due to the high-pressure condition of hydrate formation and a need for a large volume reactor, it is currently not a practical solution for implementation. Furthermore, when considering the process economics, possibility of sugar loss is present via hydrate technology, but further investigations should be performed on the large volume reactors. Due to the low-temperature requirement for the hydrate formation and dissociation process, it has the potential to replace the conventional concentration methods for the heat-sensitive material (Andersen and Thomsen, 2009).

The findings from the experimental study by (Andersen and Thomsen, 2009) confirms the concentration of sucrose up to 54 °Brix, which results in the removal of almost 90 % of its original water content. However, the major part of the sugar was found to be in the hydrate phase. Though depending on the cell volume, it is possible to remove 50 out of 1200 gr water per litre of carbon dioxide at the pressure of 3.00 MPa. A process patent (SE-2000381) was registered by Nordic Sugar in 2009 but dropped afterwards due to the process incompatibility with sugar production. The initial juice samples were 5, 15, and 30 °Brix. Additional to the concentration tests, phase boundaries of the abovementioned solutions were measured with CO_2 at temperatures between (276.29 and 280.60) K and pressures up to 3.40 MPa. Figure 4-2 shows the summary of the experimental data measured for the sucrose + CO_2, which is taken from (Andersen and Thomsen, 2009).
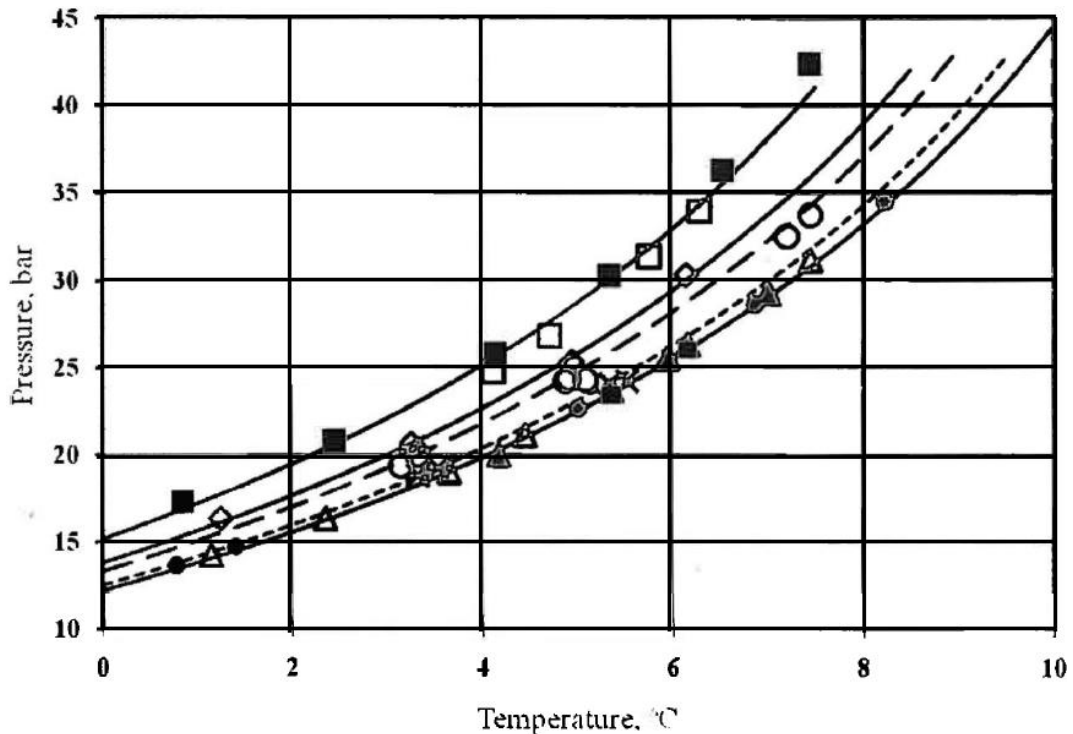
Figure 4-2. Experimental data and modelling of the sucrose solution dissociation condition with CO_2 gas hydrate; Δ Pure water (Andersen and Thomsen, 2009), × 5 ºBrix (Andersen and Thomsen, 2009), ● 15 ºBrix (Andersen and Thomsen, 2009), □ 30 ºBrix (Andersen and Thomsen, 2009), ◊ 20 ºBrix (Chun and Lee, 1999), ■ 30 ºBrix (Chun and Lee, 1999). The figure is extracted from (Andersen and Thomsen, 2009).

There is no information about the volume and structure of this equipment and only the mixing system was explained. It includes a magnetic ring inside the cell and a powerful magnetic ring outside the cell. The internal ring consisted of 12 powerful magnets which were coated with polysulfone to prevent water penetration into the magnets. The outside ring moved horizontally to induce magnetic field and provide agitation required for hydrate formation. Additional to the high-pressure units that were required for the sugar production by hydrate technology, there was a possibility of sugar loss due to the sticky nature of the sugar solution. The actual amount of sugar loss was not reported (Andersen and Thomsen, 2009).

The available studies mostly focused on the inhibition effect and phase equilibria of the carbohydrates namely, D-glucose, fructose and sucrose in the presence of several gases including methane, propane, carbon dioxide and refrigerant gases. The results indicated that glucose shows higher inhibition effect (Carbone et al., 2012, Smith et al., 2016, Tan et al., 2014). The findings from phase equilibria studies with refrigerants showed that the phase boundary is in the lower pressure range compared to that of carbon dioxide, which is an exciting discovery for the process economics point of view. However,

due to the toxic nature of most of the refrigerants, it is necessary to be cautious in the use of these chemicals for food processing and consumption. Figure 4-3 shows the schematic diagram of the equipment used for hydrate dissociation measurement, which lacks the capabilities of sample withdrawal. The highest pressure required for the phase equilibria of refrigerant gas hydrates (R410a, R507 and R134a) with sucrose solution at temperatures up to 289.15 K was 0.90 MPa (Smith et al., 2016). The cell used by (Smith et al., 2016) is one of several units used for hydrate phase equilibrium dissociation measurements in the Thermodynamics Research Unit. The reader is referred to the work of (Ilani-Kashkouli et al., 2016, Ngema et al., 2014a, Ngema et al., 2014b, Smith et al., 2016, Hashemi et al., 2015, Babaee et al., 2016, Hashemi et al., 2014, Tumba et al., 2013) for further details about the hydrate apparatus. The apparatus used by this research team and several other groups consist of an equilibrium stainless steel cell equipment with agitation. The cell is immersed in a water bath maintained at an isothermal environment using a temperature bath controller. For the nature of the experiments, a programmable bath controller is preferred since this allows one to set a temperature program for heating and cooling during the experimental procedure. The auxiliary units consist of temperature and pressure sensors, vacuum pump, power supply system for mixing mechanism sometimes gas analysis, valves, fittings lines etc.
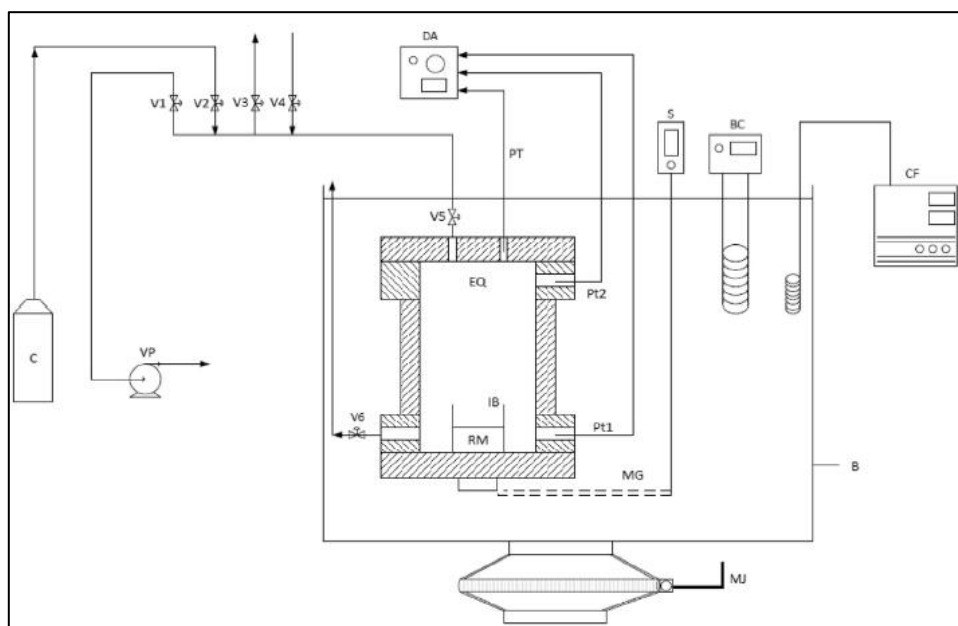
Figure 4-3. Schematic diagram of the experimental setup. B, isothermal liquid bath; BC, liquid temperature controller; C, refrigerant gas cylinder; CF, cold finger; DA, data acquisition unit; EQ, isochoric pressure equilibrium cell; IB, impeller blades; MG, mechanical gears; MJ, mechanical jack; Pt1, temperature probe; Pt2, temperature probe; PT, pressure transducer; S, overhead mechanical stirrer; V1, vacuum valve; V2, gas valve; V3, vent valve; V4, loading valve; V5, inlet valve; V6, drain valve; VP, vacuum pump. Adapted from (Smith et al., 2016).

Most of the available research in the literature focused on developing equipment for either phase equilibria or kinetics measurements. Only two studies attempted to withdraw samples from the juice. The use of various formers was tested to find the phase stability region. The studies proved the inhibition behaviour of food and carbohydrate juices. However, the phase boundary of refrigerants is below 1.00 MPa, which is considered relatively low.

Additional to the studies performed in this group there are other applications and equipment for hydrate based measurements. These include the equipment developed for food juice concentration (Purwanto et al., 2014), CO_2 capture (Li et al., 2009), desalination (Kang et al., 2014, Tohidi et al., 1995), kinetic studies of organic chemicals (Stoporev et al., 2018) and nano-particles (Mohammadi et al., 2014, Arjang et al., 2013), natural gas purification (Warrier et al., 2018) etc.

Desalination studies via gas hydrate started by developing equipment to study the effect different hydrate formers in 1960s and 1970s which led to development of the laboratory scale plants. However, due to the difficulties in crystal separation, the technologies were not commercialised (Knox et al., 1961, Barduhn et al., 1962, Barduhn, 1968). There have been recent successful efforts with optimisations required in chemical compatibilities and crystal separation techniques (McCormack and Andersen, 1995, McCormack and Niblock, 1998, McCormack and Niblock, 2000). The reader is referred to the reference of (Park et al., 2011) for further information on equipment development and separation studies.

Hydrate based CO_2 capture is a fairly new process with a considerable amount of industrial and academic interest. The studies on this technology was initiated by the phase equilibrium measurements (Duc et al., 2007, Kamath, 1984) and developed into the study of mechanical techniques to implement this technology industrially. The use of thermodynamic promotors such as tetrahydrofuran (Linga et al., 2007), tetra-n-butyl ammonium bromide (Shimada et al., 2003) improved the kinetic conditions and decreased the operating pressure. Recent advances propose the use of silica gels as it eliminates the need for energy intensive agitation by its reactive mechanism with water molecules (Kang et al., 2013). The reader is referred to (Dashti et al., 2015) for the extensive information on the experimental efforts to develop apparatus and separation techniques.

Chapter 5: Equipment description and experimental method

Engineering design is based on accurate modelling which relies on accurate empirical data (Richon, 2009). Therefore, the data collected from empirical studies is a valuable source of information that is reliable only if the methods and equipment used for its collection are accurate. The static and non-visual isochoric method was selected using a pressure cell equipped with a magnetic stirrer for this study. Another static isochoric method equipment with a 750 ml reactor volume and two viewing windows was commissioned. Among the existing static methods, the isochoric method is more beneficial as the entire process is done automatically and allows for measurements to be made overnight. Moreover, this method does not depend on the visual observation of hydrate formation, and thus eliminates this source of uncertainty. In this research study, different components were used from the literature to synthesise the new reactor cell. The new apparatus needed to be developed in a fashion such that withdrawal of the sample did not interfere with the equilibrium condition, requiring a larger reactor volume. Phase data must be obtained at the equilibrium condition. Sample withdrawal disturbs the thermodynamic equilibrium. Hence the cell volume must be large enough to overcome the problem of equilibrium disturbance after sample withdrawal. Details of the equipment design and operation of the two equipment are presented.

5.1 Isochoric pressure cell (dissociation measurements)

A high-pressure equilibrium cell reported in previous studies was used for the laboratory hydrate measurements (Smith et al., 2016). The unit includes a stainless steel (SS 316L) equilibrium cell (approximately 64 cm^3), an agitation mechanism, temperature-regulated liquid bath (43 cm x 35 cm 26 cm), programmable temperature controller (Grant 200), two 100 Ω platinum resistance thermometers (Pt100) probes (WIKA; 1/10 DIN), a pressure transmitter (WIKA; P-10; 10 MPa) with an accuracy of 0.1% of full scale, data acquisition unit (DAU) of LXI Agilent 34972A model, a desktop computer to log the data, a chilling unit (Thermo Scientific EK20 Immersion Cooler), two-stage vacuum pump (RV3 Edwards), SS316 feed lines, fittings, valves, etc. The schematic diagram of the experimental set-up is displayed in Figure 5-1. The equilibrium cell has an internal diameter of 45 mm and a height of 40 mm, with an approximate internal volume of 64 cm^3. Due to the displacement of the magnetic stirrer inside the cell, the working volume is approximately 53 cm^3. At the top of the cell, an O-ring was located in the groove between the upper flange and the cell. The top flange is connected to the cell using 6 x 10 mm SS 316L screws. The total thickness of the flange is 5 mm.

Three holes, each with a diameter of 8 mm, were drilled into the upper flange. The first hole, located on the upper right side of the cell, was used to fill and discharge the cell contents. The second hole, located on the top left of the cell, was used to connect an SS 316L tube of 1/16" to a pressure transmitter. The third hole that was located next to the flange was used to place the temperature probe. Two 8 mm holes were drilled into the flange at the bottom of the cell to place a Pt-100 at the bottom of the equilibrium cell in the first hole and to discharge the cell contents via a Swagelok valve using the second hole.

The agitation system in this equipment includes the Heidolph RZR 2041 overhead stirrer which rotates the shaft from the top of the cell, a small magnet located inside a SS 316L shaft, a four-blade stirrer and an external magnet made of neodymium to introduce the magnetic field.
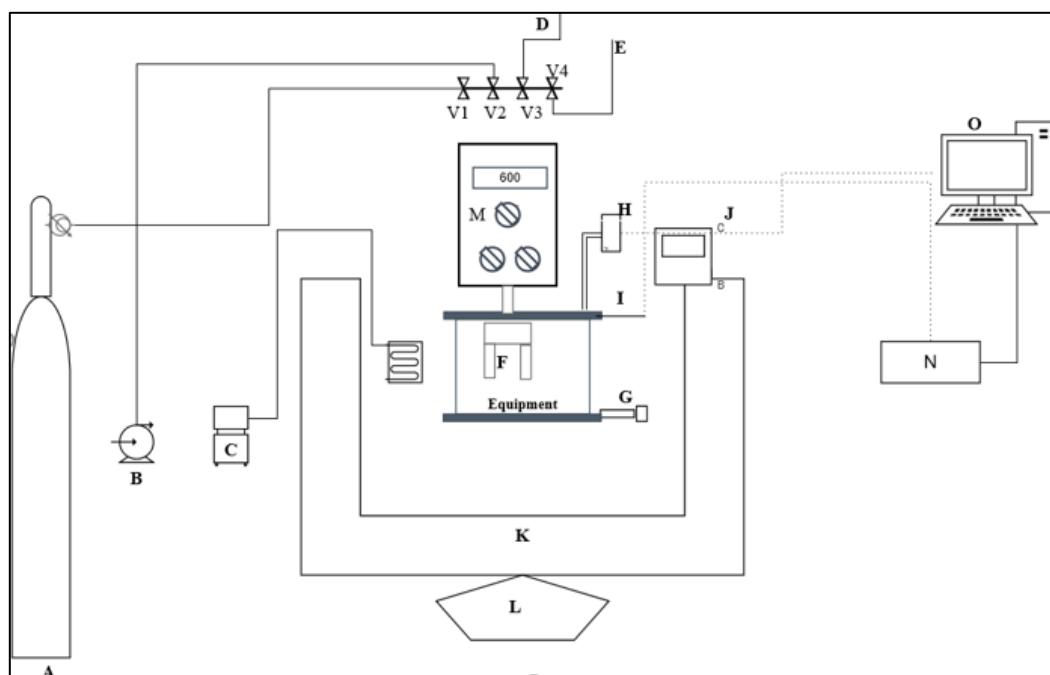
Figure 5-1. Schematic diagram of equipment which used in this study, the equipment layout, there is way below: A, CO_2 gas; B, Vacuum Pump; C, Chiller; D, Feed line; E, Vent line; F, Reactor; G, Vent line; H, Pressure Transducer; I, Pt.100 Prop; J, Programmable Temperature; K, Temperature Bath; L, Mechanical jack; M, Mechanical Stirrer; N, DAU (Data Acquisition Unit); O, PC.

5.2 New equipment (concentration studies)

In this project, a new hydrate cell was designed and commissioned in the Thermodynamics Research Unit (TRU). The new hydrate reactor was designed for the formation of hydrated crystals in sugar

solutions with an improved agitation system. Further, it was necessary to remove a sample of a concentrated solution for analysis. The new design includes a 750 ml SS 316L equilibrium cell with two polycarbonate viewing windows, an agitation system, liquid bath and frame, programmable temperature controller (Grant 200X), two Pt 100 temperature probes (accuracy of 0.05 K), a pressure sensor (WIKA; P-10, accuracy of 0.05 %), an overhead stirrer (Maxon motor), DAU (LXI Agilent 34972A), a chilling unit (Thermo Scientific EK20 Immersion Cooler), an electrical jack, and a vacuum pump (RV3 Edward). The new agitation setting was connected to a gearbox. An overview of the layout of the cell and picture are displayed in figures 5-2 and 5-3, respectively.
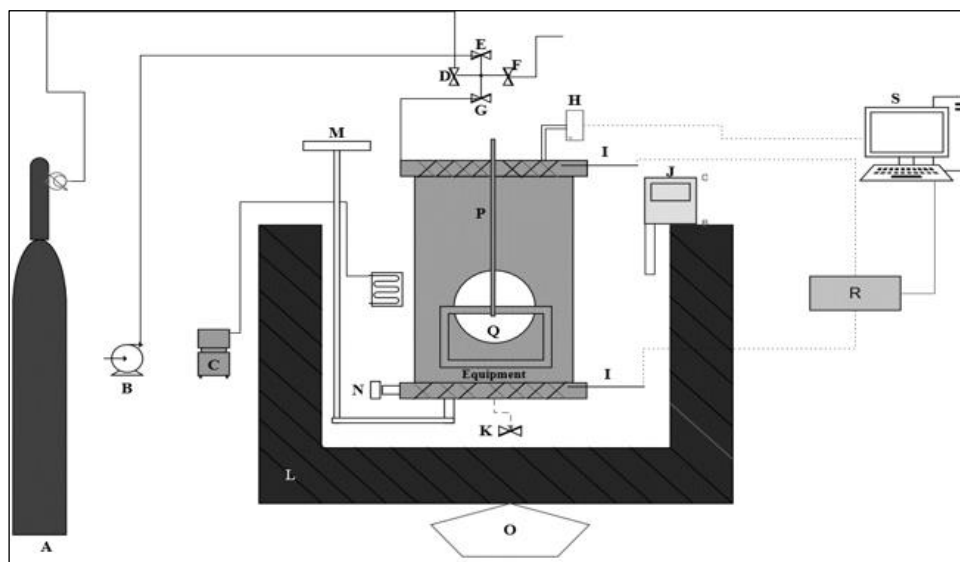
Figure 5-2. Schematic diagram of the equipment commissioned in this study, the equipment layout consists of A, CO_2 gas; B, Vacuum Pump; C, CO_2 valve; D, Filling valve; E, Vacuum Valve; F, Filling Valve; G, Inlet Valve; H, Pressure Transducer; I, Pt.100 probe; J, Programmable Temperature; K, Sampling Valve; L, Bath; M, Mixing shaft; N, Drain Valve; O, Automatic Jack, P. Agitator, Q. Housing for windows, R. DAU (Data Acquisition Unit), S. PC.
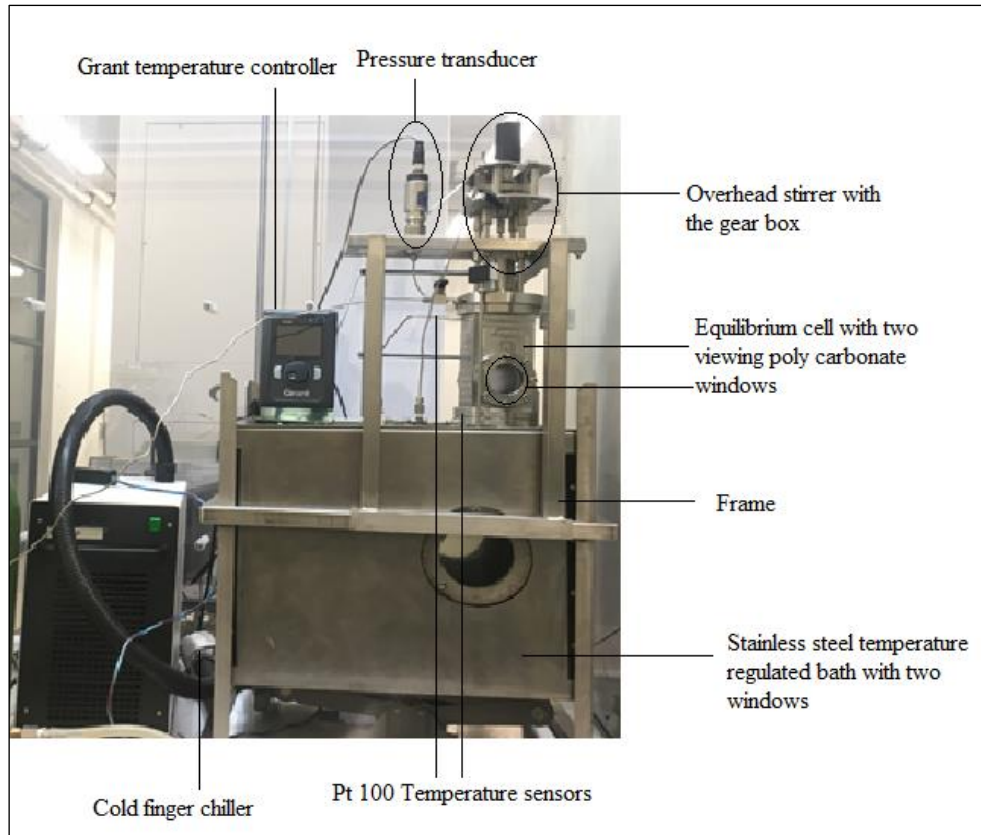
Figure 5-3. Photograph of the experimental apparatus.

5.2.1 Hydrate cell design

The unit comprises a 750 ml SS 316L vessel with two polycarbonate windows for viewing of the cell contents. A large volume is necessary to provide the ability to produce sufficient liquid for withdrawal after hydrate formation. This equipment includes a SS 316L bath with a window to view the contents and the hydrate formation inside the cell. The windows are polycarbonate disks with a diameter of 64.5 mm and thickness of 10 mm to withstand the higher operating pressures.

The internal diameter of the vessel is 75 mm, with an average thickness of 0.9 mm. Polyurethane O-rings helped with sealing between the windows and the cell body. Similarly, two SS 316L flanges provided the seal at the top and bottom. The position of the windows was not centred rather positioned towards the bottom of the cell to view the cell contents during hydrate measurements. The cell was housed in a thermo-regulated bath with two viewing windows. The bath dimensions are $43 \times 35 \times 26$ cm $\pm$ 1.9 cm and is also insulated using compressed foam made out of polystyrene. The bath is filled with the ethylene glycol solution diluted by water to $50 - 50$ volumetric fraction, which is capable of working in the range of -10 to 20 °C. An automated electrical jack is used to move the water bath up and down. The cell body is fixed to the SS 316L frame.

The pressure is measured using a transmitter which is connected to DAU. The pressure transmitter (WIKA; P-10; 8 MPa) is connected to the vessel using a 1/16" SS 316L line. Two temperature sensors (Pt100, class Aa) are also connected to the DAU. A programmable temperature controller (Grant 200X) is used for controlling the temperature inside the bath. The solution is filled to the cell through 1/8" SS 316L tube entering from the top flange of the cell. The fluid is drained using a series of arrangements of valves located in the bottom flange. All valves and fittings used are SS 316L (purchased from Swagelok) and rated for 175 bar, and 170 $^\circ$ C. Figure 5-4 shows the schematic diagram and partial picture of the experimental apparatus. Figure 5-5 shows a drawing of the cell for the top and windows flange.
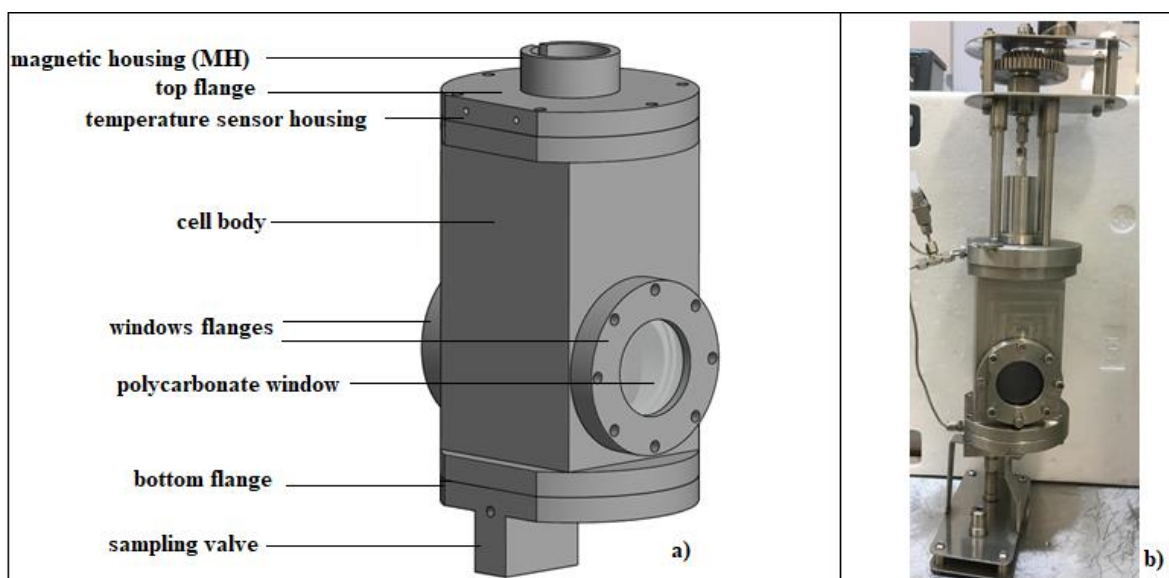
Figure 5-4. Schematic diagram of a) the equilibrium vessel with housing for the windows b) photograph of the cell body.
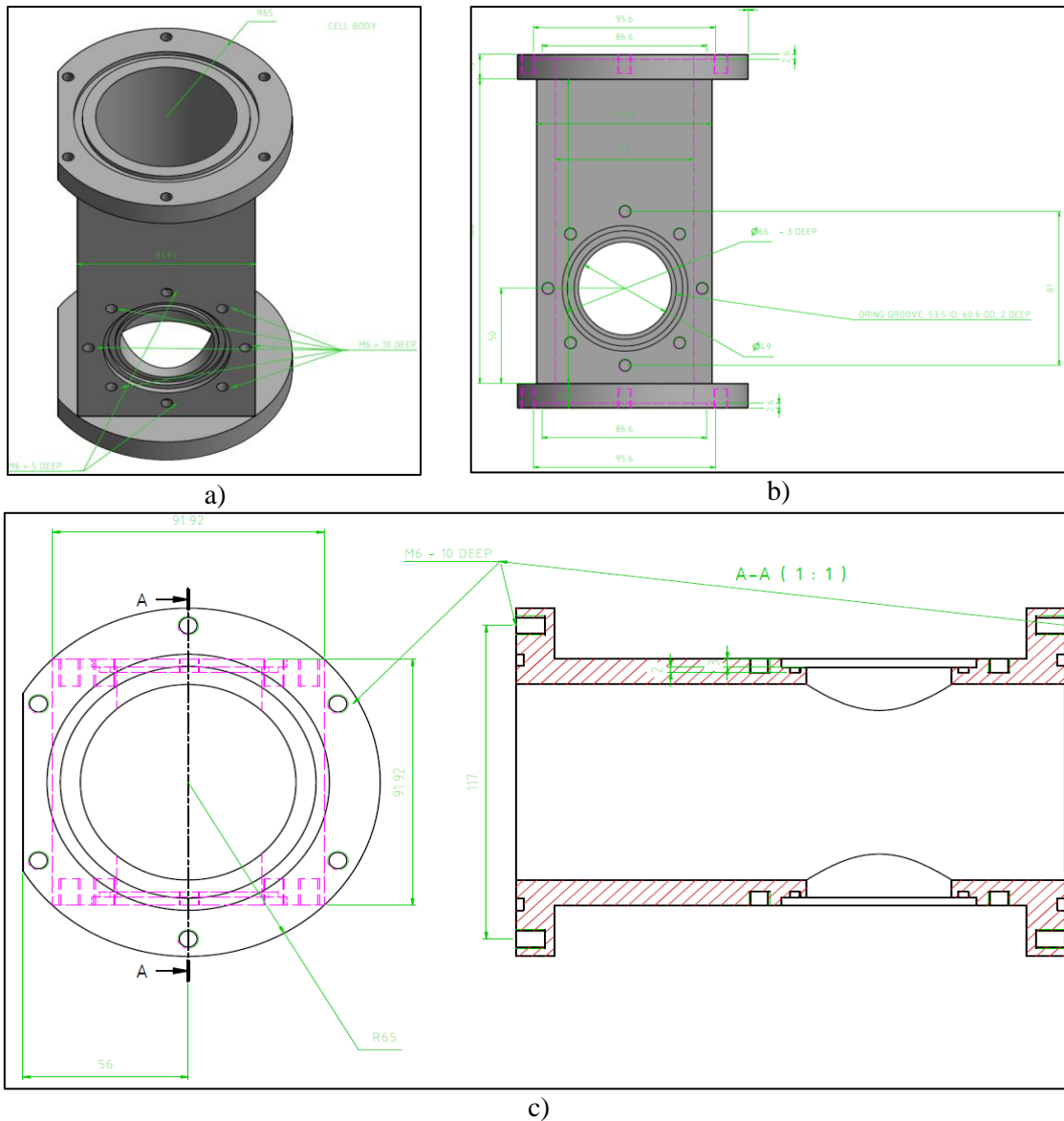
Figure 5-5. Drawing of the cell body: a) top flange and viewing windows flange, b) cell body front view, c) top flange with the grove and bolt locations
(3-D drawings drawn in Autodesk Inventor by Dr Nelson, 2017).

5.2.2 Agitation system

A Maxon motor is attached to the gearbox to aid stirring of the cell contents. The design of the gearbox and use of three different sized gears enables three speeds by 1, 1/2 and 1/3 of the motor speed providing the ability to mix in the speeds between (80-2000 rpm). Figure 5-6 shows the overhead stirring motor and the gears connected to the internal stirring rod with magnetic housing.
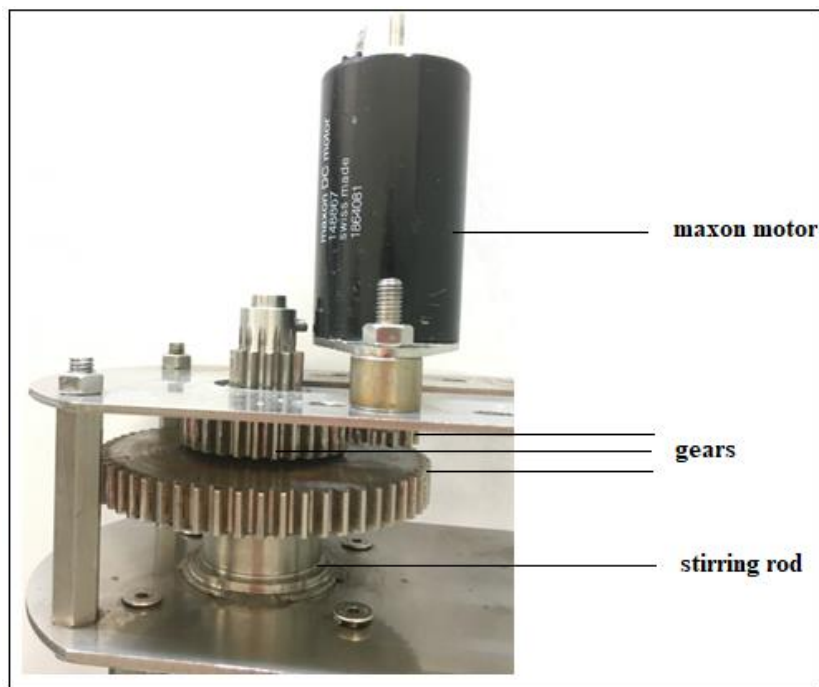
Figure 5-6. An overhead stirrer and designated three-speed gearbox.

The gears are connected to a stainless steel rod, which is attached to a stirring mechanism. The stirring mechanism consists of two arrangements of magnets with four strong Neodymium magnets outside the cell in the housing and four strong magnets inside the cell in the stirring mechanism to generate a powerful magnetic field. The outside arrangement is placed inside a stainless steel cover (housing) sealed with an O-ring to make sure there is no liquid from either condensation or liquid from the bath entering the housing. A ball bearing with the ID of 6 mm, OD of 19 mm and thickness of 6 mm is placed on the SS rod to decrease friction. Four magnets are placed inside the housing located on the top flange. There is a thrust bearing placed at the bottom of the stainless steel magnetic housing to improve the smoothness of the magnetic rotation.

The stirrer paddle is manufactured from SS 316L with a <1 mm gap between the stirrer paddle and inner wall of the cell to avoid crystal formation on the vessel walls. The bottom of the stirrer is perforated to allow the crystals to pass through the holes during mixing. With the new design of the mixing blade, the blade length was increased up to a very close point from the bottom flange to improve mixing in the liquid phase. Figure 5-7 shows a photograph of the stirring mechanism and stirring blade connected to the top flange inside the equilibrium cell.
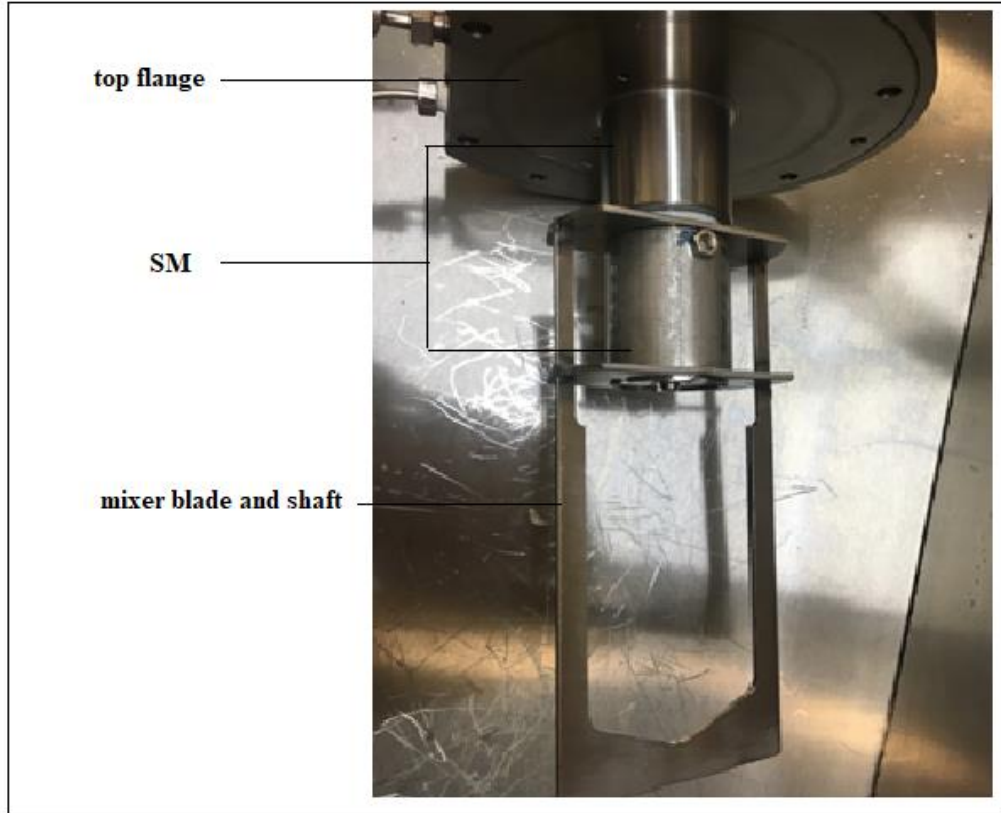
Figure 5-7. Photograph of the internal stirring mechanism.

5.2.3 Sampling withdrawal mechanism

In the bottom flange, a sintered mesh crimp is positioned to allow sampling of the concentrated solution. A valve stem is positioned to minimise the dead volume in these spaces. When the hydrate conditions are achieved (as known from phase equilibrium data and kinetic measurements), the valve is opened to allow the concentrated solution to pass through the mesh. Mesh sizes of 10, 20, 38 and 45 microns were tested to determine the appropriate sizes. These mesh screens were purchased locally from "Allied Mesh and Filters" and discs were cut from the mesh screens. The problem of being able to achieve a good separation between the crystals and the slurry were encountered by (Andersen and Thomsen, 2009). Hence, the withdrawal mechanism was adapted from (Purwanto et al., 2014) and modified. Initially, a small SS disc with four bolts was designed to hold the mesh in place. Due to space and displacement, this design was changed. The design of the bottom flange is shown in figure 5-8.
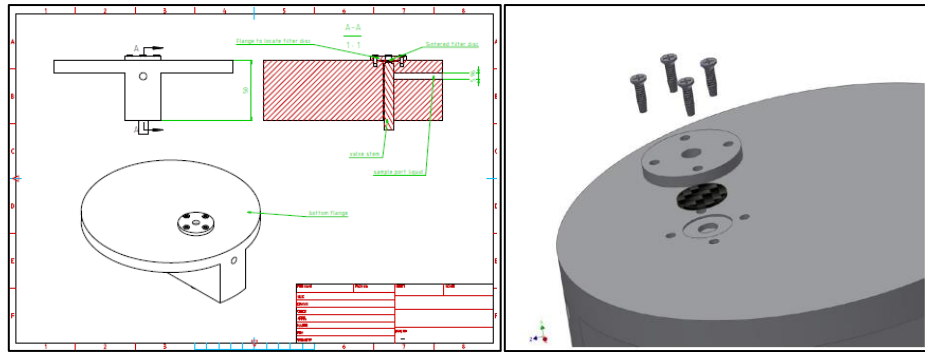
Figure 5-8. Initial drawings of the bottom flange and housing for the screen (3-D drawings drawn in Autodesk Inventor by Dr Nelson, 2017).

A crimp was designed and manufactured consisting of two delicate rings with a very small space (<10 μm) between them. This allowed the mesh to be held tightly. A groove is machined outside the crimp to screw it to the housing located in the bottom flange. Figure 5-9 shows the drawing of the bottom flange and housing for the screen. Figure 5-10 shows the manufactured crimp and the crimp placed in the housing inside the bottom flange.
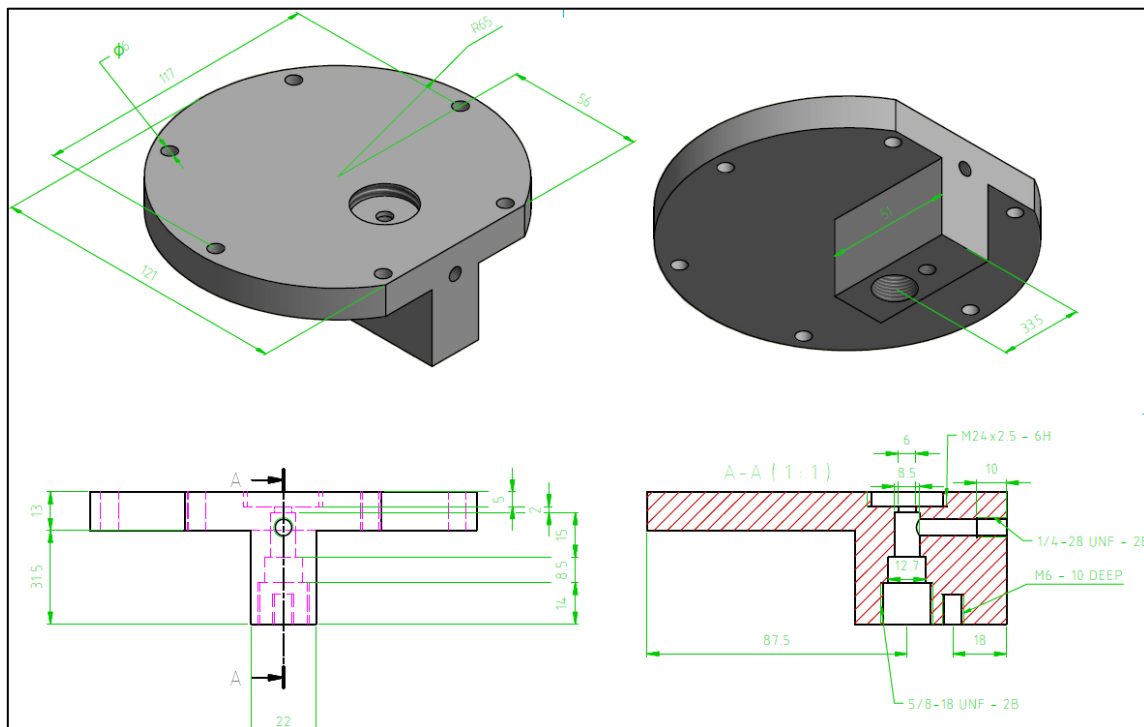
Figure 5-9. Drawing of the bottom flange and housing for the screen (3-D drawings drawn in Autodesk Inventor by Dr Nelson, 2017).
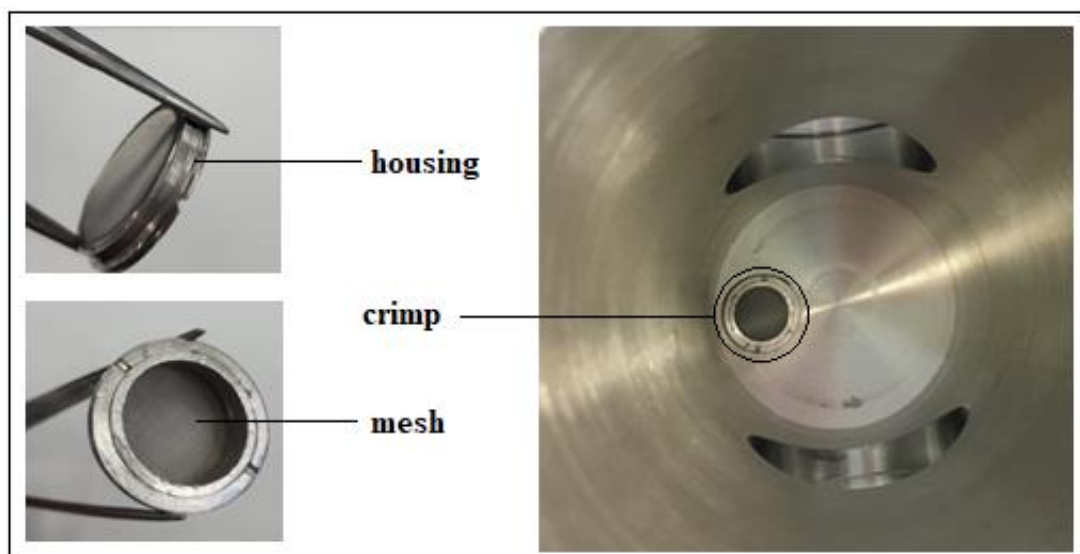
Figure 5-10. The sampling screen configuration [left]: manufactured crimp and mesh, [right]: the crimp screwed into the bottom flange.

With the revised design, it was not necessary to include filters in the withdrawal lines (as performed by (Purwanto et al., 2014)). Therefore, by opening the bottom valve, the fluid passed through the space within the discharge line. Initially, it was attempted to use a small Hamilton syringe connected via 1/4" tubing to the outlet into which the sample would fill, once the valve was opened. However, with the withdrawal of the sample at higher pressures this was not successful.

With the improved design, the needle valve (Swagelok sampling valve) on the discharge line was extended to the outside of the bath such that the valve stem could be opened. The feature of this extension is to open the bottom flange valve from the top side while the cell is submerged to the thermo-regulated bath. This configuration allows withdrawing a sample without interfering the equilibrium condition (i.e. raising the cell out of the bath). A 1/8" line was added to the needle valve using a reducer (1/4" to 1/8") and extended to the top flange for the ease of sampling. The far end of the line was connected to an SS 316L Swagelok valve rated for 175 bar and 170 °C.

5.3 Preparation of the equilibrium cell for measurements

Before starting the measurements, the equilibrium cell and all connection lines should be cleaned and washed with distilled water (deionised directly from Q5 Ultrapure (MilliporeTM)) so that the effect of any contamination on the measurement is eliminated. Then, using high-pressure nitrogen, the water inside the cell was drained via the discharge valve. The cell and connecting lines were then evacuated to 0.00039 MPa for 30 minutes to remove air and any volatile compounds in the cell using the vacuum

pump. Leak test, pressure transducer calibration, temperature probe calibration and sample preparation are part of the preparation procedure.

5.3.1 Leak test

The leak test was performed after connecting all the lines and connections in the setup. The equilibrium cell was filled with nitrogen to 4.00 MPa to perform the leak test. The temperature was then maintained at 40 ^{o} C to eliminate the effect of temperature fluctuations. The leak rate was determined over 24 hours. A leak detection fluid (Snoop®) was used on all connections and fittings. A leak is determined by the presence of bubbles around the joints as a result of the exiting gas from the point of attachment. Another test was performed to detect any leakage in the system in which the equilibrium cell was evacuated for 15 minutes at 0.00039 MPa. After that, the pressure is recorded, and an increase in cell pressure indicates a potential leak in the system. With the newly designed equilibrium cell, another leakage testing method involved submerging the cell into a clear bath of water while pressurised to detect any small bubbles released through the fittings.

5.3.2 Pressure calibration

The standard pressure calibration device CPH 6000 (from WIKA) was used to calibrate the transducer. During the calibration of the pressure transmitter, the temperature of the equilibrium cell was maintained at 298.15 K. The pressure calibration was carried out at a pressure range of 0.35 to 7.00 MPa. For this purpose, the nitrogen was loaded into the cell and left for calibration. After pressure stabilisation, pressure reading was recorded from the pressure transducer and the standard pressure gauge. For each point, data was collected for three minutes and then averaged. The same procedure was repeated for every pressure. The pressure reading was recorded and a first-order polynomial was regressed to the pressure recordings. The relationship between the standard device reading and the pressure transmitter (WIKA; P-10) is presented in figure 5-11. The standard deviation of the standard pressure is shown in figure 5-12. The maximum deviation of the pressure from the standard pressure is 1.0 kPa. The pressure calibrations were checked after a period to verify that the readings were unaltered.
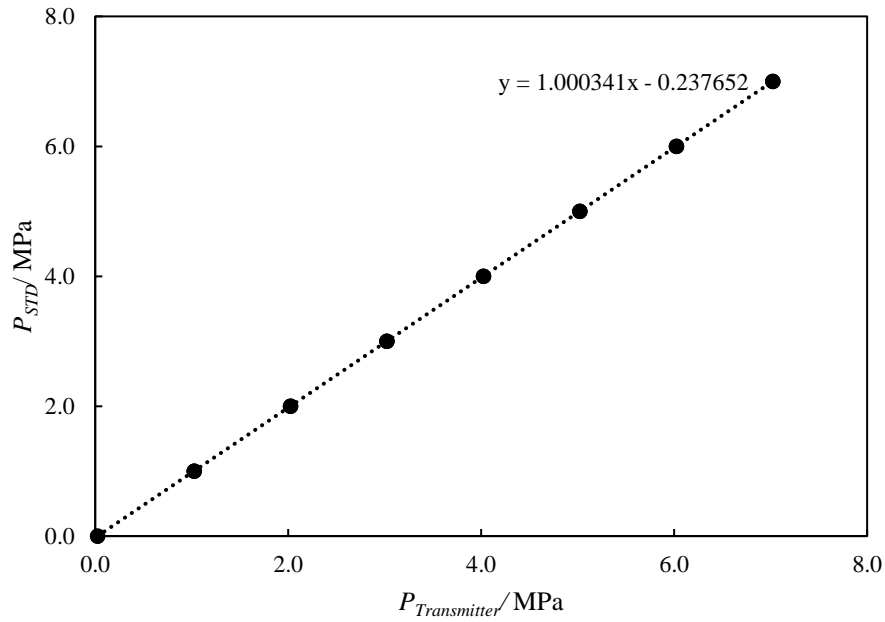
Figure 5-11. Calibration of the pressure transducer (0.00 -7.00 MPa).
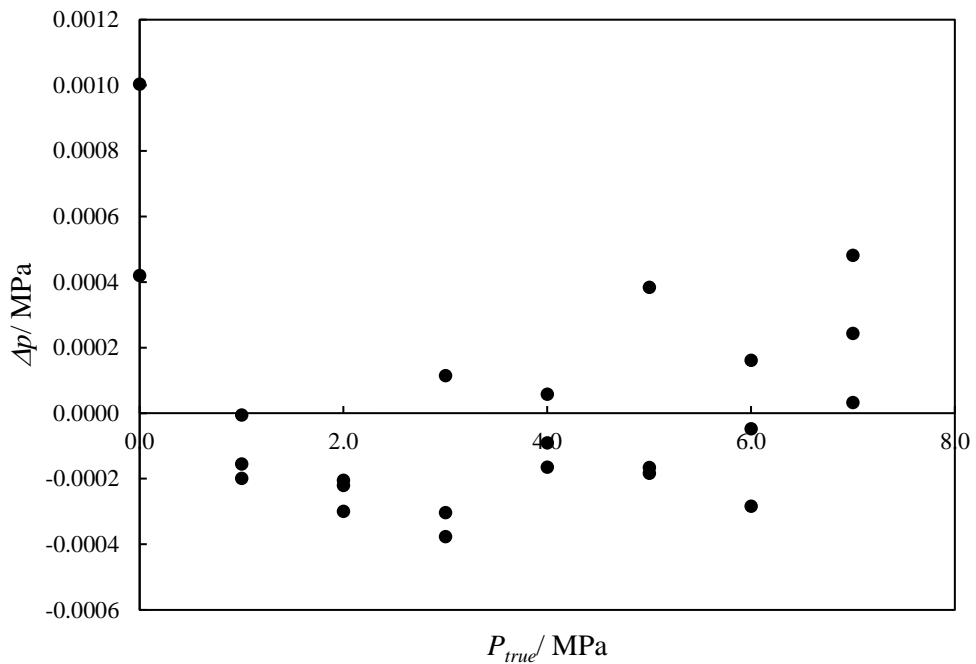
Figure 5-12. Deviation from standard pressure.

5.3.3 Temperature calibration

The precision of the standard temperature calibration unit (WIKA 2018; personal communication) is 0.03 K for the temperature range of 73.15 to 473.15 K. During the calibration of the temperature sensors, the temperature reading from the probe and the standard probes were recorded

49

simultaneously. The temperature calibration was carried out in the range of (263.15 to 298.15) K. For each point, the temperature was read for 3 minutes and then averaged. A first-order polynomial was fitted to the points measured, as shown in figure 5-13. The deviation from the standard temperature reading is plotted in Figure 5-14. The maximum temperature deviation from the standard probe is 0.018 K. The temperature calibrations were checked after a period to verify that the readings were unaltered.
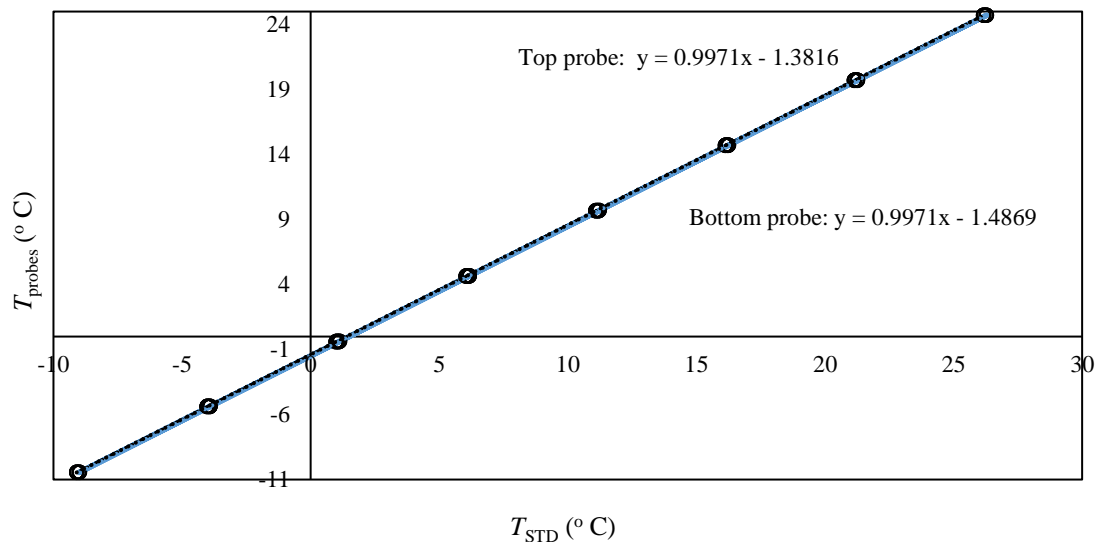
Figure 5-13. Calibration of the Pt-100 probes used in this study, -- probe 1 (top), … probe 2 (bottom)
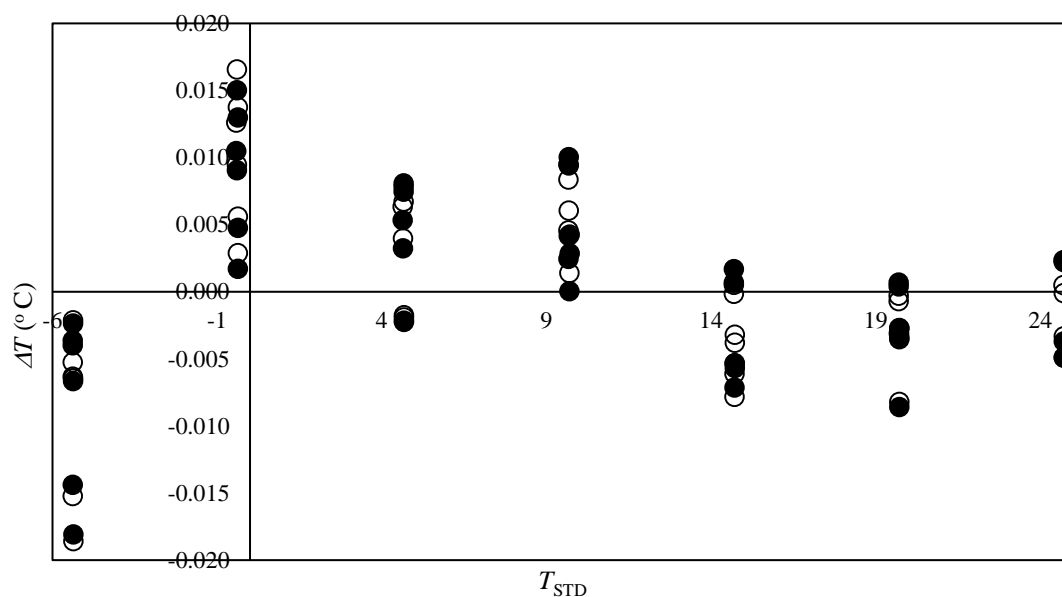
Figure 5-14. Deviation from the standard temperature, ● probe 1 (top), ○ probe 2 (bottom).

5.3.4 Sample preparation

Samples and mixtures were prepared using an OHAUS AV 114 digital scale. The scale has a full uncertainty of $\pm\,0.01$ g. First, the mass of the empty beaker was weighed. Then, the substance (several sugars) mass was measured. The required amount of water was then added slowly with a syringe until the substance was completely dissolved in aqueous solution.

5.4 Operating procedure for the isochoric pressure cell

5.4.1 Start-up procedure – Loading of equilibrium cell

Once the cell was cleaned the vacuum pump was used to evacuate the cell to 0.0002 MPa for $\pm\,5$ minutes. The inlet valve was closed. The solution was then introduced into the cell. CO_2 gas was filled to set pressure.

5.4.2 Thermodynamic hydrate measurements

The thermodynamic measurements were performed on the apparatus with the 64 ml equilibrium cell. Once the gas was filled to the desired pressure and temperature stabilised, the mixer was turned on and set to the optimum mixing speed depending on the solution concentration. When the gas was completely dissolved into the solution, and the pressure of the system was stabilised, the temperature controller was programmed to 10 degrees below the hydrate dissociation temperature. For the measurements, the temperature slowly was dropped at 1 $K.h^{-1}$ to make sure that the hydrate was formed with good separation.

This method is known as a cooling curve. There are two distinct slopes in the cooling curve. A small pressure drop characterises the first slope. This pressure drop indicates the occurrence of the nucleation process so that pressure change is mainly a function of temperature change. In the event of a severe drop in pressure, the temperature will decrease further. The hydrate formation and dissociation processes are shown in figure 5-15.
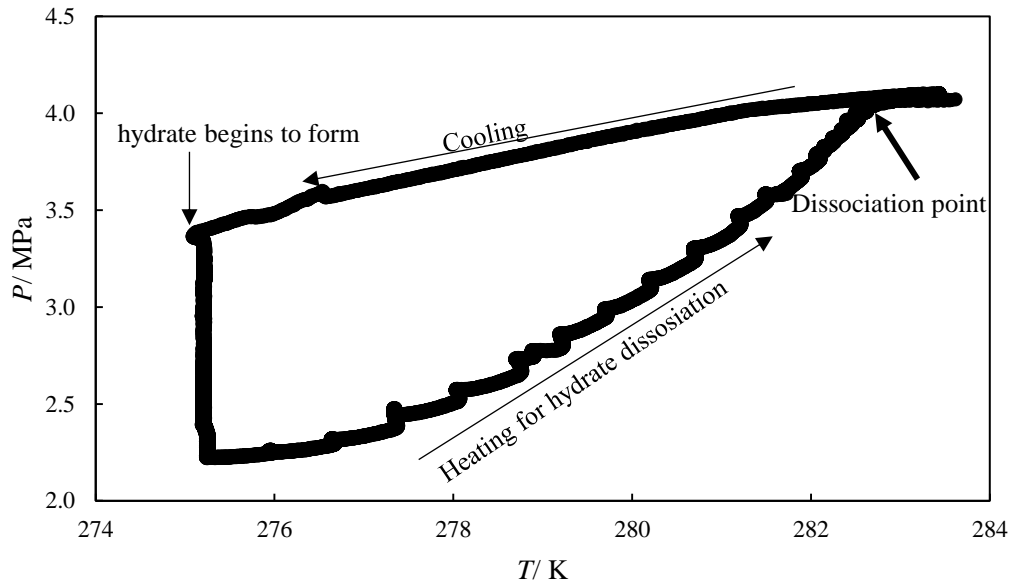
Figure 5-15. Primary cooling and heating curves for hydrate formation and dissociation in the isochoric method for CO_2+ 20 °Brix sucrose solution (this study).

After the hydrate was formed, the temperature was increased gradually. Initially, large increments (1 K) were set, however as the system approached the dissolution point 0.1 K increments were set. At any temperature increment, the system was kept for 1-1.5 hours to reach the equilibrium. The point at which the heating curve intersects the cooling curve is known as the hydrate dissociation point.

5.4.3 Kinetic measurements

The kinetic measurements were performed using the 750 ml reactor. Prior to measurements, the cell was washed with either distilled water or deionised water. Then, the cell was evacuated for about 30 minutes using a vacuum pump. Thereafter, approximately 160 ml of solution was introduced into the cell using a valve at the top of the cell. The evacuation was repeated for a short time (about 1 minute) to remove any introduced air. Afterwards, the cell is placed in the thermo-regulated bath to obtain the thermal equilibrium. After the temperature of the cell was stabilised, the gas was slowly transmitted to the cell to a pressure within the hydrate stability zone. After pressurising the cell, and the mixer was started at 200 rpm for the kinetic measurements with CO_2. Due to the formation of hydrate inside the cell by encapsulation of the former molecules, the pressure is reduced. After the kinetic data was measured, the DAU was changed to manual mode and shut down, and the stirrer was switched off. The drain valve opened to discharge the contents of the cell.

5.5 Sampling procedure

The sampling procedure follows the same method as in the kinetic measurements until the hydrate formation. Thereafter the sampling valve was opened slowly. Closing and opening of the valve should be performed meticulously and carefully to avoid damaging the valve stem tip. The sample was withdrawn into a 10 ml plastic syringe (conventional) whilst the plunger was pulled out. It was important to open the valve slowly to avoid a quick pressure build-up which would have caused the plunger in the syringe to blow off, resulting in spillage of the sample. For every test, three samples were taken after 15 minutes intervals to assess the reproducibility of the solution concentrations results. The samples were analysed using the refractive index (Anton Paar; DMA 5000; expanded uncertainty of 0.001 g/ml) and pH meter (Thermo Scientific, Orion 3 star, expanded uncertainty of 0.03).

Approximately 1-2 ml of sample solution was withdrawn. The mesh size should not exceed 26 microns to eliminate introducing the crystals into the withdrawn sample. However, the use of a mesh is to make sure that the large nuclides of hydrate are not removed along with the sample. There are crystals smaller than 26 μm which can potentially affect the solution concentration.

For the mesh size larger than 26 microns the final concentration was highly affected with time, but for the smaller mesh size, the concentration was the same ($\pm$ 0.01 ºBrix). With the smaller mesh screens, there is a slight possibility of the presence of hydrate crystals, but the volume of the crystals is very small to affect the final concentration. To avoid this (formation of small crystal sizes) a slow cooling rate also good stirring rate aids in large crystal formation which was observed visually. It was important to perform this measurement well with good stirring rate, cooling rate, and mesh size. Experiments were repeated to obtain accurate results.

5.6 NIST uncertainty analysis

The result of a measured variable is only complete when accompanied by a statement of its uncertainty (Taylor and Kuyatt, 1994). Measurement uncertainty is described with an interval around a set of measured data so that if a data point is repeated, the result must be declared within the interval.

5.6.1 Uncertainty estimation

It is very important to report all possible sources of uncertainty before providing the main measurement data. When there is more than one source of uncertainty, overall uncertainty is

combined as standard uncertainty. In this report, uncertainty was transmitted per the NIST guidelines for uncertainty reporting.

$$u_c(x) = \pm \sqrt{\sum_i u_i(x)^2}$$

<div align="right">5.1</div>

Type A uncertainty for the temperature and pressure caused by reading multiple transducers for a stable system, while type B uncertainty is the polynomial to calibration as well as the specifications of each manufacturer. Therefore, the combined standard uncertainty for a particular variable x, which may be temperature or pressure, is shown by the equation:

$$u_c(x) = \pm \sqrt{u_{instrument}(x)^2 + u_{calibration}(x)^2 + u_{repeatability}(x)^2}$$

<div align="right">5.2</div>

The upper and lower uncertainty limitation of temperature calibration was defined from first-order polynomials. From these constraints, there is a possible rectangular distribution in which there is a 100% probability of uncertainty of calibration over time. The rectangular distribution is given by the following equations:

$$u_{calibration}(x) = \frac{b}{\sqrt{3}}$$

<div align="right">5.3</div>

$$u_{instrument}(x) = \frac{b}{\sqrt{3}}$$

<div align="right">5.4</div>

Which

$$b = \left(\frac{a_+ \pm a_-}{2}\right)$$

<div align="right">5.5</div>

During the experiment, the probable temperature fluctuations were due to inadequate fluid circulation in the bath and the heat loss to the environment. Also, the fluctuations in temperature or pressure were due to the manufacturer's error. The repeatability uncertainty was determined as follows:

$$u_{repeatability}(x) = \left(\frac{1}{n(n-1)} \sum_{k=1}^{n} (x_{i,k} - \bar{x}_i)^2\right)^{0.5}$$

<div align="right">5.6</div>

Where

$$\bar{x}_i = \frac{1}{n} \sum_{k=1}^{n} x_{i,k}$$

5.7

5.6.2 Reporting uncertainty

Uncertainty may be recognised as a mixed standard uncertainty or covering factor. Covering factor plays an important role in demonstrating the confidence level of measurements with increasing uncertainty for $k > 1$. In this report $k = 2$ with a confidence level of 95 %.

$$U(x) = k u_c(x)$$

5.8

The reported uncertainties for the measured variables in this study are presented in Chapter 6.

Chapter 6: Results and Discussion

This chapter presents the experimental results of the hydrate phase equilibria for the test systems of sucrose and fructose solutions in the presence of carbon dioxide. The experimental test measurements were performed to confirm that the apparatus was suitable and to validate the experimental technique. Novel phase equilibrium data for the systems of sucrose and fructose solutions are presented together with appropriate thermodynamic modelling approaches.

The new equipment commissioned in this project was used to measure kinetic data and concentration measurements. New experimental kinetic results of the sucrose solution were generated. Concentration measurements on sucrose solutions and sugarcane juice were undertaken, and the results are presented. The first step of the hydrate experiments used a 12 °Brix feed solution and was carried out in stage-wise manner. The feed mixture for the proceeding hydrate experiment was the resulting value of the concentrated product from the previous experiment. Measurements continued until no hydrate was formed. The design and commissioning of the new experimental apparatus provided the ability of direct examination of the actual solution residue. Successful results have been achieved for the concentration of the sugar cane juice from 12 up to 60 °Brix. A comparison of the energy usage in the concentration of the sugar cane juice via current multi-effect evaporation as performed in factories, against the hydrate concentration results are presented. A discussion of the possible implementation of hydrate concentration to replace a multi-effect stage is also reported.

6.1 Materials

For the measurements in this study, sucrose ($C_{12}H_{22}O_{11}$, CAS no. 57-50-1, purity 99 wt.%) and fructose ($C_6H_{12}O_6$, CAS no. 57-48-7, purity 99 wt.%) were purchased from Sigma Aldrich. Carbon dioxide (CO_2, CAS no. 124-38-9, purity 99.9 wt.%) gas was used as the hydrate former gas. The deionised water with an electrical resistivity of 18 MΩ·cm was obtained from the laboratories and was produced by Direct-Q5 Ultrapure Water Systems (Millipore[TM]). The properties and specifications of the chemicals are listed in table 6-1. Solutions were prepared using an accurate balance (Ohaus Explorer; maximum and minimum capacity of 6100 and 0.01 g respectively, and an uncertainty of ±0.001 g).

Table 6-1. Specifications of the chemicals used in this study.

Compound	Formula	CAS number	Purity (wt.%)	Supplier
Carbon dioxide	CO_2	124-38-9	99.9	AFROX Ltd
Sucrose	$C_{12}H_{22}O_{11}$	57-50-1	99	SIGMA ALDRICH
Fructose	$C_6H_{12}O_6$	57-48-7	99	SIGMA ALDRICH
Water	H_2O	7732-18-5	99	Laboratory

6.2 Calibrations of pressure and temperature sensors

The calibration of pressure and temperature sensors (presented in Chapter 5) was done by comparing the experimental values against the values reported by the calibration standards. The expanded uncertainties (using a coverage factor of $k = 2$) on average for temperature and pressure are $U(T) = 0.1$ K and $U(P) = 0.01$ MPa, respectively. The estimates used for the calculation of uncertainties of the mass composition are provided in table 6-2.

Table 6-2. Standard uncertainty estimates and influences for the variables reported in this work.

Source of uncertainty	Estimate	Distribution
Mass balance uncertainty	0.003 g	Rectangular
V of injected liquid from the syringe	2.0 %	Rectangular
Liquid density of solutions	1.0 %	Rectangular
Repeatability (average of *max-min*) fructose and sucrose	0.04	Rectangular

A coverage factor of $k = 2$ was used to estimate the expanded uncertainty, giving a confidence level of 95 %. The expanded uncertainties for the mass fraction of the fructose and sucrose solutions are listed in table 6-3.

Table 6-3. The expanded uncertainty associated with the solution preparation of this work.

solution concentration (ºBrix)	U(x)
sucrose	
1	0.006
20	0.008
30	0.011
35	0.012
40	0.013
fructose	
15	0.007
30	0.011

6.3 Test Systems

In this study, test data points were measured for the gas hydrate dissociation condition of {CO_2 + water}, {CO_2 + sucrose (20 and 30 ºBrix) + water} and {CO_2 + fructose (30 ºBrix) + water} systems to validate the experimental methods used and validation of the equipment presented in chapter five.

6.3.1 CO₂ + water system

For the test system of CO_2 + water, measured data were compared against literature data. Table 6-4 presents experimental data for test system of CO_2 + water, and figure 6-1 provides the graphical view of the measured data against the literature. There is a good comparison of the data measured in this study against the reported data in the literature and the measured results confirm the calibrations of the sensors in the equipment.

Table 6-4. Experimental hydrate dissociation conditions for the test system of CO_2 +water.

Temperature (K)	Pressure (MPa)
276.6	1.80
277.5	1.98
280.0	2.77
280.2	2.88
280.6	3.04
281.9	3.60
282.6	3.92

U(P) = 0.01 MPa, U(T) = 0.1 K.
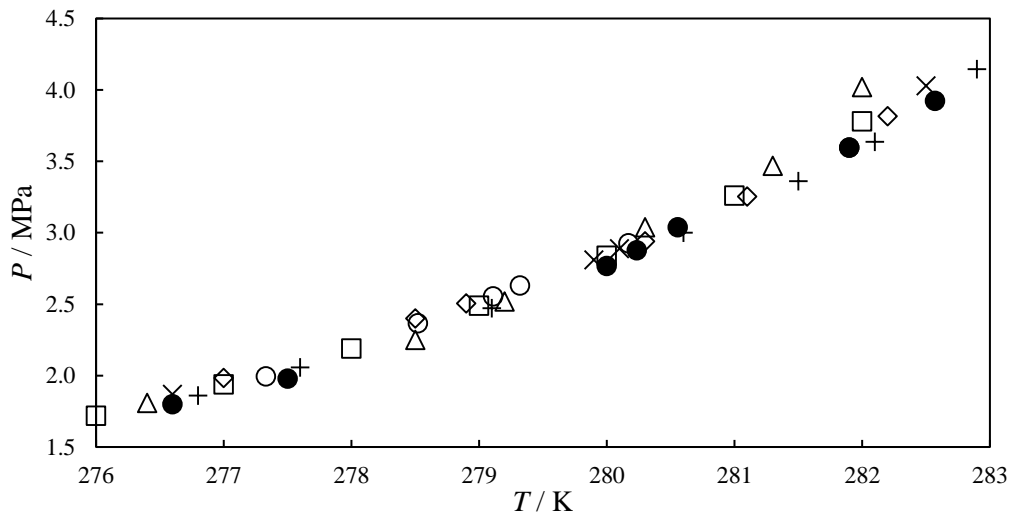
Figure 6-1. Experimental data for the CO_2 + water system. •, measured experimental data (this work); □, (Wendland et al., 1999); +, (Seo et al., 2001); Δ, (Fan and Guo, 1999); o, (Andersen and Thomsen, 2009); ×, (Maekawa, 2011); and ◊, (Smith et al., 2016).

6.3.2 CO₂ + sucrose + water system

For the test system of {sucrose + water and CO_2}, hydrate dissociation conditions were measured at two different concentrations of sucrose, viz., 0.2 and 0.3 mass fraction. The dissociation conditions for CO_2 hydrates were measured in the temperature range of (275.3 to 280.6) K and pressure ranging

from (1.94 to 4.01) MPa. The measured results are shown in figure 6-2. There is good agreement between the measured and literature data. The consistency between the measured and literature data confirms the experimental technique. The experimental data are listed in table 6-5.

Table 6-5. Experimental hydrate dissociation conditions for the test system of CO_2 + sucrose + water.

Composition of sucrose solution (ºBrix)	Temperature (K)	Pressure (MPa)
20	276.4	2.00
	279.5	3.10
	280.4	3.45
	281.4	4.10
30	275.3	1.94
	276.4	2.23
	277.1	2.37
	278.3	2.89
	279.2	3.24
	280.1	3.67
	280.6	4.01

U(P) = 0.01 MPa, U(T) = 0.1 K.
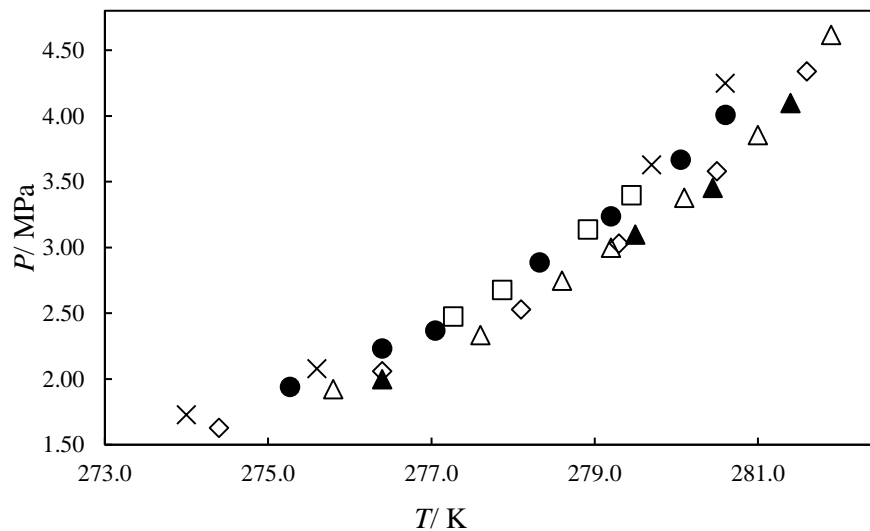
Figure 6-2. Experimental data for the CO_2 + sucrose + water system. ▲, measured experimental data in 20 ºBrix sucrose (this work); ◊, 20 ºBrix sucrose (Chun and Lee, 1999); Δ, 20 ºBrix sucrose (Smith et al., 2016); ●, measured experimental data in 30 ºBrix sucrose (this work); □, 30 ºBrix sucrose (Andersen and Thomsen, 2009) ; ×, 30 ºBrix sucrose (Chun and Lee, 1999).

6.3.3 CO₂ + fructose + water system

For the test system of fructose solutions (0.3 mass fraction fructose), the results did not show a good match with the literature data (Chun and Lee, 1999). To validate the data measured in this work, the points were repeated 2-3 times with two different experimental apparatus for each pressure and the results from successive measurements in this study overlapped. One can conclude that there seems to

be an error in the data reported in the literature (Chun and Lee, 1999), which could possibly be attributed to a mistake in the reported concentrations of the solutions or an error in experimental measurement. Experimental data for this system are listed in table 6-6 and presented in figure 6-3.

Table 6-6. Experimental hydrate dissociation conditions for the test system of CO_2 + fructose + water.

Composition of fructose solution (ºBrix)	Temperature (K)	Pressure (MPa)
30	274.3	1.93
	275.2	2.18
	275.8	2.30
	276.9	2.76
	277.8	3.09
	278.8	3.65
	278.9	3.69

U(P) = 0.01 MPa, U(T) = 0.1 K.
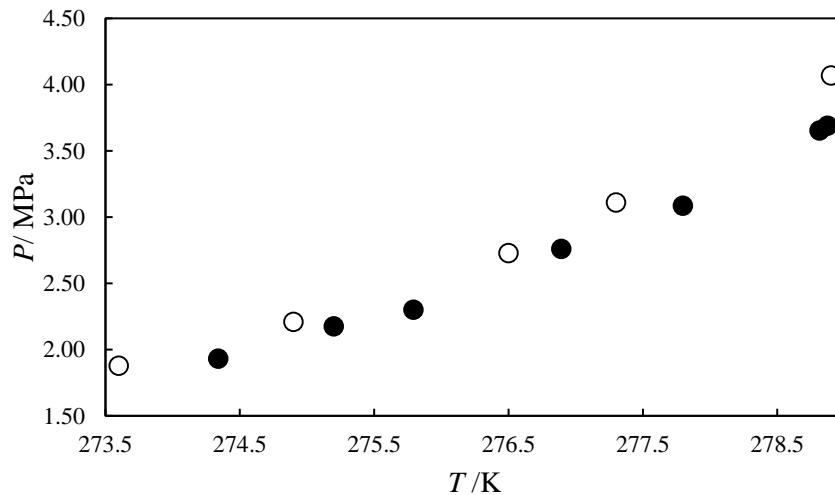
Figure 6-3. Experimental data for CO_2 + fructose (30 ºBrix) + water system. •, measured experimental data (this work); o, (Chun and Lee, 1999).

6.4 Modelling and data treatment

The description of the thermodynamic models used in correlating hydrate dissociation data was presented in chapter 3. Table 6-5 presents a list of thermodynamic modelling approaches. A combination of a Langmuir constant method (or Kihara potential function), an activity coefficient model in the liquid phase and a fugacity approach in the hydrate phase is required to couple with the solid solution theory of Van der Waals – Platteeuw to form a framework. To find the most appropriate data fit among the different available possibilities, 18 model variations were tested. The average absolute relative deviation (*AARD* (θ) %) was used to obtain the statistical analysis which was calculated as :

$$AARD(\bar{\theta})\% = 100 \times \frac{1}{N_p} \sum_{1}^{N_p} \frac{|\bar{\theta}_{exp} - \bar{\theta}_{calc}|}{\bar{\theta}_{exp}}$$

$\bar{\theta}$ represents the measured variable (pressure), subscripts *exp* and *calc* refer to the experimental and calculated values and N_p denotes the number of experimental data points. The model approaches used in this study is provided in table 6-7.

Table 6-7. A summary of the thermodynamic model approaches used in this study.

Gas-liquid interaction	Activity coefficient in the liquid phase	Fugacity in the hydrate phase
Kihara potential (K-P) (Kihara, 1953)	- UNIQUAC (Abrams and Prausnitz, 1975)	Chemical potential (C-P) (Mohammadi et al., 2005)
Parrish – Prausnitz (P-P) (Parrish and Prausnitz, 1972)	- UNIFAC (Fredenslund et al., 1975)	Empty hydrate (E-H) (Mohammadi and Richon, 2008)
Munck-Skjold-Rasmussen (M-S-R) (Munck et al., 1988)	- NRTL (Renon and Prausnitz, 1968)	

The K-P method calculated the Langmuir constant numerically by employing a model for considering the interaction between water and gas molecules inside the cavities which were explained in section 3.3.1. The P-P and M-S-R approaches are classified as empirical approaches for Langmuir constant calculation which were explained in detail in section 3.3.2. The UNIQUAC, UNIFAC, and NRTL activity coefficient models were utilised to calculate the activity coefficient in the liquid phase. The models were explained in section 3.3 of the theory chapter. With the UNIQUAC model, the energy interaction parameter of A_{ij} was optimised. With the NRTL activity coefficient model, three parameters of b_{ij}, b_{ji} and α were optimised for each system using the genetic algorithm (GA tools) following the predefined objective function using a MATLAB® code. The C-P and E-H methods were utilised to calculate the fugacity of water in the hydrate phase which was explained in section 3.2 in detail. The modelling flowchart is shown in figure 6-4. In the algorithm, the weight function of 10^{-5} was used.
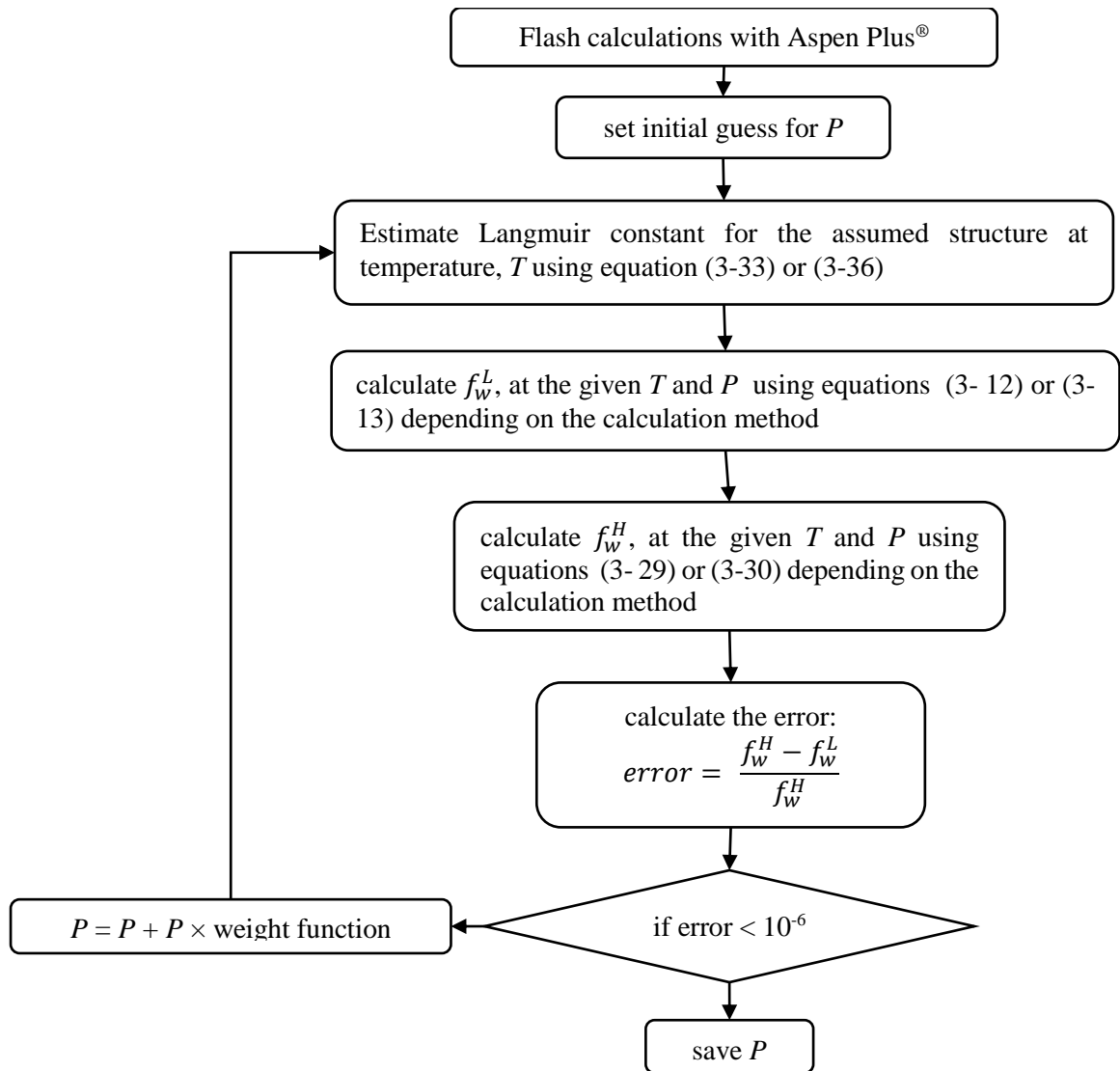
Figure 6-4. Flow chart of the algorithm used in the pressure calculation method.

Based on the model results of several model combination for each system, the most suitable correlation and model fit are presented. Some optimised parameters for UNIQUAC and NRTL are listed in Tables 6-8 and 6-9, respectively.

Table 6-8. Optimised binary energy interaction parameter, A_{ij}, for the UNIQUAC model.

A_{ij} (J/mol)	Water	Sucrose	Fructose	Glucose
Water	0	-130	64.5	-128.81
Sucrose	390	0	----	----
Fructose	47.5	----	0	----
Glucose	350.75	----	----	0

Table 6-9. Optimised binary parameters of the NRTL model for sugar–water systems.

	Sucrose-water	Glucose - water	Fructose-water
b_{12} (J/mol)	6710	3550	4300
b_{21} (J/mol)	7800	6600.99	6500
α	0.370	0.382	0.420

6.5 New systems

This section presents the novel hydrate phase equilibria data for sucrose solution at concentrations of 35 and 40 ºBrix, and fructose solution with the concentration of 15 ºBrix in the presence of carbon dioxide. The experimental data for the sucrose solution were measured at the temperatures and pressures between (275 - 280.5) K and (1.94 - 4.30) MPa, respectively. The experimental data of the fructose solution were measured at the temperatures and pressures between (276 - 281) K and (1.93 - 3.73) MPa, respectively.

6.5.1 CO_2 + sucrose + water system

A list of the systems studied along with the temperature and pressure ranges are presented in Table 6-10. New data were measured for CO_2 + sucrose (35 and 40 ºBrix) + water systems. Each system was modelled via all possible model combinations presented in section 6.4 by fitting parameters using a MATLAB® code. The model errors as determined in equation (6-1) assisted in determining the most suitable model fit. The tuned parameters were presented in chapter 3. Figures 6-5 shows the measured data in this study with the most suitable modelling result. Increasing the concentration of sucrose solutions shifts the dissociation pressure boundary to elevated values, indicating an inhibition effect, compared to the system of CO_2 + water. It was not possible to perform measurements with solutions greater than 40 ºBrix. For higher concentrations of sucrose, due to the viscous nature of the residue in the solid-liquid-vapour equilibrium (SLVE) condition, the rate of the mixer should increase (up to 2000 rpm), and it requires a powerful chiller for cooling. The activity coefficient model takes into account the deviations from ideal solutions due to the presence of an impurity in the liquid phase. In addition to the assumptions from pure CO_2 + water system, the excess Gibbs energy models were included in the modelling for the liquid phase activity coefficient.

Table 6-10. Experimental hydrate dissociation conditions for the system of CO_2 + sucrose + water.

Composition of sucrose solution (°Brix)	Temperature (K)	Pressure (MPa)
35	276.0	2.30
	277.3	2.70
	278.7	3.15
	279.7	3.74
	280.0	3.95
	280.0	3.98
	280.3	4.10
40	275.2	2.27
	276.2	2.60
	277.3	3.00
	278.3	3.54
	279.1	4.01

U(P) = 0.01 MPa, U(T) = 0.1 K.
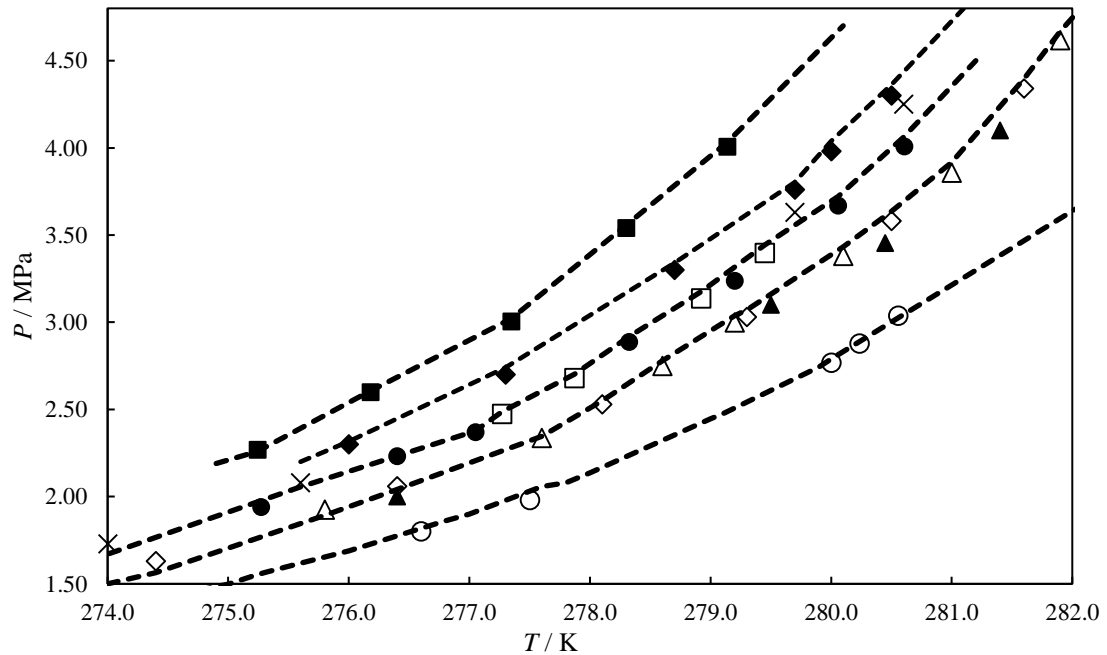
Figure 6-5. Experimental data and modelling results for the CO_2 + sucrose + water system. o, measured experimental data for water + CO_2 (this work); ▲, measured experimental data in 20 °Brix sucrose (this work) ; ◊, 20 °Brix sucrose (Chun and Lee, 1999); Δ, 20 °Brix sucrose (Smith et al., 2016); •, measured experimental data 30 °Brix sucrose (this work); □, 30 °Brix sucrose (Andersen and Thomsen, 2009); ×, 30 °Brix sucrose (Chun and Lee, 1999); ♦, measured experimental data in 35 °Brix sucrose (this work); ■, measured experimental data in 40 °Brix sucrose (this work) ,--- model.

6.5.2 CO_2 + fructose + water system

Some test and new data points were generated for the CO_2 + fructose + water system. Each system was modelled via all possible model combinations. The models show a good correlation of the experimental data. There is good consistency between the literature and measured data. Figure 6-6 shows measured data, literature data, and modelling of the CO_2 + fructose + water system. The tuned parameters were presented in chapter 3. The experimental data are presented in table 6-11.
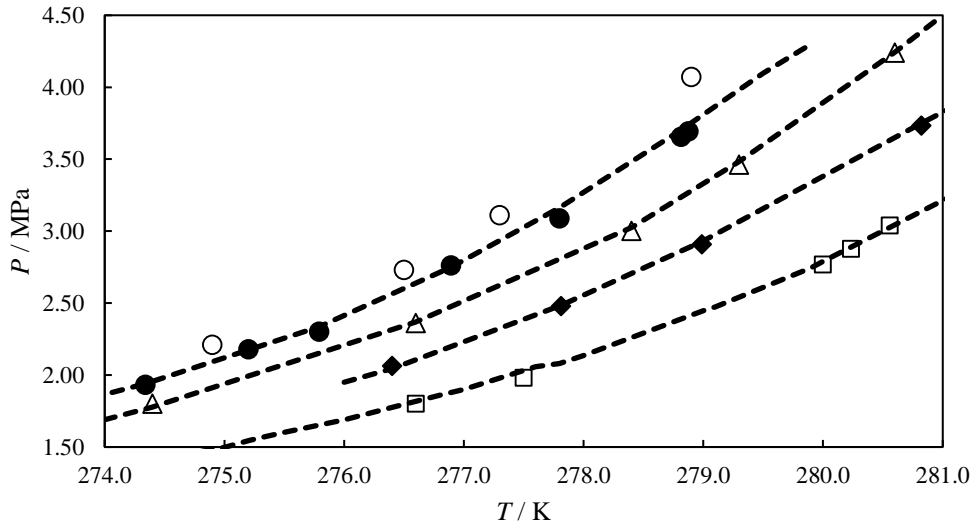
Figure 6-6. Experimental data and modelling results for the CO_2 + fructose + water system. □, measured experimental data for water + CO_2 (this work); ♦, measured experimental data in 15 ºBrix fructose (this work); Δ, 20 ºBrix fructose (Chun and Lee, 1999); ●, measured experimental data in 30 ºBrix fructose (this work); o, 30 ºBrix fructose (Chun and Lee, 1999) ,--- model.

Table 6-11. New experimental hydrate dissociation conditions for the CO_2 + fructose + water system.

Composition of fructose solution (ºBrix)	Temperature (K)	Pressure (MPa)
15	276.4	2.06
	277.8	2.48
	279.0	2.91
	280.8	3.73

U(P) = 0.01 MPa, U(T) = 0.1 K

6.5.3 Statistical analysis of the modelling approaches

The deviation of the experimental data from the calculated model was determined using equation (6.1). The model with the lowest *AARD* for the system at all concentrations is presented in table 6-12. The reader is referred to Appendix A for more information on the comparative modelling results.

Table 6-12. The models with the lowest *AARD* for the system at all concentrations.

System	Selected model	AARD (P) %
CO_2 + water	K-P + C-P	0.03
CO_2 + sucrose + water	M-S-R + NRTL + C-P	0.96
CO_2 + fructose + water	M-S-R + UNIFAC + C-P	0.75

The lowest *AARD* for the CO_2 + water system was obtained using the combination of K-P approach and C-P. The lowest *AARD* for the systems including sugar contents was obtained using the combination of M-S-R and C-P while for the sucrose system the NRTL activity coefficient model showed better representation of the experimental data while the UNIFAC group contribution model has the lowest error for the fructose system.

6.6 Kinetic result for hydrate formation of CO_2 + sucrose + water system

The kinetic studies involved determining the rate constant, rate, gas consumption and storage capacity of gas hydrate formation. The theory of crystallisation (Englezos et al., 1987) is based on calculating the difference between the fugacity of the gas species in the vapour phase and hydrate phase, which is the driving force for hydrate formation of gas hydrates, as explained in chapter 3. The effect of sucrose on hydrate formation rate constant, rate, storage capacity, and gas consumption were studied. The experimental measurements were performed in a 750 cm^3 high-pressure equilibrium cell. For the kinetic measurements, the effect of initial pressure and temperature on the induction time, the rate of formation of carbon dioxide hydrates, the apparent reaction velocity constant, storage capacity and the conversion of water-to-hydrate during the formation of gas hydrate were investigated. The kinetic experiments were performed at initial temperatures of (275.15, 275.65 and 276.15) K and initial pressures of (2.70, 2.90, 3.00 and 3.10) MPa. The kinetic results for the CO_2 + water system in terms of the parameters as mentioned earlier are presented in Appendix A. The equations and method used in determining these parameters were presented in section 3.5. The sections below report the results for the CO_2 + sucrose + water systems.

6.6.1 Induction time and effect of initial temperature and initial pressure

Experimental measurements were carried out at a constant temperature of 275.65 K and an initial pressure of 2.70, 2.90 and 3.10 MPa, to investigate the effect of primary pressure on hydrate formation for the CO_2 + sucrose + water system. Figure 6-7 shows a schematic diagram of the driving force for hydrate formation. The larger arrow length indicates the larger associated driving force. The higher the pressure difference, the greater the driving force at a set temperature.
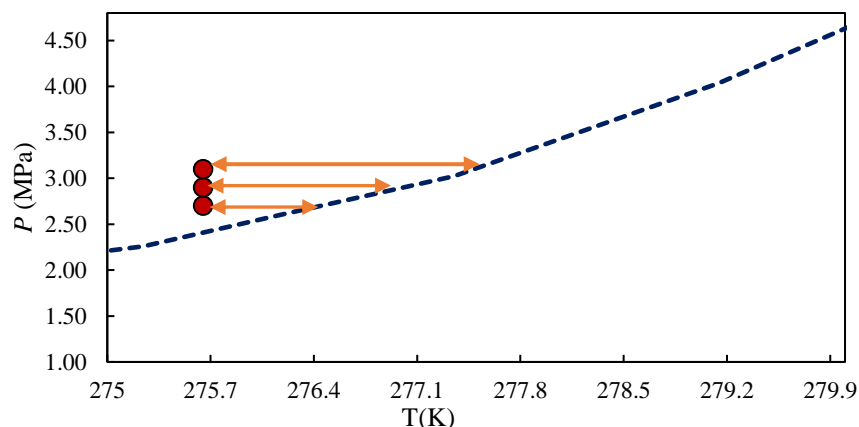
Figure 6-7. The driving force for the CO_2+ 40 ºBrix sucrose + water between the initial pressure conditions (●) and CO_2 hydrate equilibrium line (solid line) at a constant temperature of 275.65 K.

Tables 6-13 and 6-14 show that the initial temperatures, initial pressures and induction time. All measurements were repeated twice to ensure that the reported results were reproducible and accurate. The average of the measured times is reported in the table at the given pressure.

Table 6-13. Induction time (t_{in}) for CO_2 + sucrose + water system at constant temperature (275.65 K) and different pressures (2.70, 2.90 and 3.10 MPa).

CO_2 + ºBrix sucrose solution	P (MPa)	$t_{in\,average}$ (min)
	2.70	
12		18.21
20		18.36
30		22.19
35		24.25
	2.90	
12		14.22
20		15.34
30		19.45
35		20.49
	3.10	
12		12.43
20		14.15
30		14.47
35		16.57

U(P) = 0.01 MPa, U(T) = 0.1 K.

Table 6-14. Induction time (t_{in}) for the CO_2 + sucrose + water system at constant pressure (3.00 MPa) and different temperatures (275.15, 276.15 K).

CO_2 + °Brix sucrose solution	T (K)	$t_{in \, average}$ (min)
	275.15	
12		11.19
20		12.54
30		14.14
35		14.54
	276.15	
12		12.36
20		13.88
30		14.44
35		16.55

U(P) = 0.01 MPa, U(T) = 0.1 K.

The results in the tables above, show an increase in the induction time, as the temperature and sucrose mass fraction increases. This increase is in accordance with the expected trends from the thermodynamic point of view as it is an inhibitor hence, adding more sucrose to the mixture increases the inhibition effect. This shifts the hydrate phase boundary to higher pressures compared to the system with pure water. Furthermore, the results showed that sucrose is a kinetic inhibitor.

Figure 6-8 shows the variations of pressure during the formation of CO_2 + 12 °Brix sucrose+ water at an initial temperature of 275.65 K and with different initial pressures of 2.70, 2.90 and 3.10 MPa. As mentioned in chapter 3, during the formation of hydrates, three regions can be determined: 1) dissolution stage, 2) induction period, and 3) growth stage. In the first step, some CO_2 gas in the vapour phase is dissolved in the sucrose solution. During the second period or induction period, hydrated crystals form a cluster and decompose until a nucleus is created and grow to a recognisable size.

During crystal growth, CO_2 molecules are trapped inside the hydrated cavities, and the system pressure is significantly reduced to reach a constant value. As shown in Figure 6-8 and Table 6-13, the induction time for the formation of clathrate hydrates for the CO_2 + 12 °Brix sucrose + water system at a constant temperature of 275.65 K and an initial pressure of 2.70, 2.90 and 3.10 MPa is 18, 14 and 12 minutes, respectively. To design a hydrated economic process, initial temperature and pressure conditions with short induction times are considered. As shown in Figure 6-8, when the pressure is increased from 2.70 MPa to 3.10 MPa, the induction time decreases. The minimum induction time between these three conditions corresponds to the initial pressure and the temperature of 3.10 MPa and 275.65 K, respectively.
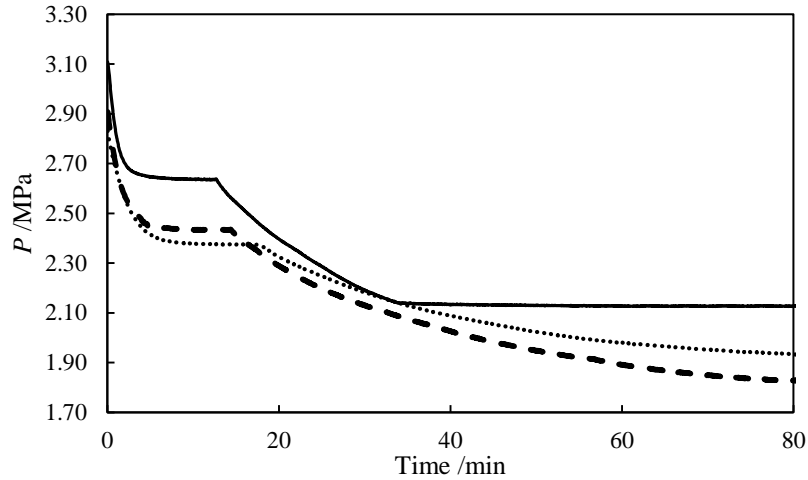
Figure 6-8. Hydrate kinetic measurements of the CO_2 + sucrose (12 ^{o}Brix) + water system at the temperature of 275.65 K and different pressures of: …2.70, --- 2.90, and $-$3.10 MPa.

Figure 6-9 shows the effect of the initial temperature on clathrate hydrates for the CO_2 + 0.12 mass fraction sucrose + water system, at a constant pressure of 3.00 MPa and at varying initial temperatures of 275.15 K and 276.15 K. As shown in figure 6-9, as the temperature increases from 275.15 K to 276.15 K, the duration of induction increases. As showed in table 6-12, the induction time for 275.15 K and 276.15 K were 11 and 12 minutes, respectively.
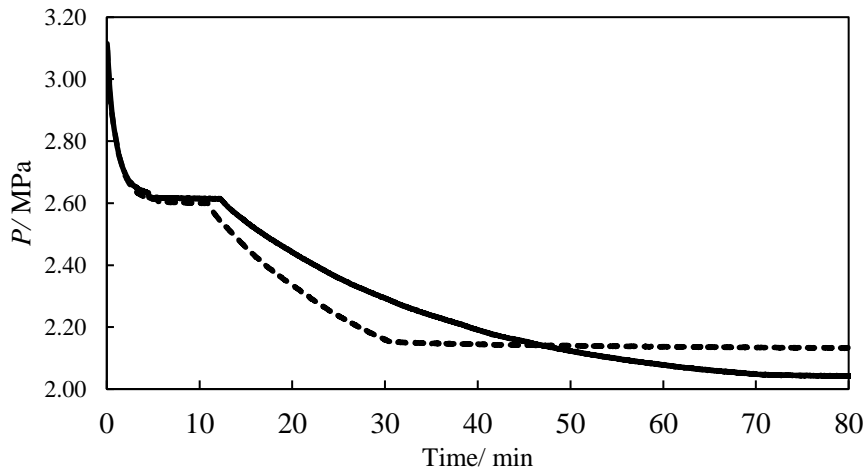
Figure 6-9. Hydrate kinetic measurements of the CO_2 + sucrose (12 ^{o}Brix) + water system at a constant pressure of 3.00 MPa and temperatures of: --- 275.15 and — 276.15 K.

Figure 6-10 presents the kinetics of hydrate formation using a pressure vs time axes. On the results of induction time at a constant temperature of 275.65 K and different pressures 2.70, 2.90 and 3.10 MPa, the higher the pressure, the lower the induction time. The results also show that as the concentration of the sucrose content increases the induction time increases. While at the constant

pressure of 3.00 MPa and different temperatures of 275.15 and 276.15 K, it can be concluded that the higher temperature has a higher induction time.

(a)

(b)

(c)

(d)

(e)

(f)

Figure 6-10. Induction time for the CO_2 + sucrose + water system. a, c and e: for different concentrations of sucrose solution (20, 30, and 35 °Brix) respectively, at a constant temperature of 275.65 K and pressures (…2.70, --- 2.90 and −3.10 MPa). b, d and f: for different concentrations of sucrose solution (20, 30, and 35 °Brix) respectively, at pressure of 3.00 MPa and temperatures (…275.15 and −276.15 K).

6.6.2 Gas consumption for CO_2 + sucrose + water system

Figures 6-11 and 6-12 show the gas consumption for CO_2 + 12 °Brix sucrose + water. By increasing the initial pressure, the CO_2 consumed increases significantly. As shown in figure 6-11 the CO_2 consumption increases by 5 mmole/mole with an increase of 0.40 MPa in initial pressure. As shown in figure 6-12 the amount of CO_2 consumed decreases to 2.34 mmole/mole by increasing the initial temperature by 1 K.
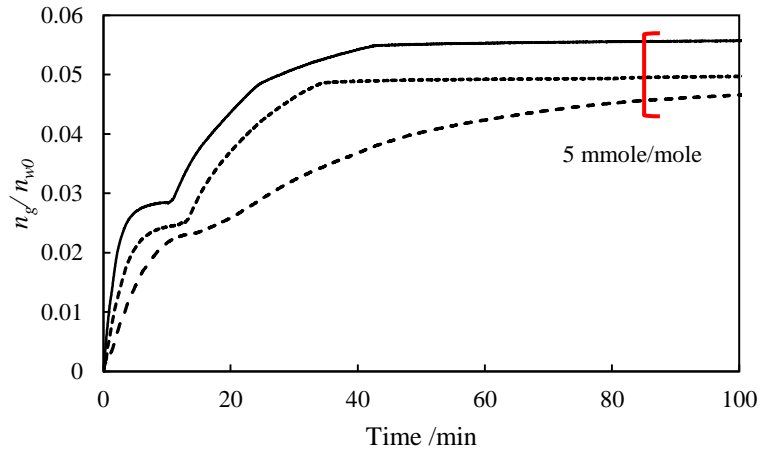
Figure 6-11. Gas consumption of CO_2 for hydrate formation of the CO_2 + sucrose (12 °Brix) + water system at constant temperature of 275.65 K and different pressures of: …2.70, --- 2.90, and −3.10 MPa.

Figure 6-12. Gas consumption of CO_2 for hydrate formation of the CO_2+ sucrose (12 °Brix) + water system at a constant pressure of 3.00 MPa and different temperatures of: …275.15 and −276.15 K.

Figure 6-13 presents the gas consumption of CO_2 at different concentrations of sucrose at a constant temperature of 275.15 K and different pressures of 2.70, 2.90 and 3.10 MPa. In figure 6-13 (a, c and

e), by increasing the initial pressure by 0.40 MPa, the gas consumption increases by 1.8, 1.44 and 1.5 mmole/mole, respectively. However, in figure 6-13 (b, d and f), by increasing the temperature from 275.15 to 276.15 K, the gas consumption decreases by 0.8, 0.6 and 0.4 mmole/mole, respectively.

Figure 6-13. Gas consumption for the CO_2 + sucrose + water system. a, c and e: for different concentrations of sucrose solution (20, 30, and 35 °Brix) respectively, at a constant temperature of 275.65 K and pressures (… 2.70, --- 2.90 and −3.10 MPa). b, d and f: for different concentrations of sucrose solution (20, 30, and 35 °Brix) respectively, at a pressure of 3.00 MPa and temperatures (… 275.15 and —276.15 K).

6.6.3 Storage capacity (SC) for CO$_2$ + sucrose + water system

As shown in figures 6-14 and 6-15, for CO$_2$ + 12 °Brix sucrose + water system, by increasing the initial pressure at a constant temperature the storage capacity (SC) increases. The increase in the SC is not significant. Figure 6-14 presents the SC for two different temperatures of 275.15 and 276.15 K at a constant pressure of 3.00 MPa which by increasing the temperature, shows a decrease in the SC.
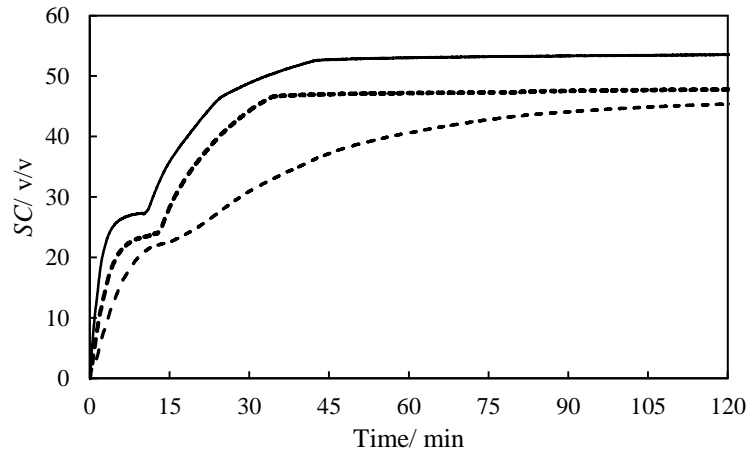
Figure 6-14. The storage capacity for hydrate formation of the CO$_2$+ sucrose (12 °Brix) + water system at a constant temperature of 275.65 K and different pressures of: …2.70, --- 2.90, and −3.10 MPa.
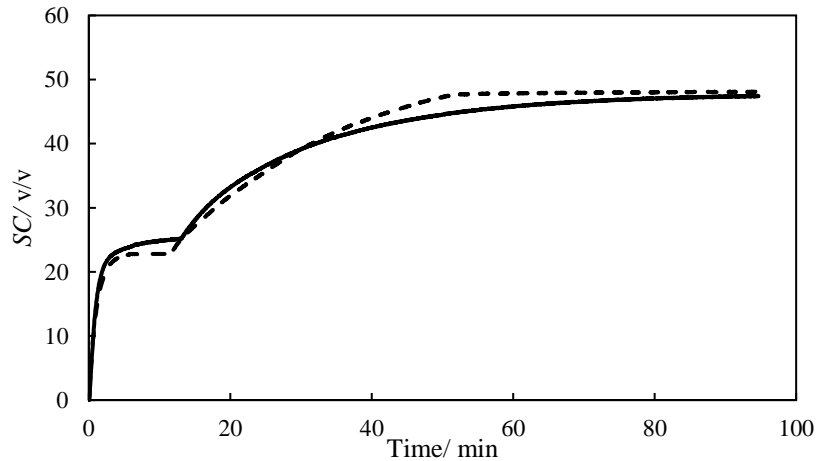
Figure 6-15. The storage capacity for hydrate formation of the CO$_2$+ sucrose (12 °Brix) + water system at the constant pressure of 3.00 MPa and different temperatures of: …275.15 and —276.15 K.

The effect of pressure variation at a constant temperature of 276.15 K as well as the variation of temperature at a constant pressure of 3.00 MPa on the SC of sucrose is shown in figure 6.16. By increasing the pressure (by 0.40 MPa) at constant temperature, the SC increases by 20 units at most.

At constant pressure of 3.00 MPa by increasing the temperature from 275.15 to 276.15 *K*, the SC decreases by seven units at most.
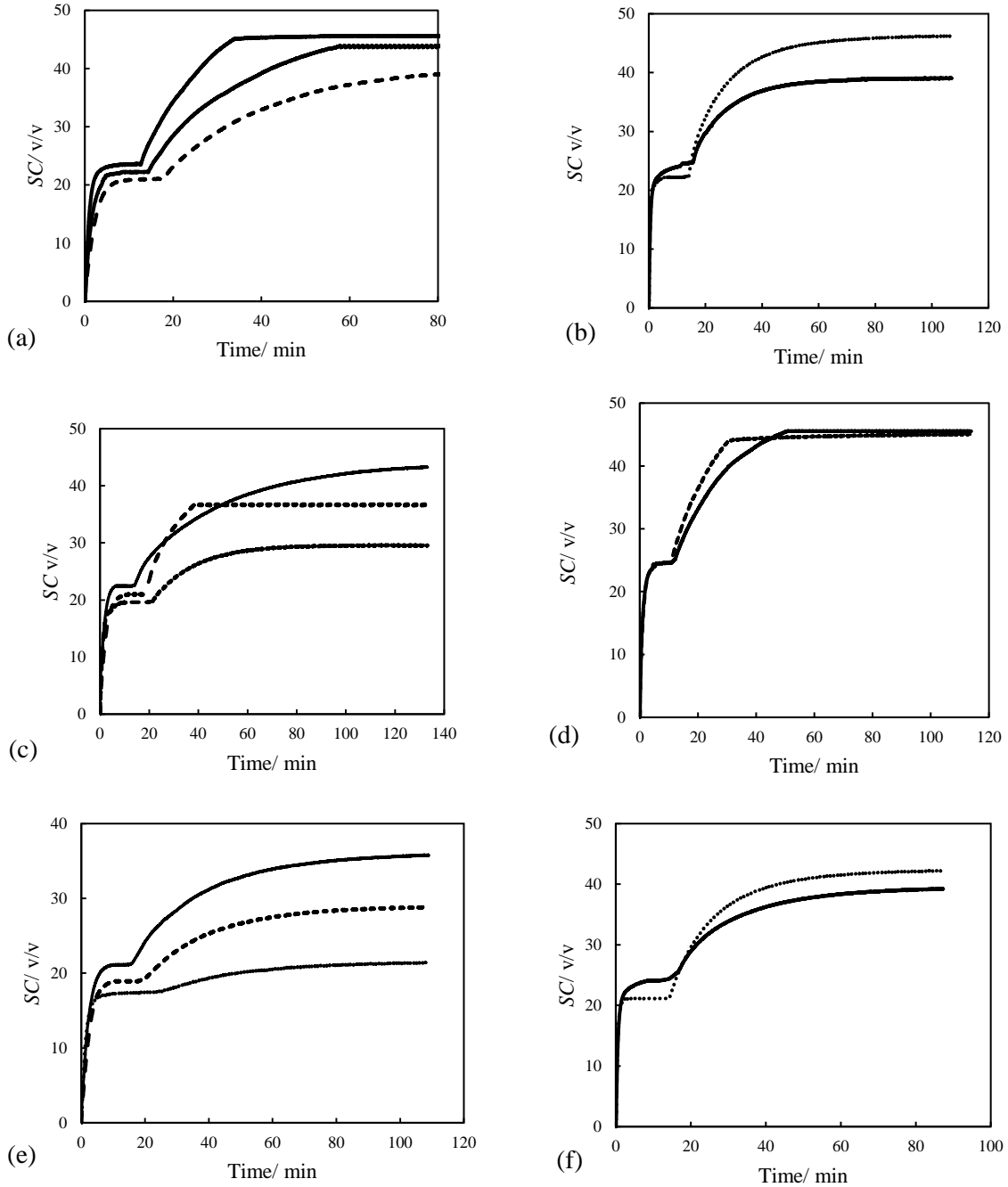
Figure 6-16. SC for the CO_2 + sucrose + water system. a, c and e: for different concentrations of sucrose solution (20, 30, and 35 °Brix) respectively, at a constant temperature of 275.65 K and pressures (…2.70, --- 2.90 and —3.10 MPa). b, d and f: for different concentrations of sucrose solution (20, 30, and 35 °Brix) respectively, at a pressure of 3.00 MPa and temperatures (…275.15 and —276.15 K).

6.6.4 Hydrate formation rate (HFR) for the CO_2 + sucrose + water system

Figure 6-17 presents the HFR for the CO_2 + 12 °Brix + water system and figure 6-18 presents HFR at constant pressure with two different temperatures of 275.15 and 276.15 K. The changes in conditions shows very slight differences whether for a change in pressure (constant T) or change in temperature (constant P). After the experiments started, an initial decrease in the system pressure was recorded until it stopped for a while followed by the second pressure decrease. The first area is the induction time for each experiment of which the concept was explained in chapter 3. The indicated peaks in the figures show the change of HFR at different time intervals. Due to the proximity of induction times and the recorded HFR, the graphs for each plot is fairly indistinguishable.
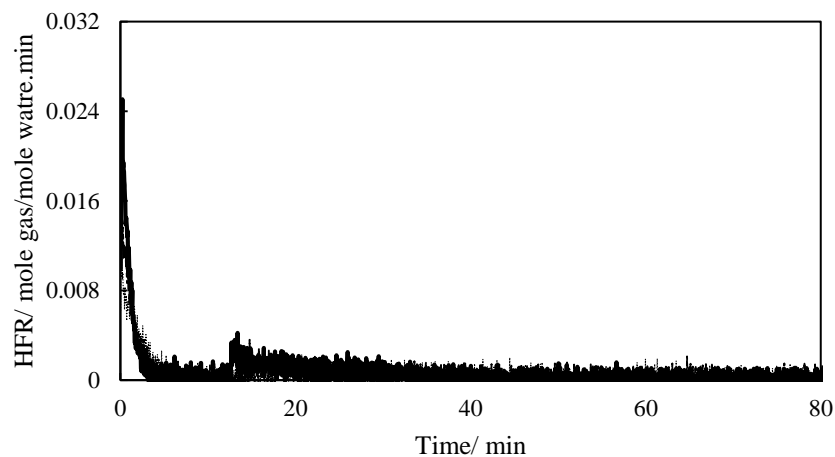
Figure 6-17. Hydrate formation rate for the CO_2 + sucrose (12 °Brix) + water system at a constant temperature of 275.65 K and different pressures of: …2.70, --- 2.90, and −3.10 MPa.
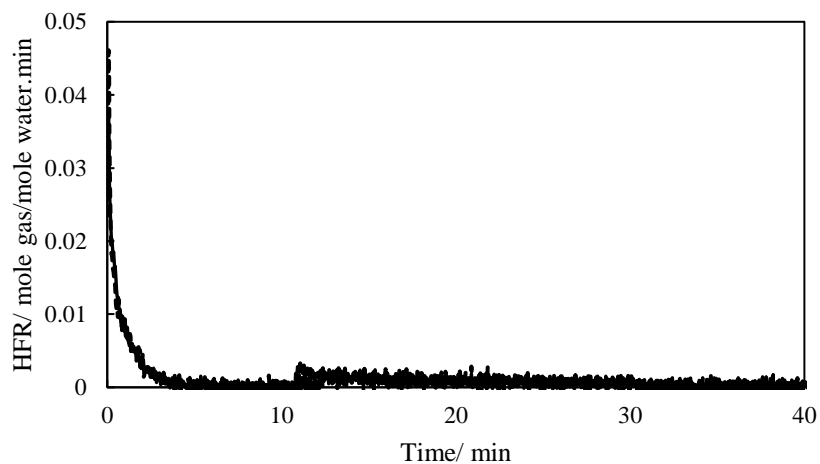
Figure 6-18. Hydrate formation rate for the CO_2 + sucrose (12 °Brix) + water system at a constant pressure of 3.00 MPa and different temperatures of: …275.15 and −276.15 K.

Figure 6-19 shows the HFR for different concentrations of sucrose (20, 30, and 35 ºBrix) at a constant temperature of 275.65 K and different pressures of 2.70, 2.90 and 3.10 MPa as well as at a constant pressure of 3.00 MPa at different temperatures of 275.15 and 276.15 K.
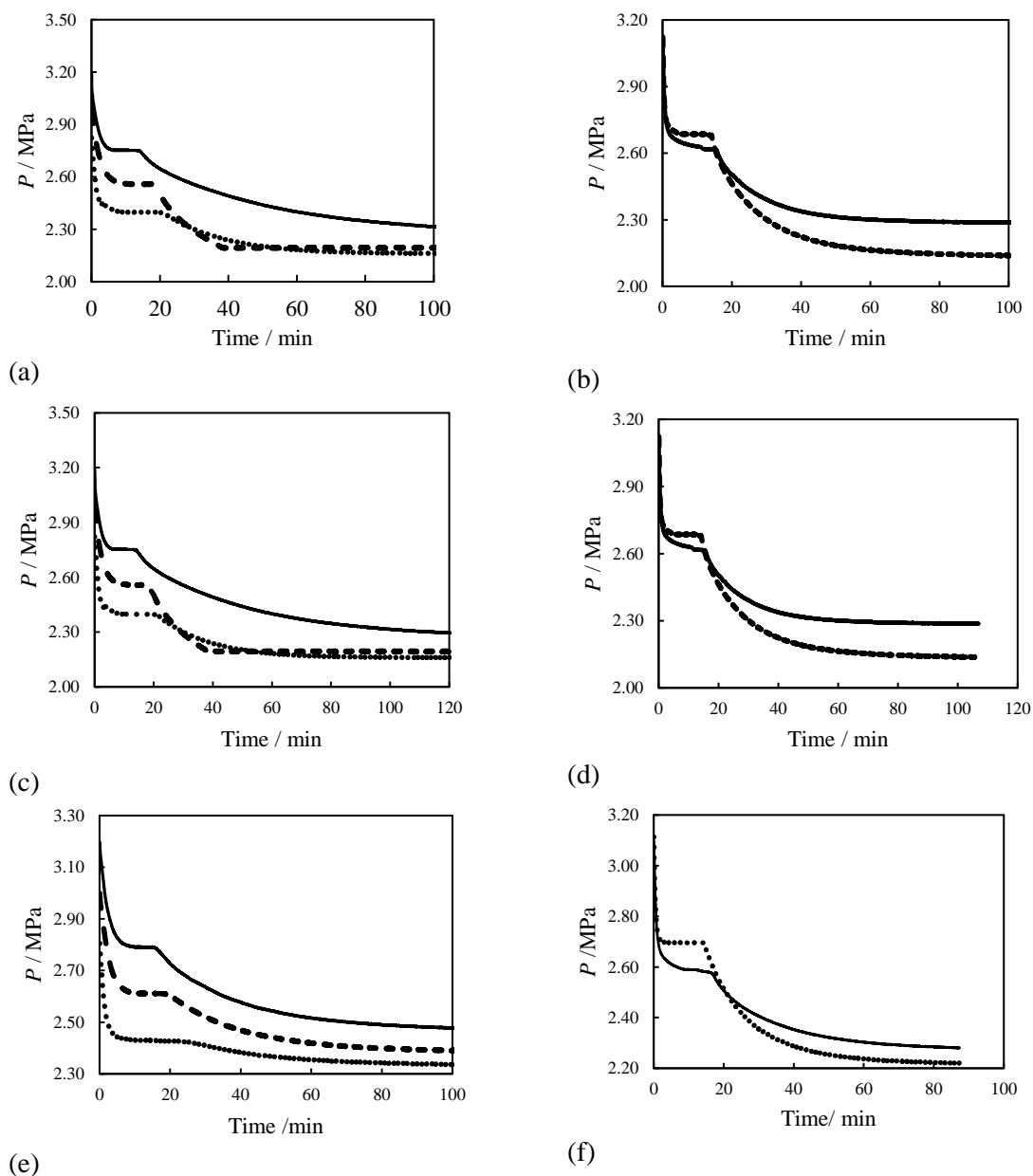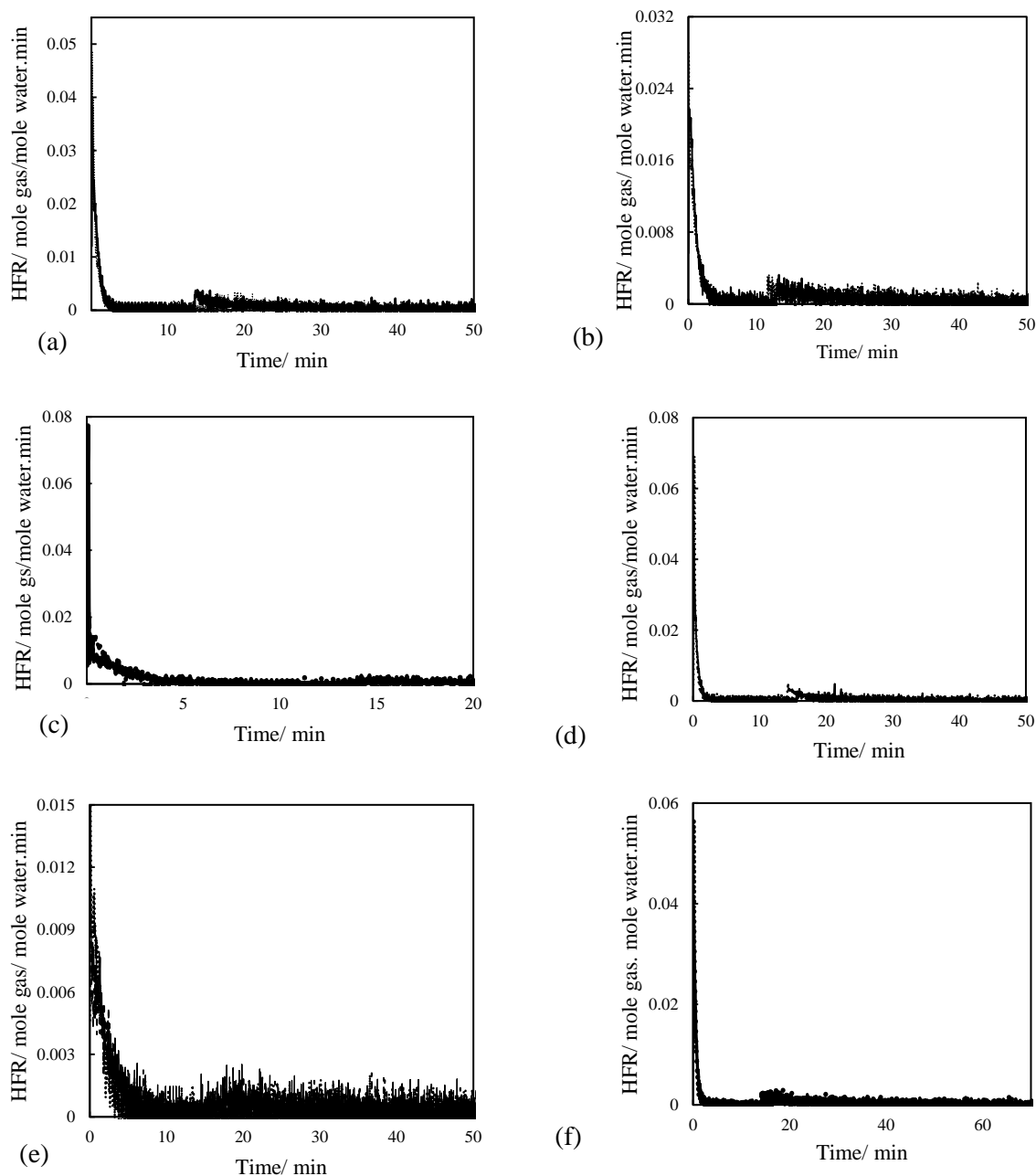

Figure 6-19. Hydrate formation rate for the CO_2 + sucrose + water system. a, c and e: for different concentrations of sucrose solution (20, 30, and 35 ºBrix) respectively, at a constant temperature of 275.65 K and pressures (…2.70, --- 2.90 and −3.10 MPa). b, d and f: for different concentrations of sucrose solution (20, 30, and 35 ºBrix) respectively, at a constant pressure of 3.00 MPa and temperatures (…275.15 and —276.15 K).

6.6.5 Rate Constant (K_{app}) for the CO_2 + sucrose + water system

Figure 6-20 shows the K_{app} for the CO_2 + 12 ºBrix sucrose + water system. By increasing the initial pressure, K_{app} increases. The K_{app} has a maximum value of 1.97×10^{-9} at a pressure of 3.10 MPa as presented in figure 6-20. Figure 6-21 shows the K_{app} at a constant pressure of 3.00 MPa and for two different temperatures of 275.15 and 276.15 K. It is observed that by increasing the temperature, the K_{app} decreases.
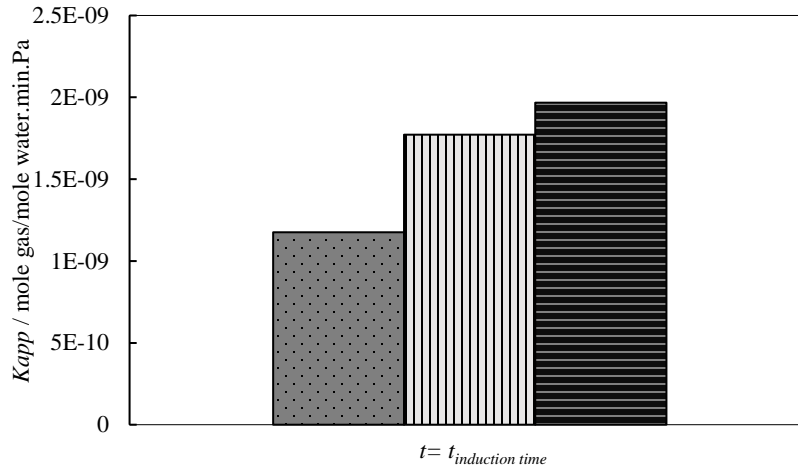
Figure 6-20. K_{app} for the CO_2 + sucrose (12 ºBrix) + water system at a constant temperature of 275.65 K and different pressures of: ▣ 2.70, ⦀ 2.90, and ▤ 3.10 MPa.
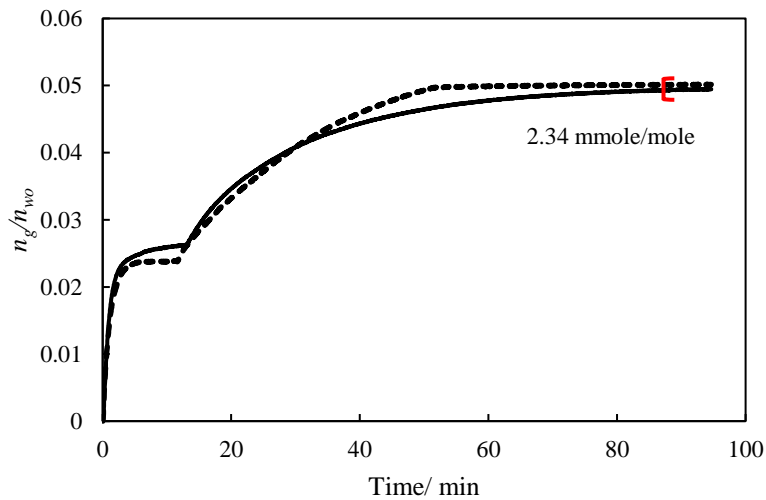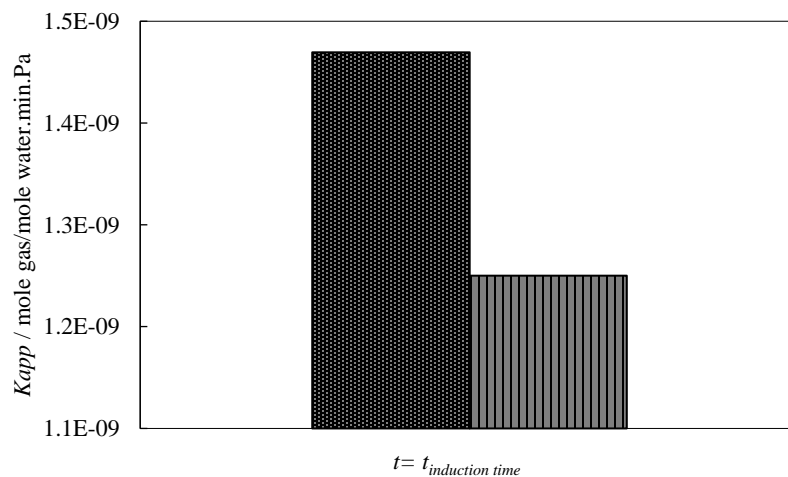

Figure 6-21. K_{app} for the CO_2 + sucrose (12 ºBrix) + water system at a constant pressure of 3.00 MPa and different temperatures of: ▦ 275.15 and ⦀ 276.15 K.

The K_{app} for different concentrations of sucrose at 20, 30, and 35 ºBrix with CO_2 + water is shown in figure 6-22. Figures a, c and e present the K_{app} at a constant temperature of 275.65 K and different

pressures of 2.70, 2.90 and 3.10 MPa. Figures b, d and f show the K_{app} at a constant pressure of 3.00 MPa and two different temperature of 275.15 and 276.15 K. By increasing the initial pressure, K_{app} increases.

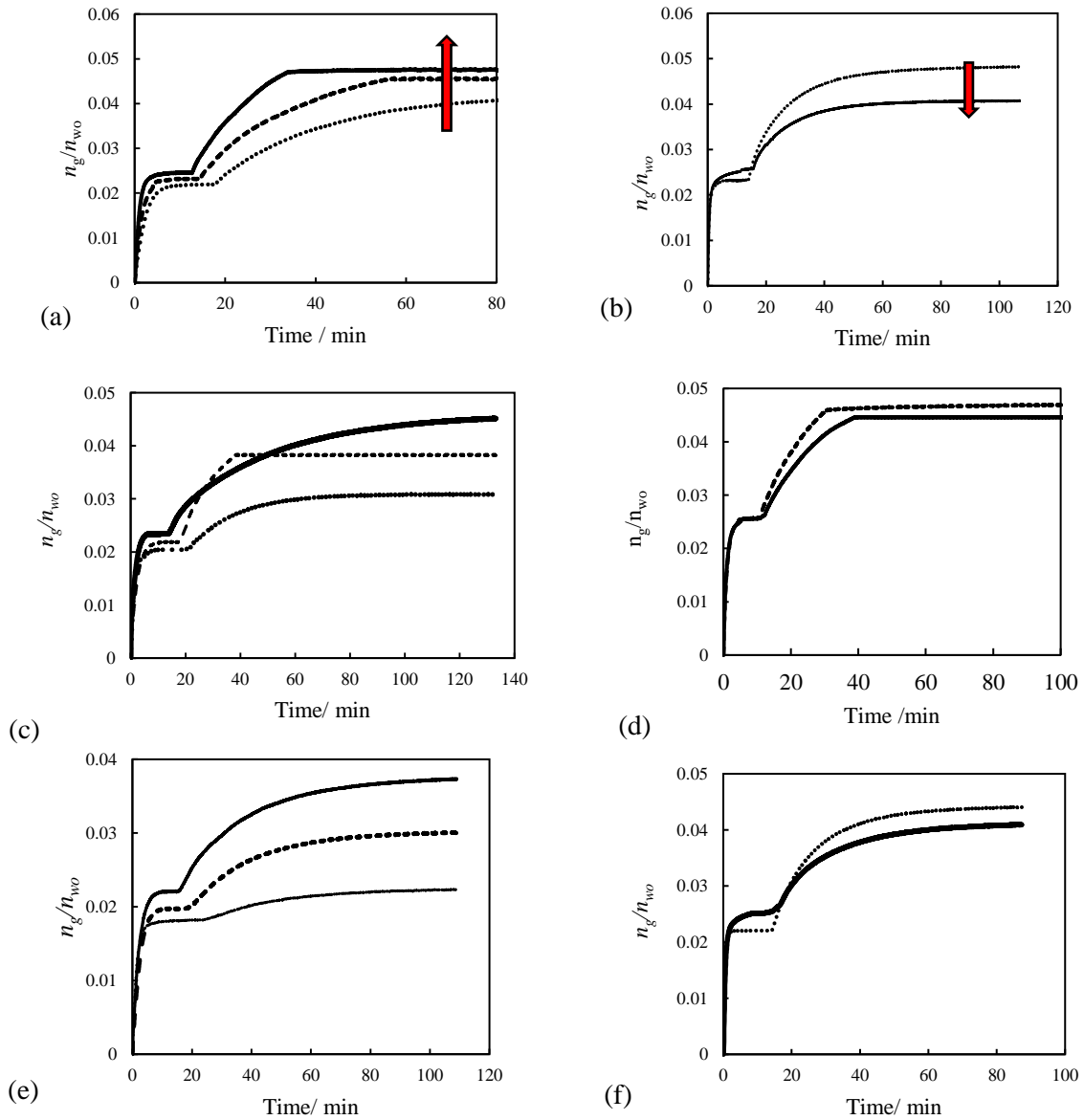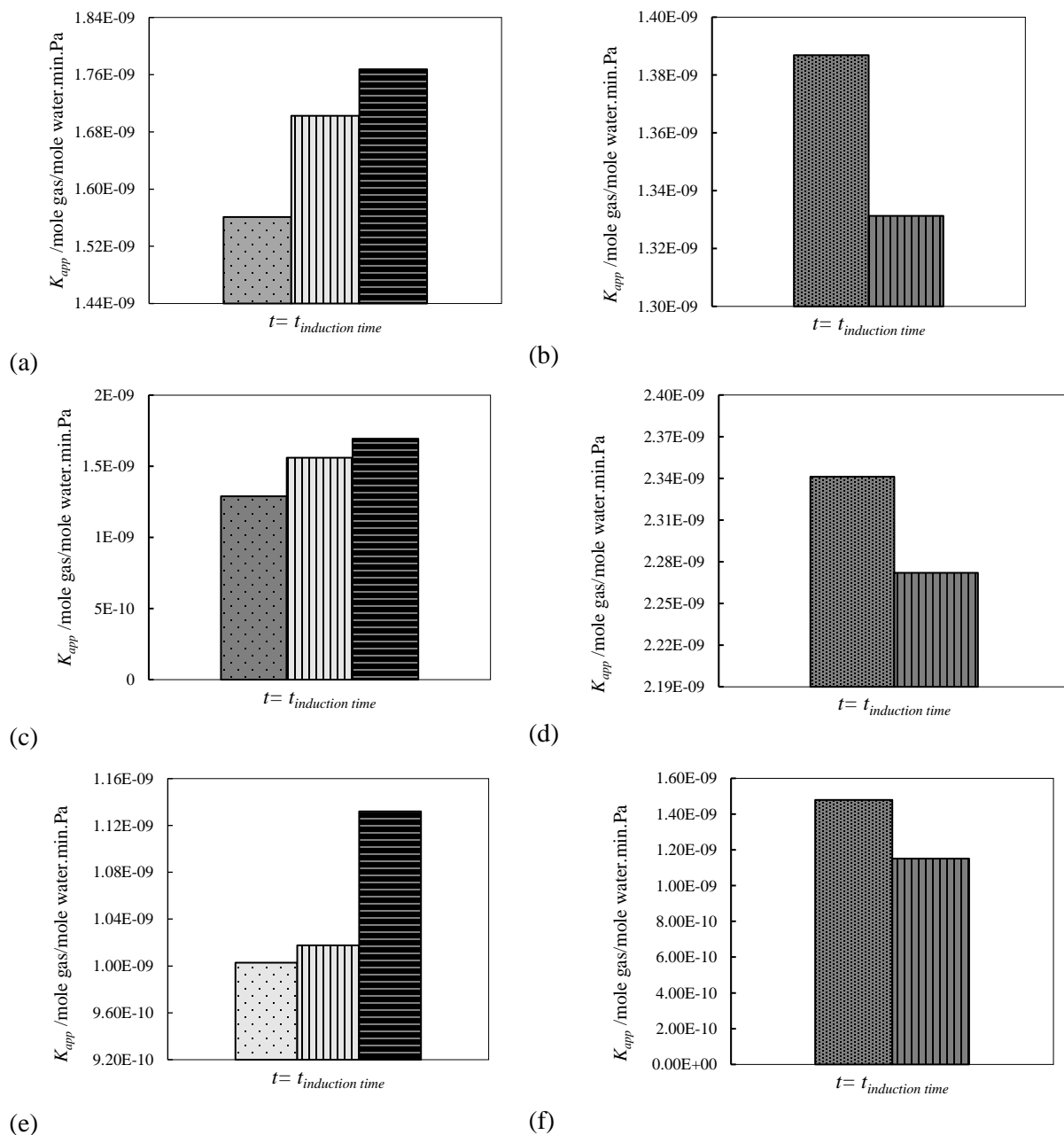**Figure 6-22.** The maximum K_{app} for the CO_2 + sucrose + water system. a, c and e: for different concentrations of sucrose solution (20, 30, and 35 °Brix) respectively, at a constant temperature of 275.65 K and pressures (▨ 2.70, ⫴ 2.90 and ▬ 3.10 MPa). b, d and f: for different concentrations of sucrose solution (20, 30, and 35 °Brix) respectively, at a pressure of 3.00 MPa and temperatures (▨ 275.15 and ⫴ 276.15 K).

6.7 Concentration measurements

6.7.1 Sucrose solutions

Several researchers attempted to concentrate and analyse the residue fluid from hydrate experiments with sucrose solutions (Andersen and Thomsen, 2009, Purwanto et al., 2014) as presented in chapter 4. The main objective of this study was to determine the concentration of the sugar cane juice, via hydrate-based concentration, using a series of hydrate concentration stages with sample analysis of the hydrate residue after each stage.

In the measurements, the effect of temperature, pressure, the speed of the mixer and the sampling screen size were investigated. The effect of each of these parameters was investigated separately, and the optimum conditions for sugar concentration were obtained. The sample concentration was determined via measurement of the refractive indices.

The concentration experiments of this study were measured in a stage-wise manner, which started with a 12 ^{o}Brix sucrose solution. The concentration obtained from each step was used as the feed for the next stage until there was no hydrate formed in the reactor. The schematic of these experiments is shown in figure 6-23.
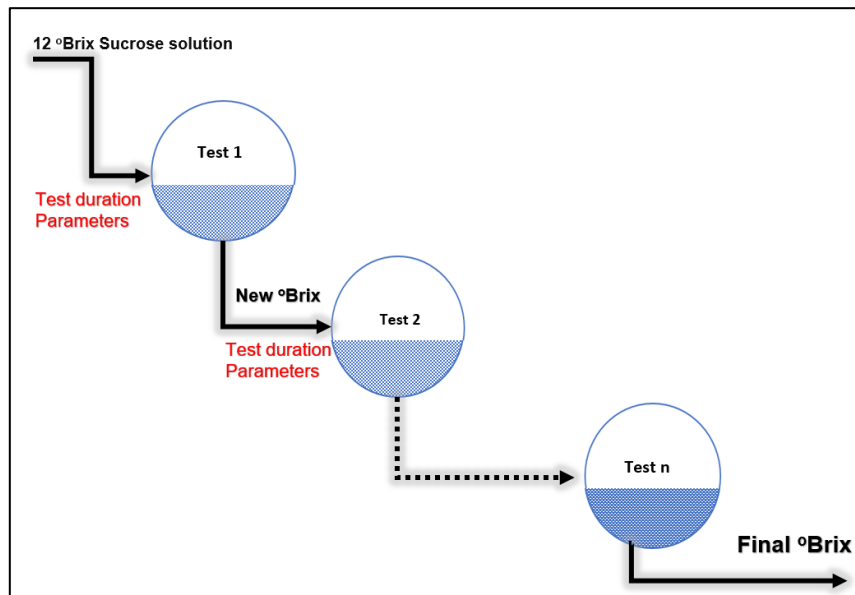
Figure 6-23. Schematic of the stage-wise experimental study for the concentration tests.

6.7.1.1 Effect of mesh size variation

At a constant temperature of 275.65 K and a pressure of 3.00 MPa, mesh sizes of 38 and 45 microns were tested. It should be noted that in each of these concentration experiments, two identical tests

were performed, and the average concentration is reported. The difference is reported as an error of ± 0.004 mass fraction. Table 6-15 shows the experimental results of a sucrose concentration with CO_2 gas hydrate at a pressure of 3.00 MPa and a temperature of 275.65 K with a mesh size of 45 µm and a stirrer speed of 260 rpm. After the first test was performed and the final pressure was stabilised, a sample was withdrawn via the sample port located in the bottom flange and tested by the refractive index to determine its concentration.

Table 6-15. Experimental results of sucrose solution concentration with CO_2 gas hydrate at an initial pressure ($P_{initial}$) of 3.00 MPa and temperature of 275.65 K using a mesh size of 45 µm and mixer speed of 260 rpm.

Stage no.	P_{final} (MPa)	$C_{initial}$ (ºBrix)	C_{final} (ºBrix)	Water removed (wt.%)	Induction time (min)
1	1.71	12.00	15.92	29	13.12
2	1.78	15.92	21.92	35	13.54
3	1.83	21.92	28.81	33	14.34
4	1.93	28.81	31.89	15	14.54
5	2.22	31.89	36.06	19	14.83
6	2.26	36.06	41.09	22	17.20
7	2.41	41.09	46.06	22	31.57

U(P) = 0.01 MPa, U(T) = 0.1 K.

During the sample withdrawal using a 45 µm mesh size, some hydrate crystals were visible in the sample vial/syringe as bubbles were generated and the sample volume was observed to gradually decrease in the sample syringe. Samples analysis via refractive index was performed at 10, 20, and 30 minutes intervals, over which the concentration of the sample changed (about 1 to 2 ºBrix). This change indicated the presence of hydrate nuclei inside the sample vial. However, after approximately 10 minutes, the concentration did not change significantly. For this first set of experiments, at a temperature of 275.65 K, a pressure of 3.00 MPa and a mixer speed of 260 and a mesh size of 45 µm, initial sucrose ºBrix of 12, a final concentration of 46.06 ºBrix was obtained after 7 consecutive concentration stages, In each step, the amount of water isolated from the initial solution was calculated. According to Table 6-15, the more viscous the final product, the greater the water recovery in the hydrate. As observed in Table 6-15, the induction time increases significantly as the initial concentration of the solution increases from 12 to 41 ºBrix. Further concentration beyond stage 7 is not possible when considering the hydrate stability zone, as it is not possible to form stable hydrates.

The second set of concentration measurements, under the same (T, P and mixer speed) conditions, used a mesh size of 38 µm to examine the effect of mesh size on concentration. Table 6-16 presents

the results for this series of measurements. By visual examination of the withdrawn sample, for stage 1, although hydrate residues were visible in the sample syringe, the number of observed bubbles in the sample vial/syringe decreased compared to when the larger mesh size was used. This indicated that the smaller size crystal passed through the mesh. The withdrawn samples were tested via refractometer three times within 10 minutes of each to study the effect of time on the sample concentration. The effect of time variations on the concentration of the sample was found to be much lower (less than 0.5 °Brix) compared to the previous set of experiments, indicating that crystals with a core size greater than 38 μm did not pass through the screen. The concentration of the final product after seven stages was 48.21 °Brix using a mesh size of 38 μm. Similar to the previous experiments, it was not possible to form stable hydrates beyond stage 7.

Table 6-16. Experimental results of sucrose solution concentration with CO_2 gas hydrate at initial pressure ($P_{initial}$) of 3.00 MPa and temperature of 275.65 K using a mesh size of 38 μm and mixer speed of 260 rpm.

Stage no.	P_{final} (MPa)	$C_{initial}$ (°Brix)	C_{final} (°Brix)	Water removed (wt.%)	Induction time (min)
1	1.76	12.00	16.99	36	13.10
2	1.82	16.99	22.50	32	13.75
3	1.93	22.50	28.96	31	14.41
4	2.06	28.96	33.75	22	14.73
5	2.26	33.75	38.69	22	15.65
6	2.53	38.69	43.98	23	17.84
7	2.61	43.98	48.28	19	36.10

U(P) = 0.01 MPa, U(T) = 0.1 K.

Meshes size of 26 and 10 μm were also tested at constant temperature and pressure of 274.65 K and 3.70 MPa, respectively and 130 rpm mixer speed which are shown in tables 6-17 and 6-18. In table 6-17, the changes in concentration were more noticeable than the previous experiments, with a concentration increase from $C_{initial}$ of 12 to 38.62 °Brix. In the previous experiments, a 4-5 °Brix increase was observed over the initial stages. Table 6-17 presents the results for experiments using the 26 μm mesh size and a mixer speed of 130 rpm.

Table 6-17. Experimental results of t sucrose solution concentration with CO_2 gas hydrate at initial pressure ($P_{initial}$) of 3.70 MPa and temperature of 274.65 K using a mesh size of 26 μm and mixer speed of 130 rpm.

Stage no.	P_{final} (MPa)	$C_{initial}$ (°Brix)	C_{final} (°Brix)	Water removed (wt.%)	Induction time (min)
1	2.36	12.00	38.62	82	25.15
2	2.93	38.62	52.83	51	45.35
3	3.40	52.83	58.43	25	246.20

U(P) = 0.01 MPa, U(T) = 0.1 K.

The results show that after three stages of concentration hydrate formation experiments, the sucrose solution concentration in the final solution reached 58.43 ºBrix. The conditions and mesh size in this third set of concentration experiments resulted in the least number of stages (three). With the use of the 26 μm mesh size, the probability of crystals of a size greater than 26 μm passing through the mesh decreased, and a very slight change in the concentration of the withdrawn sample (on the average ±0.05 ºBrix) over time confirmed this claim. But given the fact that the presence of stable and unstable nuclei, much smaller than 26 μm, is very high, such small amounts of suspended nuclei were retained in the solution by passing through the mesh. These nuclei are not visible through the eye, and changes in concentration of the withdrawn sample after 10, 20 and 30 minutes, was less than 0.05 ºBrix.

The concentration results using the 10 μm mesh size were the final set of experiments to assess the effect of mesh size on product achieved. Table 6-18 shows the experimental results of a sucrose solution concentration with CO_2 gas hydrate at a pressure of 3.70 MPa and a temperature of 274.65 K using a mesh size of 10 μm and a stirrer speed of 130 rpm. At these conditions, four concentrations were required to reach a final concentration of 59.94 ºBrix. Due to the very small size of the mesh in the device, removal of a sample was much more difficult than in previous concentration experiments, and the system experienced a significant drop in pressure of 0.10 - 0.20 MPa, in the first stage. Samples did not show any change in concentration as time passed. With the removal of two 3 ml samples for each experiment, it proved impossible to remove the third sample probably due to obstruction of the mesh with hydrates. In general, the use of a 26 μm mesh gave better results especially in the first stage of the concentration experiment. Due to the higher concentration obtained in the last stage of the experiment with the 10 μm mesh, it is recommended to use this mesh size for the final stage of the concentration experiment.

Table 6-18. Experimental results of sucrose solution concentration with CO_2 gas hydrate at initial pressure ($P_{initial}$) of 3.70 MPa and temperature of 274.65 K using a mesh size of 10 μm and mixer speed of 130 rpm.

Stage no.	P_{final} (MPa)	$C_{initial}$ (ºBrix)	C_{final} (ºBrix)	Water removed (wt.%)	Induction time (min)
1	2.23	12.00	29.30	70	25.13
2	2.35	29.30	44.61	54	37.50
3	2.36	44.61	54.46	39	130.20
4	3.00	54.46	59.94	25	258.25

$U(P) = 0.01$ MPa, $U(T) = 0.1$ K.

The results of this series of experiments show that the reduction of the mesh size to a certain extent increases the concentration. However, there were far more difficulties in the physical removal of the

samples with the lowest mesh size of 10um to outweigh the greatest concentration effect. Given the mesh size available in the market, the 26 µm mesh showed the most promising result for the concentration of the sucrose solution.

6.7.1.2 Effect of pressure variation

The effect of pressure on the concentration of sucrose solution was studied at 275.65 K and 3.70 MPa, using a 38 µm mesh size and 260 rpm mixer speed. A summary of this set of results is presented in Table 6-19. The results presented were compared to Table 6-16. The results show that after five stages (each experiment was repeated for each stage), a final concentration of 52.10 °Brix was achieved.

Table 6-19. Experimental results of sucrose solution concentration with CO_2 gas hydrate at initial pressure ($P_{initial}$) of 3.70 MPa and temperature of 275.65 K using a mesh size of 38 µm and mixer speed of 260 rpm.

Stage no.	P_{final} (MPa)	$C_{initial}$ (ºBrix)	C_{final} (ºBrix)	Water removed (wt.%)	Induction time (min)
1	2.35	12.00	19.29	45	13.10
2	2.49	19.29	29.50	46	14.10
3	2.47	29.50	41.63	46	14.95
4	2.90	41.63	48.71	29	31.90
5	3.22	48.71	52.10	15	45.20

$U(P) = 0.01$ MPa, $U(T) = 0.1$ K.

In this method, the pressure difference with the hydrate dissociation zone is considered as the driving force. Therefore, the greater the distance from the stability curve, the greater the driving force, such that the hydrates consume more gas and liquid. It should be noted that this difference means an increase in pressure, and this increase in pressure should be economically justifiable. Two fewer stages are required in this experiment compared to the previous experiment with 3.00 MPa pressure. These results indicate that pressure is a crucial variable in concentration via hydrate technology.

6.7.1.3 Effect of temperature variation

The effect of temperature on the concentration of sucrose solution was studied at temperatures of 274.65 and 275.65 K. The measured results for the experiment set of 274.65 K at 3.70 MPa, the mixer speed of 260 rpm and using a 38 µm mesh are given in Table 6-20. After completing this series of experiments, the results were compared with the data presented in Table 6-19. The results at the lower temperature (274.75 K) showed better concentration effects at the constant pressure. At this temperature, only three equilibrium stages are needed to obtain a concentration of 55.12 °Brix sucrose solution, which is much higher than the previous result (52.10 °Brix). At these thermodynamic conditions, clearly, with constant pressure and variation of temperature, two hydrate stability lines

were encountered, which the lower temperature curve has a higher pressure difference compared to the higher temperature one. This difference means a greater driving force, resulting in increased water consumption and better concentration of the final product.

Table 6-20. Experimental results of sucrose solution concentration with CO_2 gas hydrate at initial pressure ($P_{initial}$) of 3.70 MPa and temperature of 274.65 K using a mesh size of 38 µm and mixer speed of 260 rpm.

Stage no.	P_{final} (MPa)	$C_{initial}$ (ºBrix)	C_{final} (ºBrix)	Water removed (wt.%)	Induction time (min)
1	2.40	12.00	20.05	48	12.80
2	2.42	20.05	35.82	59	13.56
3	3.00	35.82	55.12	63	16.75

U(P) = 0.01 MPa, U(T) = 0.1 K.

6.7.1.4 Effect of mixer speed variation

To investigate the effect of mixer speed, experiments at a temperature of 274.15 K, a pressure of 3.70 MPa, with a mesh size of 38 microns and a mixer speed of 130 rpm was performed. The results of this experiment are presented in Table 6-21. The results presented are compared to Table 6-20.

Table 6-21. Experimental results of sucrose solution concentration with CO_2 gas hydrate at initial pressure ($P_{initial}$) of 3.70 MPa and temperature of 274.65 K using a mesh size of 38 µm and mixer speed of 130 rpm.

Stage no.	P_{final} (MPa)	$C_{initial}$ (ºBrix)	C_{final} (ºBrix)	Water removed (wt.%)	Induction time (min)
1	2.23	12.00	*32.80*	75	25.18
2	2.48	*32.80*	47.33	52	39.50

U(P) = 0.01 MPa, U(T) = 0.1 K.

These results indicate that only two equilibrium stages are needed to reach the final concentration of 47.33 ºBrix. Results indicate that the lower speed favours water recovery/removal. The distinguishing feature of this test is the time taken to reach the equilibrium, which varies from 4 to 5 hours depending on the initial concentration of the solution. It should be noted that at lower mixer speeds the hydrates take longer to form, resulting in a slower rate of gas encapsulation, and longer time to reach equilibrium. Figure 6-24 shows a summary of the information presented for the CO_2 + sucrose + water system.
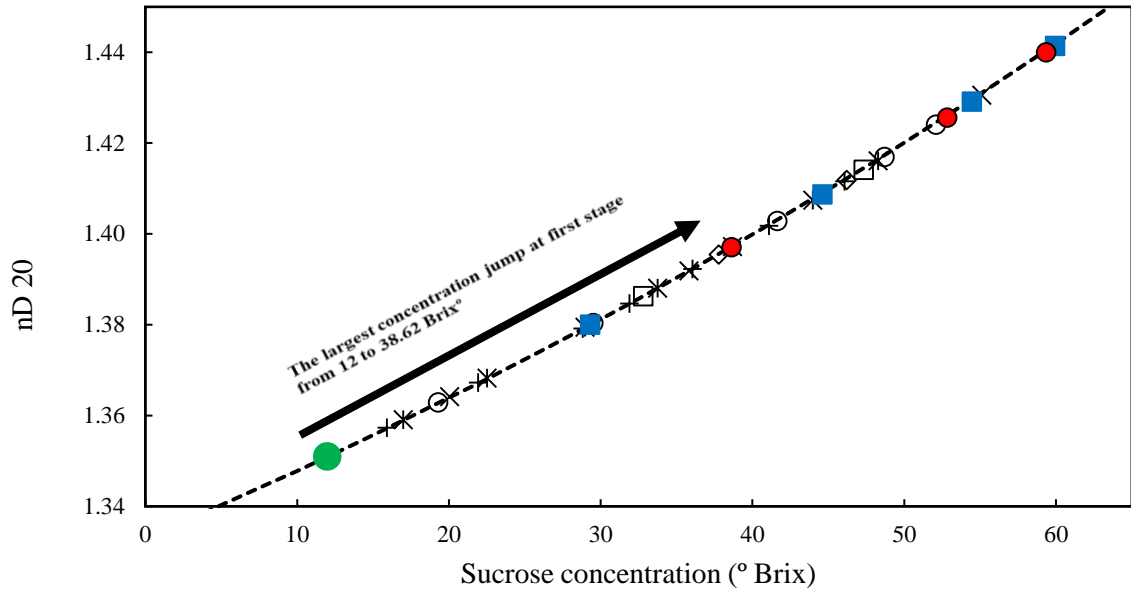
Figure 6-24. Experimental results (refractive index nD20) of the sucrose solution concentration with CO_2 gas hydrate. ●: Starting point at 12 °Brix (feed concentration); +: 3.0 MPa, 275.65 K, 45 μm and 260 rpm (7 stages); ●: 3.7 MPa, 275.65 K, 45 μm and 260 rpm (5 stages); *: 3.0 MPa, 275.65 K, 38 μm and 260 rpm (7 stages); ×: 3.7 MPa, 274.65 K, 38 μm and 260 rpm (3 stages); ◊: 3.7 MPa, 274.65 K, 38 μm and 260 rpm (5 stages); □: 3.7 MPa, 274.65 K, 38 μm and 130 rpm (2 stages); ■: 3.7 MPa, 274.65 K, 10 μm and 130 rpm (4 stages); ●: 3.7 MPa, 274.65 K, 26 μm and 130 rpm (3 stages); --- data from this work.

All experiments for the concentration studies began with an initial sucrose solution of 12 °Brix. The largest concentration increase in the first experiment was achieved using the conditions of 274.65 K, 3.70 MPa, mesh size of 26 μm and mixing speed of 130 rpm. For this stage, a final sucrose solution with a concentration of 38.62 °Brix was achieved. Figure 6-25 shows the schematic diagram of the proposed process for concentration of a sucrose solution with CO_2 hydrate.
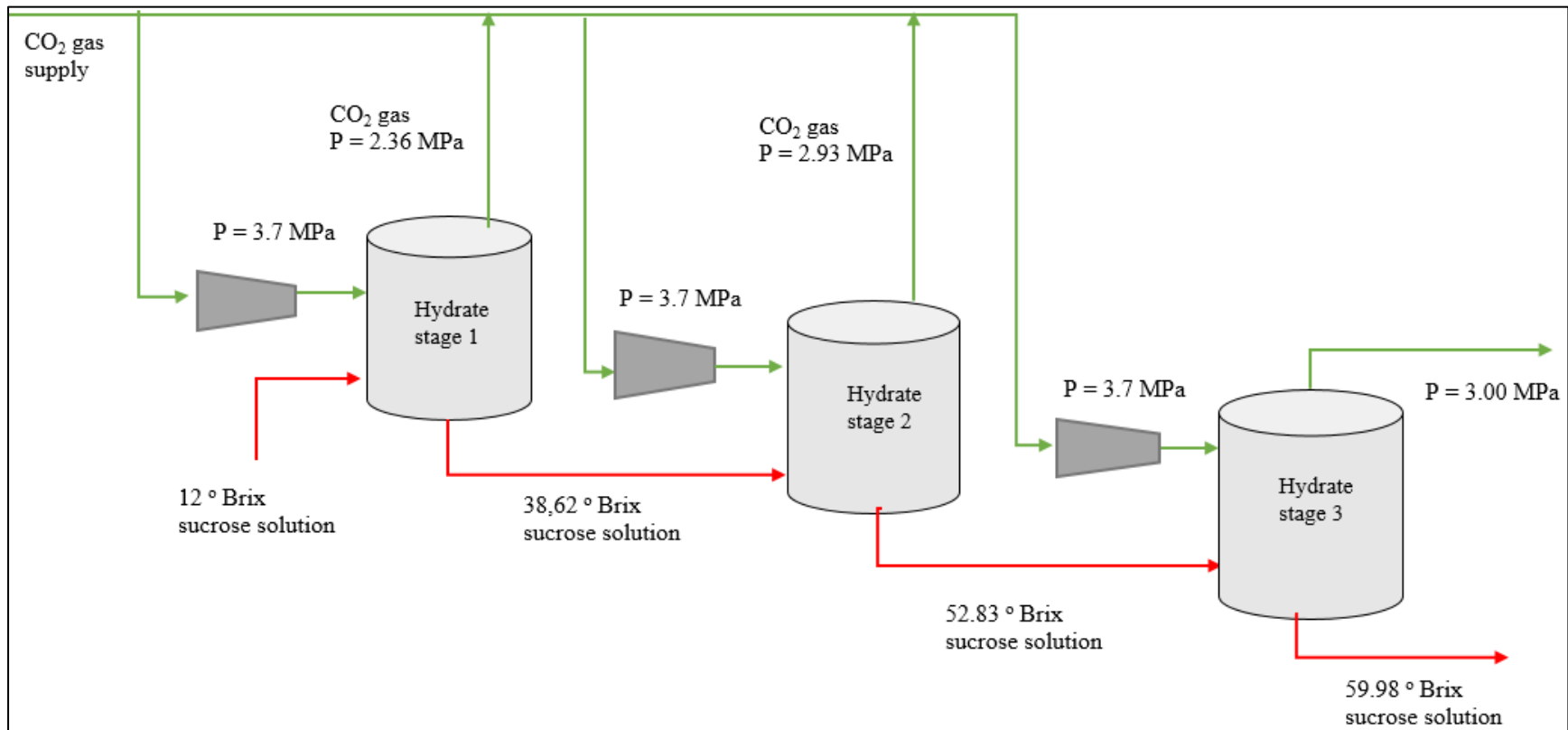
Figure 6-25. Conceptual hydrate process for sucrose solution concentration using CO_2 gas hydrate to recover water from the solution. Hydrate formation was carried out at 274.65 K and 3.70 MPa and mixer speed of 130 rpm in the three stages.

6.7.2 Concentration experiments using sugar cane juice

Concentration measurements were performed using sugar cane juice supplied by SMRI (South African Sugar Milling Institute). Regarding the sensitivity of the materials to storage and time (one-week limit), experiments were performed as quickly as possible with samples being stored in the fridge when not being used. In some cases, the duration of the experiment lasted more than 15 hours to assess the concentration-effect over one stage. The first batch of the sugar juice received began to ferment after a week, most likely due to the microbial contamination using sucrose, glucose and fructose as substrate. Its pH had decreased dramatically to 3, and the experiments had to be repeated with a new batch of sugarcane juice samples with the pH of new results being acceptable at approximately >5. The new batch of the samples were kept in the refrigerator and was only defrosted when required for use. This ensured that the new samples did not ferment.

The optimal conditions for sucrose solution hydrate conditions from earlier hydrate and kinetic measurements were 274.65 K, 3.70 MPa, 130 rpm mixer speed using a 26 μm mesh size. Therefore, concentration measurements using the cane juice were studied under these conditions. Furthermore, additional experiments were performed at 275.65 K, to assess the effect of temperature. Due to the presence of amino acids in sugarcane juice, its pH was tested. Table 6-22 shows the results of the concentration of sugar cane juice at a temperature of 274.65 K.

Table 6-22. Experimental results for sugarcane juice concentration with CO_2 gas hydrate at initial pressure ($P_{initial}$) of 3.70 MPa and temperature of 274.65 K with a mesh size of 26 μm and mixer speed of 130 rpm.

Stage no.	P_{final} (MPa)	$C_{initial}$ (ºBrix)	C_{final} (ºBrix)	Induction time (min)	pH $_{initial}$	pH $_{final}$
1	2.49	12.00	30.10	25.86	6.73	5.76
2	2.70	30.10	41.22	40.25	6.46	5.44
3	2.90	41.22	52.30	135.24	6.30	5.33
4	3.10	52.30	56.20	265.00	6.21	5.30

U(P) = 0.01 MPa, U(T) = 0.1 K.

The results from these experiments showed that a greater time was needed to reach equilibrium for sugar cane juice compared to measurements using sucrose solutions. Furthermore, as the solution concentration increased, the time to reach equilibrium increased. Depending on the concentration of each step, the time to reach equilibrium varied from 6 to 15 hours. The induction time rises dramatically from 4 to 15 hours. Four equilibrium steps were required to achieve a concentration of 56.2 ºBrix (at 274.65 K, 3.70 MPa, 130 rpm mixer speed and 26 μm mesh size). The pH was measured for the feed (pH of 6.73) and product sample, with results showing a decrease after every stage of

concentration. The final pH obtained was 5.5, on average. The pH must remain constant and a change is considered as a concern.

Table 6-23 shows the results of the concentration of sugar cane juice at a temperature of 275.65 K. The results show that the change in temperature affects the final concentration of the product, and the final concentration after four stages was 54.4 ºBrix. The pH is most affected by the temperature change with a noticeable increase in pH. The results show that the lower the solution temperature, the lower the final pH of the product. Due to the increase in the temperature of the test condition compared to the previous one, it can be seen that an average pH of 5.7 is obtained for the final product. In general, four equilibrium steps are required to reach a concentration of 55 ºBrix from a feed of sugar cane juice solution.

Table 6-23. Experimental results for sugarcane juice concentration with CO_2 gas hydrate at initial pressure ($P_{initial}$) of 3.70 MPa and temperature of 275.65 K with the mesh size of 26 µm and mixer speed of 130 rpm.

Stage no.	P_{final} (MPa)	$C_{initial}$ (ºBrix)	C_{final} (ºBrix)	Induction time (min)	pH $_{initial}$	pH $_{final}$
1	2.49	12.00	28.70	28.45	6.73	5.85
2	2.7	28.70	40.65	39.85	6.46	5.71
3	2.9	40.65	47.37	128.52	6.3	5.7
4	3.18	47.37	54.40	260.1	6.21	5.69

U(P) = 0.01 MPa, U(T) = 0.1 K.

In general, four equilibrium steps are required to reach a concentration of 54.4 ºBrix from a sugar cane juice solution. Each stage was repeated and the average value is reported for each stage. Figure 6-26 shows the schematic diagram of the proposed process for the concentration of sugarcane juice with CO_2 hydrate.
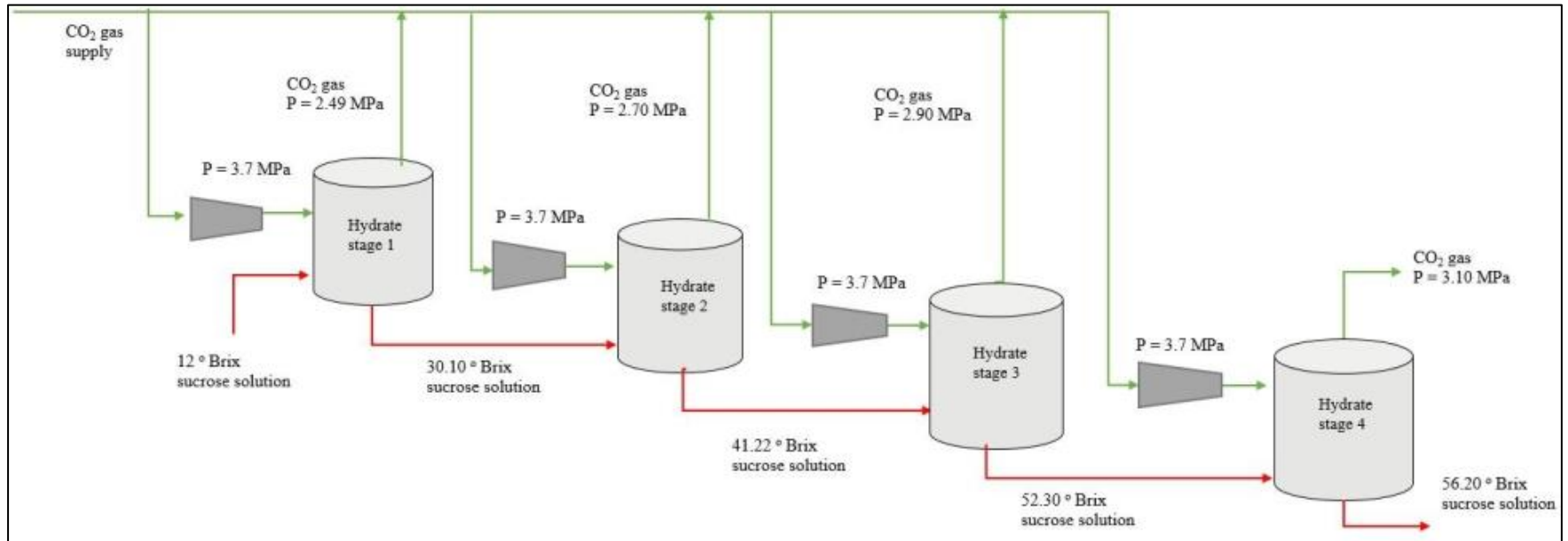
Figure 6-26. Conceptual hydrate process for sugarcane juice concentration using CO_2 gas hydrate at 274.65, 3.70 MPa, 130 rpm stirrer speed and mesh size of 26 μm in the four stages.

6.7.3 Sample withdrawal procedure

For the withdrawn sucrose samples using mesh sizes of 38 or 45 microns, small bubbles appeared in the syringe as time passed. This is due to dissociation of the withdrawn hydrate crystals within the sucrose solution. Therefore, it is important that the sample withdrawn using the larger mesh size should be tested very quick (well within 20 seconds) to obtain accurate concentration readings. There is a possibility that there will be small bubbles detected immediately after sample withdrawal because of the dissolved gas in the liquid phase, which will disappear quickly.

For the sampling of the concentrated sugarcane juice solution, after reaching concentrations higher than 40 °Brix, the samples withdrawn looked more like foam. It took at least 10 minutes for the foam to disappear and form a normal liquid solution. On comparison of the bubbles released from hydrate crystals in sucrose solution to those in the sample of sugar cane juice at higher Brix, after a while, the bubbles of the sucrose solution were larger, and the volume of the liquid in the syringe decreased by almost 0.1 ml, indicating the release of gas. Figure 6-27 shows photographs of the samples withdrawn from sucrose and sugarcane juice solutions. It was, therefore, possible to form stable hydrate which was confirmed in this study. (Smith et al., 2016) only measured thermodynamic phase boundary of the sucrose solution using refrigerants. The equipment used did not include features to withdraw the sample from the solution. Furthermore, (Smith et al., 2016) were not able to measure kinetic data (Smith et al., 2016). As a part of this research study, for the first time, reliable samples from concentration experiments using sucrose and sugarcane juice solutions were withdrawn with the new equipment developed in the Thermodynamic Research Unit (TRU). Due to the innovative technique employed for the design of the sampling mechanism, the samples were validated via three repeatable experiments providing a high confidence level for the data measured.

a)   b)   c)
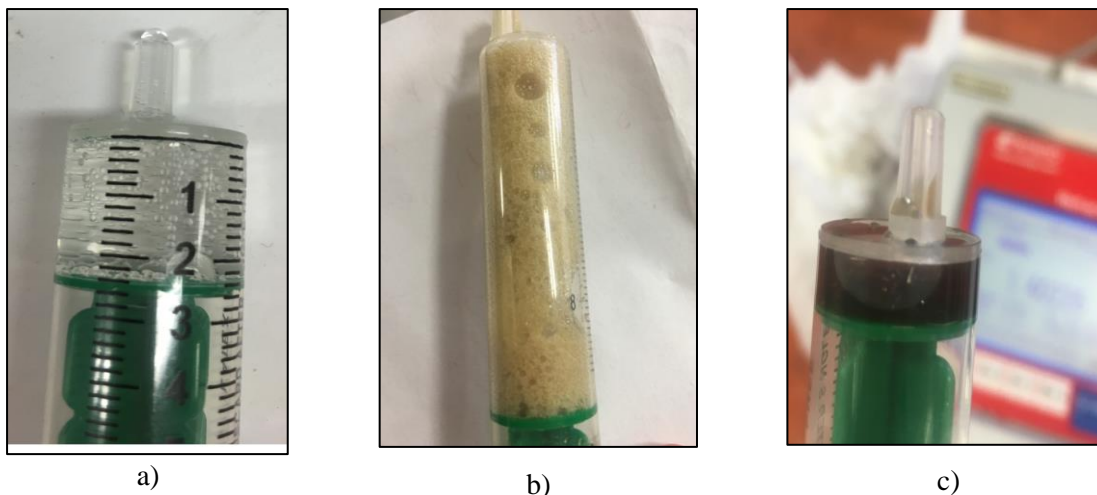
Figure 6-27. Withdrawn samples from the hydrate cell; **a**: sample from sucrose solution containing hydrate crystals, **b**: initial sample taken from sugarcane juice solution with the concentration higher than 40 °Brix, **c**: sample from sugarcane juice solution after the foam disappeared.

Figure 6-28 shows the pictures of hydrates formed for sucrose and sugarcane juice solutions once the cell was opened. The hydrate crystals were withdrawn from the equilibrium cell once the gas was vented and the cell was opened. Due to the change in equilibrium condition, the crystals were not the same as in their equilibrium state. The taste of the crystals was also sweet. The crystals withdrawn from the sucrose solution were white and strong, however, the crystals removed from sugarcane juice were brownish with a softer texture.

a)   b)
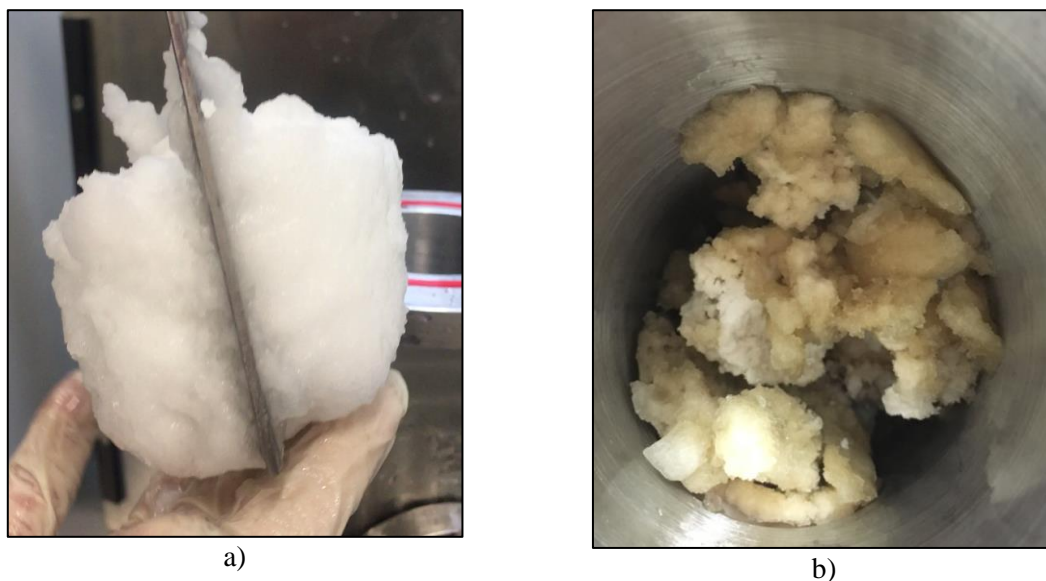
Figure 6-28. Photographs of the hydrate crystals after measurements; **a**: hydrate crystals from sucrose solution; **b**: hydrate crystals from sugarcane juice.

6.8 Evaluation of energy requirement

6.8.1 Energy requirement for evaporation

In the sugar factory, before the evaporation process, juice flows through a mixed and clear juice tank at temperatures between 338.15 to 348.15 K. It is then preheated to a temperature 2-3 K hotter than the juice boiling point which is normally 376.15 K. Thereafter hot lime is added to the juice at the same temperature and it is flashed down to its boiling point. The juice is then clarified. Due to the design of the clarifier, the juice is cooled down to 368.15 K. It is then preheated, pressurised, and introduced to the first effect at the temperature of 385.15 K.

In a typical quadruple evaporation process, sugar cane juice is heated using four continuous evaporators, bringing the initial concentration of 12 to 55 °Brix. The final product reported at current sugar factories is at 60 to 70 °Brix with a target of around 65 °Brix (Foxon, 2019). This batch-based process shown in figure 6-29 is adapted from the Handbook of cane sugar engineering (Hugot, 2014).
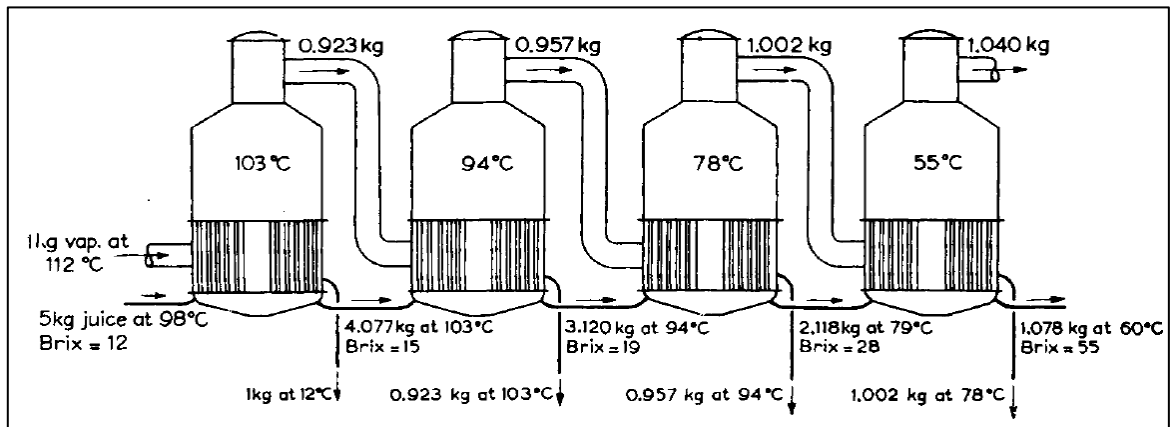
Figure 6-29. A typical relative multi-effect evaporation configuration for sugar cane juice concentration process (Hugot, 2014).

An energy balance was used to calculate the energy required for the process in figure 6-29. The specific heat capacity of juices, syrups, and molasses were calculated as follows (Hugot, 2014):

$$c_p = 1 - 0.006 \times B \hspace{3cm} 6.2$$

Where C_p is the specific heat (kcal.kg^{-1}.C^{-1}), and B is the °Brix of the solution. Figure 6-30 shows detailed information about the energy balance over the first effect. The calculated heat entering and exiting the first effect are listed in table 6-24. The three streams of juice condensate (stream 3), sugar cane juice (stream 4), and vapourised water (stream 5) leaving each effect add to the heat loss. The

heat loss for the first to fourth effects are 1.25, 1, 0.75 and 0.5 % of total heat entering each effect (Hugot, 2014). It can also be calculated from the difference of the entering and exiting heat.

6.8.1.1 Energy balance over the first effect

During the evaporation process, the pressurized feed of sugarcane juice and steam enters the first evaporator and undergoes a physical reaction of phase change. Furthermore, the internal energy of the material involved is changed. Based on the conservation of energy, the total energy of the evaporator remains constant. Considering the heat loss, the energy balance is:

$$\sum H_{in} = H_{heatloss} + \sum H_{out}$$
6.3

The heat of steam entering is taken from a steam table of dry saturated steam. The temperature gradient is the temperature difference of the current state with the reference state which is 0 °C (Hugot, 2014). The enthalpy of the feed sugar cane juice is calculated as follows:

$$Q_{juice} = m_{juice} \times C_{p_{juice}} \times \Delta T_{juice}$$

$$\Delta T_{juice} = T_{juice} - T_{ref} = T_{juice}$$

$$Q_{juice} = m_{juice} \times C_{p_{juice}} \times T_{juice}$$
6.4

$$Q_{steam} = m_{steam} \times \lambda_{steam}$$
6.5

Where *m, C_p, T,* and λ are mass, heat capacity, temperature and the latent heat of the steam, respectively. Three streams of the recovered water from juice, the residue of the juice and condensed vapour exits the evaporator adding to the heat loss.

Figure 6-30. Detailed information on the energy balance around the 1st effect.

The enthalpy of steam is calculated via the steam table, and equation 6.4 is applied for the juice and condensate. The heat loss on the first effect is 1.25 % of total internal energy entering the evaporator. The summarised results of the calculated values for the first effect are provided in table 6.24.

$$Q_{stream_1} = 1 \, kg \times 643 \, kcal.\,kg^{-1} = 643 \, kcal$$
$$Q_{stream_2} = 5 \, kg \times 0.93 \, kcal.\,kg^{-1}.\,C^{-1} \times 98 \, C = 456 \, kcal$$
$$Q_{stream_3} = 1 \, kg \times 1 \, kcal.\,kg^{-1}.\,C^{-1} \times 112 \, C = 112 \, kcal$$
$$Q_{stream_4} = 4.077 \, kg \times 0.91 \, kcal.\,kg^{-1}.\,C^{-1} \times 103 \, C = 382 \, kcal$$
$$Q_{stream_5} = 0.923 \, kg \times 640 \, kcal.\,kg^{-1} = 591 \, kcal$$
$$Q_{heatloss_1} = 0.0125 \times (643 \, kcal + 456 \, kcal) = 14 \, kcal$$

Table 6-24. Calculated energy entering and exiting the first effect (as shown in figure 6-30).

Substance	Stream in		Stream out	
	m_{in} (kg)	H_{in} (kcal)	m_{out} (kg)	H_{out} (kcal)
stream 1	1.000	643	——	——
stream 2	5.000	456	——	——
stream 3	——	——	1.000	112
stream 4	——	——	4.077	382
stream 5	——	——	0.923	591
heat loss	——	——	——	14

6.8.1.2 Energy balance over the second effect

The steam generated from the first effect is the heat source for evaporation in the second effect. Concentrated juice enters the second evaporator as the feed. Figure 6-31 shows detailed information on the energy balance around the second effect. The calculation of the enthalpy of the streams is the same as the previous section. The only difference is that the heat loss on the second effect is 1 % of the total energy entering the evaporator (Hugot, 2014). The calculated energies of the streams entering and exiting the second effect are listed in table 6-25.
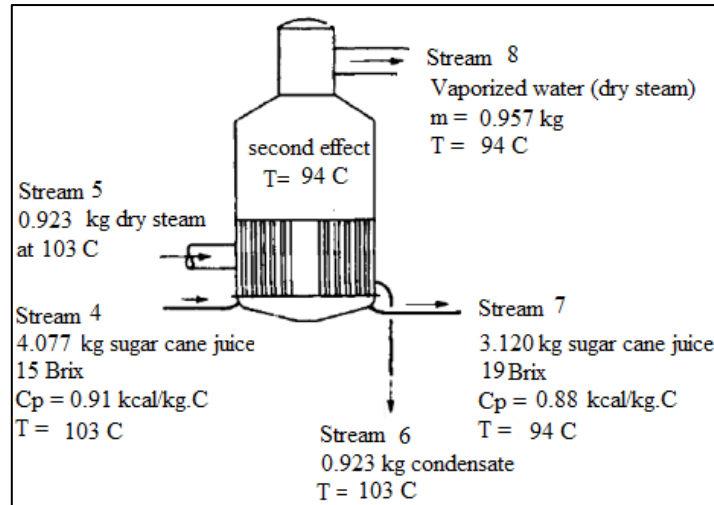
Figure 6-31. Detailed information on the energy balance around the 2nd effect.

The enthalpy of steam is calculated via the steam table, and equation 6.4 is applied for the juice and condensate. The summarised results of the calculated values for the 2nd effect is provided in table 6.25.

$$Q_{stream_6} = 0.923 \text{ kg} \times 1 \text{ } kcal.kg^{-1}.\text{ }°C^{-1} \times 103\text{ }°C = 95 \text{ } kcal$$
$$Q_{stream_7} = 3.120 \text{ } kg \times 0.88 \text{ } kcal.kg^{-1}.\text{ }°C^{-1} \times 94 \text{ }°C = 258 \text{ } kcal$$
$$Q_{stream_8} = 0.957 \text{ } kg \times 637 \text{ } kcal.kg^{-1} = 610 \text{ } kcal$$
$$Q_{heatloss_2} = 0.01 \times (591 \text{ } kcal + 382 \text{ } kcal) = 10 \text{ } kcal$$

Table 6-25. Calculated heat entering and exiting the 2nd effect (as shown in figure 6-31).

	Stream in		Stream out	
Substance	m_{in} (kg)	H_{in} (kcal)	m_{out} (kg)	H_{out} (kcal)
stream 4	0.923	591	——	——
stream 5	4.077	382	——	——
stream 6	——	——	0.923	95
stream 7	——	——	3.120	258
stream 8	——	——	0.957	610
heat loss	——	——	——	10

6.8.1.3 Energy balance over the third effect

The steam generated from the second effect is used as a heating medium for the third effect, and the residue of the sugarcane juice enters the third effect as the feed. Figure 6-32 shows detailed information on the energy balance around the second effect.
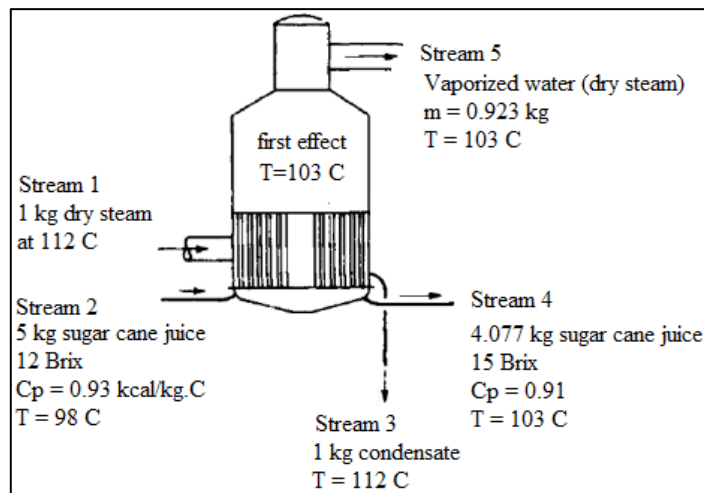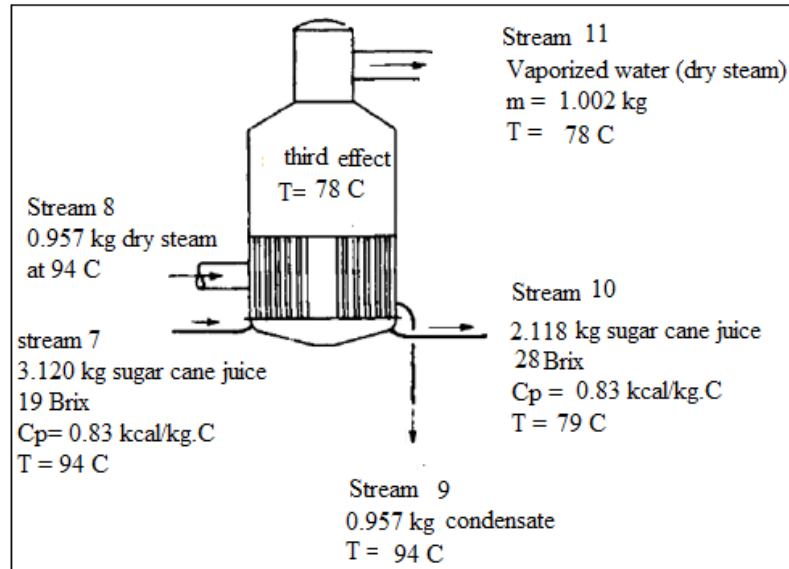
Figure 6-32. Detailed information on the energy balance around the 3ʳᵈ effect.

The enthalpy of steam is calculated using the steam table, and equation 6.4 is applied for the juice and condensate. The heat loss on the 3ʳᵈ effect is 0.75 % of total internal energy entering the evaporator. The summarised results of the calculated values for the 2ⁿᵈ effect is provided in table 6.26.

$$Q_{stream_9} = 0.957 \text{ kg} \times 1 \text{ kcal.kg}^{-1}.\,°C^{-1} \times 94 \,°C = 90 \text{ kcal}$$
$$Q_{stream_{10}} = 2.118 \text{ kg} \times 0.83 \text{ kcal.kg}^{-1}.\,°C^{-1} \times 79 \,°C = 139 \text{ kcal}$$
$$Q_{stream_{11}} = 1.002 \text{ kg} \times 631 \text{ kcal.kg}^{-1} = 632 \text{ kcal}$$
$$Q_{heatloss_3} = 0.0075 \times (610 \text{ kcal} + 258 \text{ kcal}) = 7 \text{ kcal}$$

Table 6-26. Calculated heat entering and exiting the 3ʳᵈ effect (as shown in figure 6-32).

Substance	Stream in		Stream out	
	m_{in} (kg)	H_{in} (kcal)	m_{out} (kg)	H_{out} (kcal)
stream 7	3.120	258	——	——
stream 8	0.957	610	——	——
stream 9	——	——	0.957	90
stream 10	——	——	2.118	139
stream 11	——	——	1.002	632
heat loss	——	——	——	7

In general, to achieve 28 °Brix from 12 °Brix, 2940 kcal (12301 kJ) is required. With the total 1 kg of supplied steam at the temperature of 112 ° C, 0.923, 0.957, 1.002 and 1.040 kg of water was removed from the first to fourth effect, respectively. The heat supplied was transferred to the juice to remove water as steam, and the generated steam is used in the next effect. These calculations were only performed for a simple case of the evaporation up to a certain concentration as a preliminary benchmarking exercise. There is an additional energy demand for vapour bleeds in the sugar factory.

Consequently, the amount of steam that goes into the first effect is substantially greater than calculated for this case.

6.8.1.4 Estimation of the energy requirement for hydrate-based concentration

From the hydrate experiments performed, only one effect of gas hydrate technology is required to achieve a concentration of 30.10 from 12 °Brix sugarcane juice. The energy required for just one effect is obtained via an energy balance around the hydrate system. The sugarcane juice provided upstream is at 95 °C and a pressure of 0.10 MPa. Here the system is considered as the reactor which operates at the optimum temperature and pressure of 274.65 K and 3.70 MPa, respectively. The gas must therefore be pressurised to 3.70 MPa using a compressor, and the juice must be cooled to the desired temperature. The schematic diagram of the system proposed is shown in figure 6-33.

After the juice is cooled from 95 to 1.5 °C in the heat exchanger, it is mixed with pressurised CO_2 gas in the reactor. When the hydrate forms, the slurry and gas is transferred to the centrifuge to separate the juice from the hydrate crystals. The juice residue and gas is then transferred to the separation column to recover the gas and remove the concentrated juice. The separated hydrate is moved to the melter where clean water and released gas from decomposed gas hydrates are separated. The recovered gases are combined with the CO_2 feed gas to be recycled in the process.
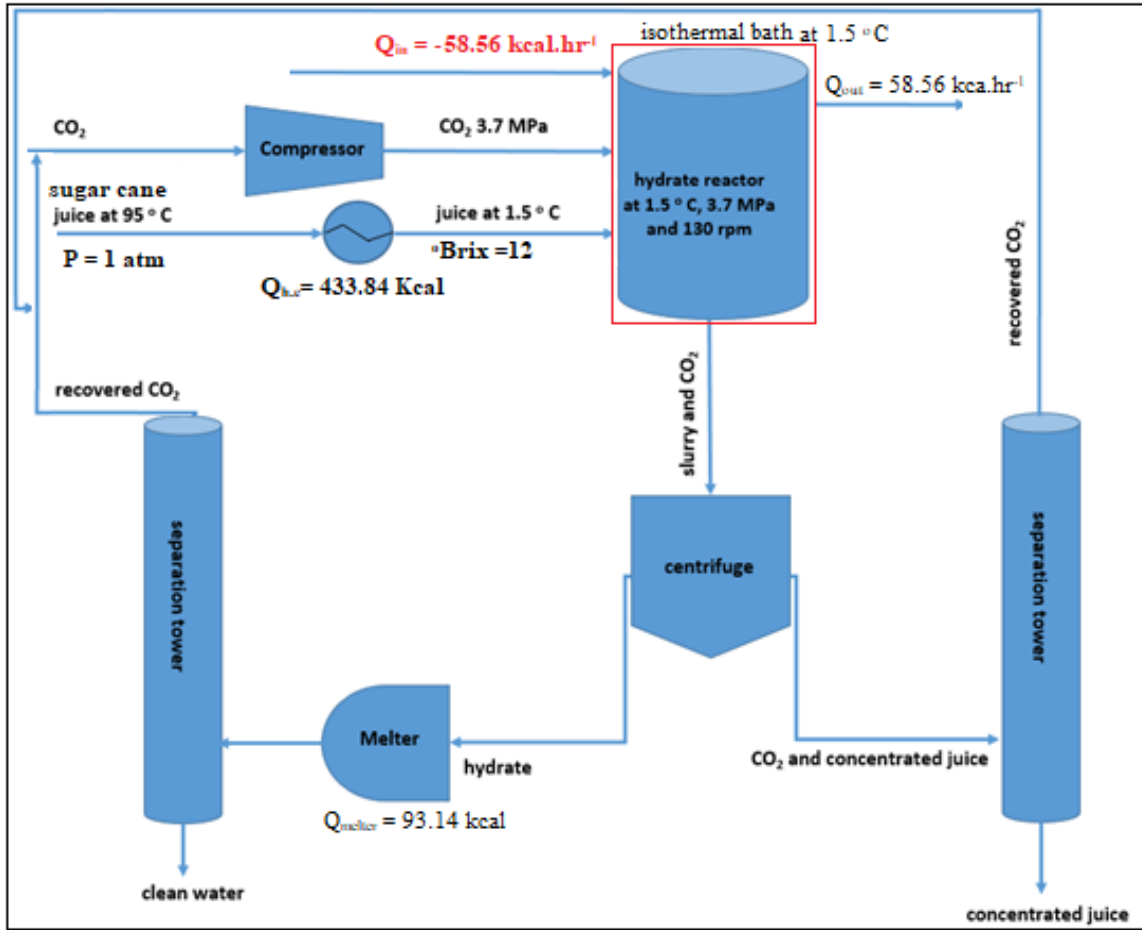
Figure 6-33. The proposed process for concentrating sugar cane juice from 12 to 30 °Brix using gas hydrate technology.

The total heat required for the process in forming hydrates consists of three elements; the heat exchanger, hydrate formation and melter. The reactor walls are assumed to be thin and with no effect on heat transfer. The reactor operates at 1.5 °C which is below the ambient temperature. It is assumed to be isolated from the environment with a cold water jacket around it to maintain the temperature at the desired level for the duration of hydrate formation. For a 5 kg feed, a reactor with an optimal volume of 24 litres is required. It is assumed that the reactor is kept in a jacket containing 72 litres water.

$$Q_{total} = Q_{heat\ exchanger} + Q_{hydrate\ formation} + Q_{chilling\ unit} - Q_{melter} \qquad 6.6$$

The heat required for the heat exchanger is calculated as follows:

$$Q_{heat\ exchanger} = m \times Cp \times \Delta T = 5kg \times (1 - 0.006 \times 12\ kcal.kg^{-1}.°C^{-1}) \times (1.5 - 95)°C$$
$$= -433.84\ kcal$$

The heat required in the reactor is the latent heat of phase change. The enthalpy of CO_2 gas hydrate formation is 333.12 kJ.kg^{-1} (79.61 kcal/kg) at pressures between (1.00 to 4.00) MPa and temperatures between (273.35 to 284.15) K (Jemai et al., 2014). The mass of hydrate formed was previously calculated from the kinetic measurements and for this case is 1.117 kg. The heat required is calculated as follows:

$$Q_{reactor} = Q_{phase\ change} = -m_{formedhydrate} \times H_{phase\ change} = 1.117\ kg \times 79.61\ kcal.kg^{-1}$$
$$= -93.14\ kcal$$

The mass of the decomposed hydrates in the melter is the same as the mass in the reactor. Therefore, one can assume that the same amount of energy is required to melt the hydrate that is formed. Further assumptions include the energy required to decrease the temperature of the reactor, firstly from room temperature to the hydrate formation conditions, then to maintain this during the process. To determine this energy demand, the energy requirement was determined on the laboratory scale requirement of an insulated isothermal bath (SS 316L with internal dimensions of 40 × 40 × 60 cm, with a composite wall made of two stainless steel sheets of 1 mm thickness and 10 mm space between, filled with glass wool). The energy required by the chilling unit is:

$$Q_{chilling\ unit} = Q_{bath\ liquid} - Q_{heat\ flux}$$
$$Q_{bath\ liquid} = m \times Cp \times \Delta T = 72\ kg \times (1\ kcal.kg^{-1}.°C^{-1}) \times (1.5 - 25)°C = -1692\ kcal$$

The energy required to maintain the system temperature in the desired temperature of 1.5 °C is calculated via the heat flux of the walls. The heat flux of glass wool and SS 316L are 0.023 and 15 W.m^{-1}.K^{-1}, respectively. The overall heat transfer coefficient is calculated as follows:

$$U = \frac{1}{\frac{L_1}{K_1} + \frac{L_2}{K_2} + \frac{L_3}{K_3}} \qquad 6.7$$

$$U = \frac{1}{\frac{0.001}{15} + \frac{0.01}{0.023} + \frac{0.001}{15}} = 2.299\ W.m^{-2}.K^{-1}$$

L and K are wall thickness and conduction heat transfer coefficient. The heat flux is calculated as follows:

$$Q_{heat\ flux} = UA\Delta T = 2.299\ W.m^{-2}.K^{-1} \times 1.26\ m^2 \times (25 + 273.15 - 1.5 - 273.15)K =$$
$$68.06\ \left(\frac{J}{s}\right) = 245.02\ \frac{kJ}{hr} = 58.56\ \frac{Kcal}{hr}$$

The hydrate formation process takes approximately 4 hours. This requires a significant amount of energy input. The total energy requirement for maintaining this stage of the process is calculated as follows.

$$Q_{chilling\ unit} = -1692\ kcal - 4\ hr \times 58.56\ kcal.hr^{-1} = -1926.24\ kcal$$

The total heat required for the process is calculated using equation 6.6:

$$Q_{total} = Q_{heat\ exchanger} + Q_{hydrate\ formation} - Q_{melter} + Q_{chilling\ unit}$$
$$= -433.84\ kcal - 93.14\ kcal + 93.14\ kcal - 1926.24\ kcal = -2360.08\ kcal$$

In summary, the total energy required is 9912.34 kJ (2360.08 kcal) for 5 kg 12 Brix sugar cane juice. To obtain a 30 °Brix juice from an initial concentration of 12 °Brix, the energy requirement is 20 % less than a three-stage evaporator train (2940 kcal; 12301 kJ). No capital costs have been accounted for, rather this is based solely on a preliminary assessment of the energy requirements (heating and cooling). A summary of the assessment of the utilities is presented in table 6-27.

Table 6-27. Summary of the benchmarking studies for gas hydrate and evaporation studies.

Technology	C final (°Brix)	No. of stages	Energy input (kcal)	T (° C)	P (MPa)
Hydrate	up to 60	3	2360 (1 stage ≈ 30 °Brix)	1.5	3.70
Evaporation	up to 70	5-6	2940 (3 stages ≈ 28 °Brix)	55 - 112	0.01-0.10

With evaporation technology, 3 stages are required to concentrate the sugarcane juice from 12 to 28 °Brix, while with hydrate technology only 1 stage is required to obtain a product of higher concentration, with 30 °Brix. The first 3 trains of evaporation technology operate at a temperatures range from 78 – 113 ° C with the last evaporator operating at 55 ° C, while hydrate technology operates at 1.5 ° C. The primary source of energy required for the hydrate process is the reactor cooling which uses +80% of the energy demand. A more efficient design of the cooling system with energy integration in the sugar cane factory could provide options for decreasing the energy demand. Furthermore, it is possible to perform further studies to enable higher operating temperatures for hydrate formation by the use of promoters or changing the gas (former) used. Given the number of

simplifications and assumptions in the presented work, consideration must be given to the energy demand for downstream heating in a sugar factory which will no longer be available by the evaporator station (the vapour bleeds). Furthermore, the actual sugar manufacturing processes takes place on a much bigger scale (e.g. 100 tonnes/hr). In order to consider such processes, one needs to put a lot of effort into the design of the chilling and maintenance of low temperature, which could lead to lower heat loss rates per unit flow of sugar juice. Hence, the cooling costs will probably be a lot lower than what is proposed in this study.

Evaporation is costly from the energy point of view but the technology is easily understood. It is a traditional well-understood process compared to the hydrate which is a new technology. Evaporation operates at the high-temperature range which is one of the major reasons (in addition to pH lower than 5) to initiate sucrose inversion. In addition, possibility of the caramelisation on the hot surfaces, sugar entrainment as well as the scale deposition on the internal walls of the evaporators are among other disadvantages. These factors can be overcome using hydrate technology. However, more research and work needs to be spent on understanding the physical separation aspects. The design of the separators needs to be improved such that maintenance of the system at low temperature does not require significant energy. The current development level of the gas hydrate technology shows that more efforts need to be done to develop the equipment, reactor and separator which would provide the possibility of commercialisation.

Chapter 7: Conclusion

A new pilot rig, with a 750 ml reactor designed in the Thermodynamics Research Unit was commissioned in this study. The new design included windows for viewing the cell content, an improved agitation system and enabled samples withdrawal for analysis of the concentrated solution. Thermodynamic phase equilibria data were generated for the systems {CO_2 + sucrose or fructose solution} at the temperature range of (274.3 – 282.6) K and pressures up to 4.01 MPa.

The measured data were regressed via the gamma-phi ($\gamma - \emptyset$) approach using the PR EOS in combination with the NRTL, UNIQUAC or the UNIFAC group contribution model. Satisfactory correlation of the experimental and model data was well within 1% AAD (P).

Kinetic data were measured for the systems {CO_2 + sucrose solution} in the concentration range of 0, 12, 20, 30, and 35 °Brix sucrose solution.

The effect of initial pressure and temperature were tested on the kinetics of hydrate measurement in the ranges of 2.70 – 3.10 MPa and 275.15 – 276.15 K, respectively, indicating the shorter induction time at higher pressures, lower temperatures and lower initial concentration of the sucrose solution.

The kinetic model was developed to obtain the hydrate formation rate (maximum of 0.043 $n_g.n_w^{-1}.min^{-1}$ at temperature, pressure and sucrose solution concentration of 275.15 K, 3.10 MPa, and 12 °Brix, respectively), apparent rate constant (maximum of 1.99 $\times$ 10^{-9} $n_g.n_w^{-1}.min^{-1}.Pa^{-1}$ at temperature, pressure and sucrose solution concentration of 275.65 K, 3.10 MPa, and 12 °Brix, respectively), gas consumption (maximum of 0.055 $n_g.n_{w0}^{-1}$ at temperature, pressure and sucrose solution concentration of 275.65 K, 3.10 MPa, and 12 °Brix, respectively), and storage capacity (maximum of 53.52 $v.v^{-1}$ at temperature, pressure and sucrose solution concentration of 275.65 K, 3.10 MPa, and 12 °Brix, respectively).

An increase of pressure at constant temperature affects the above-mentioned parameters directly. By contrast, a rise in temperature at constant pressure has an inverse effect.

The study of the effect of initial pressure (3.00 and 3.70 MPa), temperature (274.65 – 275.65 K), mixer speed (130 and 260 rpm) and mesh size (10, 26, 38 and 45 μm) on the concentration of the sucrose solutions helped achieved the optimum operating condition.

Hydrate formation for {CO_2 + sucrose solution} at temperature, pressure, mixer speed, and mesh size of 274.65 K, 3.70 MPa, 130 rpm, and 26 μm, respectively, resulted in the concentration of 12 °Brix feed to approximately 59.98 °Brix over three stages.

The concentration of the sugarcane juice solutions was performed at the optimum conditions with only four stages required to concentrate the sugarcane juice from 12 to 56.20 °Brix.

An analysis of the hydrate process for implementation in a sugar factory showed that using one hydrate stage to concentrate feed of 12 to 30 ℃Brix has the possibility to replace three evaporation units. A comparison of the energy usage was performed, which showed an approximate 20 % decrease in the energy requirement for this one stage over a three-effect evaporation train. The calculations were performed for a simple case with an aim to benchmark the initial concentration levels. This excluded the consideration of vapour bleed from evaporation trains as well as the temperature maintenance of the hydrate reactor. The vapour bleeds are normally used as an energy supply to the other parts of the sugar factory.

Chapter 8: Recommendations

As a continuation of this work, various measurements, modelling considerations, and equipment developments can be performed.

i.   Further experimental measurements using different gases such as methane, ethane, propane etc. should be performed to obtain the hydrate phase boundary for the new systems {of hydrate former + solutions}

ii.   Hydrate dissociation measurements for other carbohydrates such as fructose, glucose, dextrose and fruit juices either in pure or mixture form should be investigated.

iii. A comprehensive study of integrating the hydrate technology should be performed to combine the gas hydrate technology with the available evaporation trains to reduce the energy and cost requirements. This includes more attention to the evaporator station as a source of heating medium for other factory processes

iv.   Further equipment development should be conducted to study the crystal size at different thermodynamic conditions. This can be done by modifying the hydrate equipment to withdraw samples from hydrate crystals, which also will provide the possibility to analyse the composition of the samples to investigate the carbohydrates retained in the crystals.

v.   Further work on the hydrate formation process and the change in crystal size at various thermo-physical conditions should be studied. This will enable an understanding of the hydrate structure during hydrate formation and the dissociation process.

vi.   The thermodynamic model used for the inhibition effect of the carbohydrates is based on empirical data. This can be extended via including experimental phase equilibrium data.

vii. Further work can be performed to investigate the cause of the pH change in the gas hydrate experiments and to propose strategies to mitigate this effect.

References

ABRAMS, D. S. & PRAUSNITZ, J. M. 1975. Statistical thermodynamics of liquid mixtures: a new expression for the excess Gibbs energy of partly or completely miscible systems. *AIChE Journal,* 21**,** 116-128.

ALVAREZ, V., ALVAREZ, S., RIERA, F. & ALVAREZ, R. 1997. Permeate flux prediction in apple juice concentration by reverse osmosis. *Journal of Membrane Science,* 127**,** 25-34.

ALVES, V., KOROKNAI, B., BÉLAFI-BAKÓ, K. & COELHOSO, I. 2004. Using membrane contactors for fruit juice concentration. *Desalination,* 162**,** 263-270.

ANDERSEN, T. B. & THOMSEN, K. 2009. Separation of water through gas hydrate formation. *International Sugar Journal,* 111**,** 632-636.

ARJANG, S., MANTEGHIAN, M. & MOHAMMADI, A. 2013. Effect of synthesized silver nanoparticles in promoting methane hydrate formation at 4.7 MPa and 5.7 MPa. *Chemical Engineering Research and Design,* 91**,** 1050-1054.

BABAEE, S., HASHEMI, H., MOHAMMADI, A. H., NAIDOO, P. & RAMJUGERNATH, D. 2016. Experimental measurement and thermodynamic modelling of hydrate phase equilibrium conditions for krypton+n-butyl ammonium bromide aqueous solution. *The Journal of Supercritical Fluids,* 107**,** 676-681.

BAILEY, A., BARBE, A., HOGAN, P., JOHNSON, R. & SHENG, J. 2000. The effect of ultrafiltration on the subsequent concentration of grape juice by osmotic distillation. *Journal of Membrane Science,* 164**,** 195-204.

BÁNVÖLGYI, S., HORVÁTH, S., STEFANOVITS-BÁNYAI, É., BÉKÁSSY-MOLNÁR, E. & VATAI, G. 2009. Integrated membrane process for blackcurrant (Ribes nigrum L.) juice concentration. *Desalination,* 241**,** 281-287.

BARDUHN, A. J. 1968. The state of the crystallization processes for desalting saline waters. *Desalination,* 5**,** 173-184.

BARDUHN, A. J., TOWLSON, H. E. & HU, Y. C. 1962. The properties of some new gas hydrates and their use in demineralizing sea water. *AIChE Journal,* 8**,** 176-183.

BELANDRIA, V., ESLAMIMANESH, A., MOHAMMADI, A. H., THÉVENEAU, P., LEGENDRE, H. & RICHON, D. 2011. Compositional analysis and hydrate dissociation conditions measurements for carbon dioxide+ methane+ water system. *Industrial & Engineering Chemistry Research,* 50**,** 5783-5794.

BERNARDO, P., DRIOLI, E. & GOLEMME, G. 2009. Membrane gas separation: a review/state of the art. *Industrial & Engineering Chemistry Research,* 48**,** 4638-4663.

BOND, D. C. & RUSSELL, N. B. 1949. Effect of antifreeze agents on the formation of hydrogen sulphide hydrate. *Transactions of the AIME,* 179**,** 192-198.

CAO, Z., TESTER, J. W., SPARKS, K. A. & TROUT, B. L. 2001. Molecular computations using robust hydrocarbon−water potentials for predicting gas hydrate phase equilibria. *The Journal of Physical Chemistry B,* 105**,** 10950-10960.

CARBONE, A. S., IVALL, J. R. & SERVIO, P. D. 2012. H–Lw–V Equilibrium measurements of pure methane gas in the presence of d-(+)-glucose. *Journal of Chemical & Engineering Data,* 57**,** 974-977.

CARROLL, J. 2014. *Natural gas hydrates: a guide for engineers*, Gulf Professional Publishing.

CASSANO, A., CONIDI, C. & DRIOLI, E. 2018. 8 Membrane-based operations and integrated membrane systems in fruit juice processing. *Membrane Engineering*, 255.

CASSANO, A., CONIDI, C., TIMPONE, R., D'AVELLA, M. & DRIOLI, E. 2007. A membrane-based process for the clarification and the concentration of the cactus pear juice. *Journal of Food Engineering,* 80, 914-921.

CASSANO, A. & DRIOLI, E. 2007. Concentration of clarified kiwifruit juice by osmotic distillation. *Journal of Food Engineering,* 79, 1397-1404.

CASSANO, A., DRIOLI, E., GALAVERNA, G., MARCHELLI, R., DI SILVESTRO, G. & CAGNASSO, P. 2003. Clarification and concentration of citrus and carrot juices by integrated membrane processes. *Journal of Food Engineering,* 57, 153-163.

CHEN, G.-J. & GUO, T.-M. 1996. Thermodynamic modeling of hydrate formation based on new concepts. *Fluid Phase Equilibria,* 122, 43-65.

CHEN, J. C. & CHOU, C. C. 1993. *Cane sugar handbook: a manual for cane sugar manufacturers and their chemists*, John Wiley & Sons.

CHEN, P., CHEN, X. D. & FREE, K. W. 1998. Solute inclusion in ice formed from sucrose solutions on a sub-cooled surface—an experimental study. *Journal of Food Engineering,* 38, 1-13.

CHEN, P., CHEN, X. D. & FREE, K. W. 1999. An experimental study on the spatial uniformity of solute inclusion in ice formed from falling film flows on a sub-cooled surface. *Journal of Food Engineering,* 39, 101-105.

CHEN, X. D., WU, W. D. & CHEN, P. 2015. An analytical relationship of concentration-dependent interfacial solute distribution coefficient for aqueous layer freeze concentration. *AIChE Journal,* 61, 1334-1344.

CHUDOTVORTSEV, I. & YATSENKO, O. 2007. Concentration and temperature of eutectic points in glucose-water and saccharose-water systems, determined by the method of fractional melting of ice. *Russian Journal of Applied Chemistry,* 80, 201-205.

CHUN, M.-K. & LEE, H. 1998. Phase equilibria of R22 ($CHClF_2$) hydrate system in the presence of sucrose, glucose and lactic acid. *Fluid Phase Equilibria,* 150-151, 361-370.

CHUN, M.-K. & LEE, H. 1999. Phase equilibria of carbon dioxide hydrate system in the presence of sucrose, glucose, and fructose. *Journal of Chemical & Engineering Data,* 44, 1081-1084.

CURCIO, S., CALABRO, V., IORIO, G. & DE CINDIO, B. 2001. Fruit juice concentration by membranes: effect of rheological properties on concentration polarization phenomena. *Journal of Food Engineering,* 48, 235-241.

DAHL, S. & MICHELSEN, M. L. 1990. High-pressure vapor-liquid equilibrium with a UNIFAC-based equation of state. *AIChE Journal,* 36, 1829-1836.

DARDE, V., VAN WELL, W. J. M., STENBY, E. H. & THOMSEN, K. 2010. Modeling of Carbon Dioxide Absorption by Aqueous Ammonia Solutions Using the Extended UNIQUAC Model. *Industrial & Engineering Chemistry Research,* 49, 12663-12674.

DASHTI, H., ZHEHAO YEW, L. & LOU, X. 2015. Recent advances in gas hydrate-based CO_2 capture. *Journal of Natural Gas Science and Engineering,* 23, 195-207.

DEATON, W. & FROST, E. 1937. Gas hydrates in natural gas pipe lines. *American Gas Journal.;(United States),* 146.

DEHAGHANI, A. H. S. & BADIZAD, M. H. 2016. Thermodynamic modeling of gas hydrate formation in presence of thermodynamic inhibitors with a new association equation of state. *Fluid Phase Equilibria,* 427**,** 328-339.

DELAHAYE, A., FOURNAISON, L., MARINHAS, S., CHATTI, I., PETITET, J.-P., DALMAZZONE, D. & FÜRST, W. 2006. Effect of THF on equilibrium pressure and dissociation enthalpy of CO_2 hydrates applied to secondary refrigeration. *Industrial & Engineering Chemistry Research,* 45**,** 391-397.

DELAVAR, H. & HAGHTALAB, A. 2015. Thermodynamic modeling of gas hydrate formation conditions in the presence of organic inhibitors, salts and their mixtures using UNIQUAC model. *Fluid Phase Equilibria,* 394**,** 101-117.

DESTANI, F., CASSANO, A., FAZIO, A., VINCKEN, J.-P. & GABRIELE, B. 2013. Recovery and concentration of phenolic compounds in blood orange juice by membrane operations. *Journal of Food Engineering,* 117**,** 263-271.

DHARMAWARDHANA, P., PARRISH, W. & SLOAN, E. 1980. Experimental thermodynamic parameters for the prediction of natural gas hydrate dissociation conditions. *Industrial & Engineering Chemistry Fundamentals,* 19**,** 410-414.

DUC, N. H., CHAUVY, F. & HERRI, J.-M. 2007. CO_2 capture by hydrate crystallization–A potential solution for gas emission of steelmaking industry. *Energy Conversion and Management,* 48**,** 1313-1322.

DURAN-VALENCIA, C., VALTZ, A., GALICIA-LUNA, L. A. & RICHON, D. 2001. Isothermal vapor−liquid equilibria of the carbon dioxide (CO_2)−n,n-dimethylformamide (DMF) system at temperatures from 293.95 K to 338.05 K and pressures up to 12 MPa. *Journal of Chemical & Engineering Data,* 46**,** 1589-1592.

ECHAVARRÍA, A., FALGUERA, V., TORRAS, C., BERDUN, C., PAGÁN, J. & IBARZ, A. 2012. Ultrafiltration and reverse osmosis for clarification and concentration of fruit juices at pilot plant scale. *LWT-Food Science and Technology,* 46**,** 189-195.

ENGLEZOS, P. 1994. The freeze concentration process and its applications. *Developments in Chemical Engineering and Mineral Processing,* 2**,** 3-15.

ENGLEZOS, P. & BISHNOI, P. 1991. Experimental study on the equilibrium ethane hydrate formation conditions in aqueous electrolyte solutions. *Industrial & Engineering Chemistry Research,* 30**,** 1655-1659.

ENGLEZOS, P., KALOGERAKIS, N., DHOLABHAI, P. & BISHNOI, P. 1987. Kinetics of formation of methane and ethane gas hydrates. *Chemical Engineering Science,* 42**,** 2647-2658.

ESLAMIMANESH, A., MOHAMMADI, A. H. & RICHON, D. 2011. Thermodynamic model for predicting phase equilibria of simple clathrate hydrates of refrigerants. *Chemical Engineering Science,* 66**,** 5439-5445.

FAN, S.-S. & GUO, T.-M. 1999. Hydrate formation of CO_2-rich binary and quaternary gas mixtures in aqueous sodium chloride solutions. *Journal of Chemical & Engineering Data,* 44**,** 829-832.

FARHANG, F., NGUYEN, A. V. & HAMPTON, M. A. 2014a. Influence of sodium halides on the kinetics of CO_2 hydrate formation. *Energy & Fuels,* 28**,** 1220-1229.

FARHANG, F., NGUYEN, A. V. & SEWELL, K. B. 2014b. Fundamental investigation of the effects of hydrophobic fumed silica on the formation of carbon dioxide gas hydrates. *Energy & Fuels,* 28**,** 7025-7037.

FARNWORTH, E., LAGACE, M., COUTURE, R., YAYLAYAN, V. & STEWART, B. 2001. Thermal processing, storage conditions, and the composition and physical properties of orange juice. *Food Research International,* 34**,** 25-30.

FASTONLINE 2017. Raw sugar manufacturing flow chart. *Faith and Sustainability Journal.*

FAZLALI, A., KAZEMI, S. A., KESHAVARZ-MORAVEJI, M. & MOHAMMADI, A. H. 2013. Impact of different surfactants and their mixtures on methane-hydrate formation. . *Energy Technology,* 1**,** 471-477.

FLESLAND, O. 1995. Freeze concentratton by layer crystallization. *Drying Technology,* 13**,** 1713-1739.

FOXON, K. 2019. Personal communication, Sugar Milling Research Institute.

FREDENSLUND, A., JONES, R. L. & PRAUSNITZ, J. M. 1975. Group-contribution estimation of activity coefficients in nonideal liquid mixtures. *AIChE Journal,* 21**,** 1086-1099.

FRENKEL, M., CHIRICO, R., DIKY, V., YAN, X., DONG, Q. & MUZNY, C. 2005. NIST ThermoData Engine 6.0. National Institute of Standards and Technology. Thermodynamics Research Center (TRC). NIST Applied Chemicals and Materials Division: USA.

GARCIA-CASTELLO, E. M., MCCUTCHEON, J. R. & ELIMELECH, M. 2009. Performance evaluation of sucrose concentration using forward osmosis. *Journal of Membrane Science,* 338**,** 61-66.

GNANENDRAN, N. & AMIN, R. 2004. Equilibrium hydrate formation conditions for hydrotrope–water–natural gas systems. *Fluid Phase Equilibria,* 221**,** 175-187.

GUIGNON, B., APARICIO, C., SANZ, P. & OTERO, L. 2012. Orange juice pvT-properties for high pressure processing and modeling purposes: Importance of soluble solids concentration. *Food Research International,* 46**,** 83–91.

GUL, S. & HARASEK, M. 2012. Energy saving in sugar manufacturing through the integration of environmental friendly new membrane processes for thin juice pre-concentration. *Applied Thermal Engineering,* 43**,** 128-133.

GUNKO, S., VERBYCH, S., BRYK, M. & HILAL, N. 2006. Concentration of apple juice using direct contact membrane distillation. *Desalination,* 190**,** 117-124.

HAMMERSCHMIDT, E. 1934. Formation of gas hydrates in natural gas transmission lines. *Industrial & Engineering Chemistry,* 26**,** 851-855.

HAPPEL, J., HNATOW, M. A. & MEYER, H. 1994. The study of separation of nitrogen from methane by hydrate formation using a novel apparatus. *Annals of the New york Academy of Sciences,* 715**,** 412-424.

HASHEMI, H., BABAEE, S., MOHAMMADI, A. H., NAIDOO, P. & RAMJUGERNATH, D. 2015. Experimental measurements and thermodynamic modeling of refrigerant hydrates dissociation conditions. *The Journal of Chemical Thermodynamics,* 80**,** 30-40.

HASHEMI, H., BABAEE, S., NAIDOO, P., MOHAMMADI, A. H. & RAMJUGERNATH, D. 2014. Experimental measurements and thermodynamic modeling of clathrate hydrate dissociation conditions for refrigerants R116, R23, and their mixture R508B. *Journal of Chemical & Engineering Data,* 59**,** 3907-3911.

HOLDER, G., CORBIN, G. & PAPADOPOULOS, K. 1980. Thermodynamic and molecular properties of gas hydrates from mixtures containing methane, argon, and krypton. *Industrial & Engineering Chemistry Fundamentals,* 19**,** 282-286.

HONGVALEERAT, C., CABRAL, L. M., DORNIER, M., REYNES, M. & NINGSANOND, S. 2008. Concentration of pineapple juice by osmotic evaporation. *Journal of Food Engineering,* 88**,** 548-552.

HONIG, P. 1963. The Chemistry of evaporation process. Elsevier Publishing Company Amsterdam-London-New York.

HOUGH, J. S., BRIGGS, D. E., STEVENS, R. & YOUNG, T. W. 2012. *Malting and Brewing Science: volume II hopped wort and beer*, Springer.

HU, A., ZHENG, J. & QIU, T. 2006. Industrial experiments for the application of ultrasound on scale control in the Chinese sugar industry. *Ultrasonics Sonochemistry,* 13**,** 329-333.

HUANG, C. P., FENNEMA, O. & POWRIE, W. D. 1965. Gas hydrates in aqueous-organic systems: I. Preliminary studies. *Cryobiology,* 2**,** 109-115.

HUGOT, E. 2014. *Handbook of cane sugar engineering*, Elsevier.

HUIGE, N. & THIJSSEN, H. 1972. Production of large crystals by continuous ripening in a stirrer tank. *Journal of Crystal Growth,* 13-14**,** 483-487.

IGWEMMAR, N., KOLAWOLE, S. & IMRAN, I. 2013. Effect of heating on vitamin C content of some selected vegetables. *International Journal of Scientific &Technology Research,* 2**,** 209-212.

ILANI-KASHKOULI, P., MOHAMMADI, A. H., NAIDOO, P. & RAMJUGERNATH, D. 2016. Hydrate phase equilibria for CO_2 , CH_4, or N_2+ tetrabutylphosphonium bromide (TBPB) aqueous solution. *Fluid Phase Equilibria,* 411**,** 88-92.

JAVANMARDI, J., AYATOLLAHI, S., MOTEALLEH, R. & MOSHFEGHIAN, M. 2004. Experimental measurement and modeling of R22 ($CHClF_2$) hydrates in mixtures of acetone+ water. *Journal of Chemical & Engineering Data,* 49**,** 886-889.

JAVANMARDI, J., BABAEE, S., ESLAMIMANESH, A. & MOHAMMADI, A. H. 2012. Experimental measurements and predictions of gas hydrate dissociation conditions in the presence of methanol and ethane-1, 2-diol aqueous solutions. *Journal of Chemical & Engineering Data,* 57**,** 1474-1479.

JAVANMARDI, J., NASRIFAR, K., NAJIBI, S. & MOSHFEGHIAN, M. 2005. Economic evaluation of natural gas hydrate as an alternative for natural gas transportation. *Applied Thermal Engineering,* 25**,** 1708-1723.

JEMAI, K., KVAMME, B. & VAFAEI, M. T. 2014. Theoretical studies of CO_2 hydrates formation and dissociation in cold aquifers using RetrasoCodeBright simulator. *Reactive transport modelling of hydrate phase transition dynamics in porous media*.

JESUS, D., LEITE, M., SILVA, L., MODESTA, R., MATTA, V. & CABRAL, L. 2007. Orange (Citrus sinensis) juice concentration by reverse osmosis. *Journal of Food Engineering,* 81**,** 287-291.

JIAO, B., CASSANO, A. & DRIOLI, E. 2004. Recent advances on membrane processes for the concentration of fruit juices: a review. *Journal of Food Engineering,* 63**,** 303-324.

KAMATH, V. A. 1984. *Study of heat transfer characteristics during dissociation of gas hydrates in porous media.* Pittsburgh Univ., PA (USA).

KANG, K. C., LINGA, P., PARK, K.-N., CHOI, S.-J. & LEE, J. D. 2014. Seawater desalination by gas hydrate process and removal characteristics of dissolved ions (Na^+, K^+, Mg^{2+}, Ca^{2+}, B^{3+}, Cl^-, $SO4^{2-}$). *Desalination,* 353**,** 84-90.

KANG, S.-P., LEE, J. & SEO, Y. 2013. Pre-combustion capture of CO_2 by gas hydrate formation in silica gel pore structure. *Chemical Engineering Journal,* 218**,** 126-132.

KAWASAKI, K., MATSUDA, A. & KADOTA, H. 2006. Freeze concentration of equal molarity solutions with ultrasonic irradiation under constant freezing rate: effect of solute. *Chemical Engineering Research and Design,* 84**,** 107-112.

KELLAND, M. A., MOI, N. & HOWARTH, M. 2013. Breakthrough in synergists for kinetic hydrate inhibitor polymers, hexaalkylguanidinium salts: tetrahydrofuran hydrate crystal growth inhibition and synergism with polyvinylcaprolactam. *Energy & Fuels,* 27**,** 711-716.

KESHAVARZ, L., JAVANMARDI, J., ESLAMIMANESH, A. & MOHAMMADI, A. H. 2013. Experimental measurement and thermodynamic modeling of methane hydrate dissociation conditions in the presence of aqueous solution of ionic liquid. *Fluid Phase Equilibria,* 354**,** 312-318.

KHOKHAR, A., GUDMUNDSSON, J. & SLOAN, E. 1998. Gas storage in structure H hydrates. *Fluid Phase Equilibria,* 150-151**,** 383-392.

KHOSRAVANI, E., MORADI, G. & SAJJADIFAR, S. 2013. An accurate thermodynamic model to predict phase behavior of clathrate hydrates in the absence and presence of methanol based on the genetic algorithm. *The Journal of Chemical Thermodynamics,* 57**,** 286-294.

KIHARA, T. 1953. Virial coefficients and models of molecules in gases. *Reviews of Modern Physics,* 25**,** 831.

KLAUDA, J. B. & SANDLER, S. I. 2000. A fugacity model for gas hydrate phase equilibria. *Industrial & Engineering Chemistry Research,* 39**,** 3377-3386.

KNOX, W. G., HESS, M., JONES, G. & SMITH, H. 1961. The hydrate process. *Chem. Eng. Prog,* 57**,** 66-71.

KOBAYASHI, A., SHIRAI, Y., NAKANISHI, K. & MATSUNO, R. 1996. A method for making large agglomerated ice crystals for freeze concentration. *Journal of Food Engineering,* 27**,** 1-15.

KOBAYASHI, R. & KATZ, D. L. 1949. Methane Hydrate at High Pressure. *Journal of Petroleum Technology,* 1**,** 66-70.

KONDORI, J., ZENDEHBOUDI, S. & JAMES, L. 2018. Evaluation of gas hydrate formation temperature for gas/water/salt/alcohol systems: utilization of extended UNIQUAC model and PC-SAFT equation of state. *Industrial & Engineering Chemistry Research,* 57**,** 13833-13855.

KONTOGEORGIS, G. M., FOLAS, G. K., MURO-SUÑÉ, N., VON SOLMS, N., MICHELSEN, M. L. & STENBY, E. H. 2007. Modelling of associating mixtures for applications in the oil & gas and chemical industries. *Fluid Phase Equilibria,* 261**,** 205-211.

KOROKNAI, B., CSANÁDI, Z., GUBICZA, L. & BÉLAFI-BAKÓ, K. 2008. Preservation of antioxidant capacity and flux enhancement in concentration of red fruit juices by membrane processes. *Desalination,* 228**,** 295-301.

KUJAWSKI, W., GIERSZEWSKA-DRUSYNSKA, M., SOBOLEWSKA, A., DOBRAK, A., GUELL, C., FERRANDO, M., LOPEZ, F. & WARCZOK, J. 2008. Application of pervaporation and osmotic membrane distillation in fruits and fruit juices processing. *International Symposium on Physico-Chemical Methods of the Mixtures Separation.*

KUJAWSKI, W., SOBOLEWSKA, A., JARZYNKA, K., GÜELL, C., FERRANDO, M. & WARCZOK, J. 2013. Application of osmotic membrane distillation process in red grape juice concentration. *Journal of Food Engineering,* 116**,** 801-808.

KUMAR, A., SAKPAL, T., LINGA, P. & KUMAR, R. 2013. Influence of contact medium and surfactants on carbon dioxide clathrate hydrate kinetics. *Fuel,* 105**,** 664-671.

KURIHARA, K., TOCHIGI, K. & KOJIMA, K. 1987. Mixing rule containing regular-solution and residual excess free energy. *Journal of Chemical Engineering of Japan,* 20**,** 227-231.

LI, S.-F., SHEN, Y.-M., LIU, D.-B., FAN, L.-H., ZHANG, Z.-G. & LI, W.-X. 2014. Orange juice concentration method based on C_2H_4 clathrate hydrate formation. . *Advance Journal of Food Science and Technology,* 6**,** 780-783.

LI, S., FAN, S., WANG, J., LANG, X. & LIANG, D. 2009. CO_2 capture from binary mixture via forming hydrate with the help of tetra-n-butyl ammonium bromide. *Journal of Natural Gas Chemistry,* 18**,** 15-20.

LI, S., QI, F., DU, K., SHEN, Y., LIU, D. & FAN, L. 2017. An energy-efficient juice concentration technology by ethylene hydrate formation. *Separation and Purification Technology,* 173**,** 80-85.

LI, S., SHEN, Y., LIU, D., FAN, L. & TAN, Z. 2015. Concentrating orange juice through CO_2 clathrate hydrate technology. *Chemical Engineering Research and Design,* 93**,** 773-778.

LINGA, P., KUMAR, R. & ENGLEZOS, P. 2007. Gas hydrate formation from hydrogen/carbon dioxide and nitrogen/carbon dioxide gas mixtures. *Chemical Engineering Science,* 62**,** 4268-4276.

LIRIO, C. F. D. S., PESSOA, F. L. P. & ULLER, A. M. C. 2013. Storage capacity of carbon dioxide hydrates in the presence of sodium dodecyl sulfate (SDS) and tetrahydrofuran (THF). *Chemical Engineering Science,* 96**,** 118-123.

LIU, L., FUJII, T., HAYAKAWA, K. & MIYAWAKI, O. 1998. Prevention of initial supercooling in progressive freeze-concentration. *Bioscience, Biotechnology, and Biochemistry,* 62**,** 2467-2469.

LOPEZ-QUIROGA, E., WANG, R., GOUSETI, O., FRYER, P. & BAKALIS, S. 2015. Modelling freezing processes of high concentrated systems. *IFAC-PapersOnLine,* 48**,** 749-754.

MA, Q.-L., CHEN, G.-J. & GUO, T.-M. 2003. Modelling the gas hydrate formation of inhibitor containing systems. *Fluid Phase Equilibria,* 205**,** 291-302.

MADAENI, S. & ZERESHKI, S. 2010. Energy consumption for sugar manufacturing. Part I: evaporation versus reverse osmosis. *Energy Conversion and Management,* 51**,** 1270-1276.

MADHURA, L., KANCHI, S., SABELA, M. I., SINGH, S., BISETTY, K. & INAMUDDIN 2018. Membrane technology for water purification. *Environmental Chemistry Letters,* 16**,** 343-365.

MAEKAWA, T. 2011. Equilibrium conditions of clathrate hydrates formed from carbon dioxide and aqueous acetone solutions. *Fluid Phase Equilibria,* 303**,** 76-79.

MAGNUSSEN, T., RASMUSSEN, P. & FREDENSLUND, A. 1981. UNIFAC parameter table for prediction of liquid-liquid equilibriums. *Industrial & Engineering Chemistry Process Design and Development,* 20**,** 331-339.

MAKOGON, T. Y., MEHTA, A. P. & SLOAN, E. D. 1996. Structure H and Structure I hydrate equilibrium data for 2,2-dimethylbutane with methane and xenon. *Journal of Chemical & Engineering Data,* 41**,** 315-318.

MANTEGHIAN, M., SAFAVI, S. M. M. & MOHAMMADI, A. 2013. The equilibrium conditions, hydrate formation and dissociation rate and storage capacity of ethylene hydrate in presence of 1, 4-dioxane. *Chemical Engineering Journal,* 217**,** 379-384.

MATTA, V., MORETTI, R. & CABRAL, L. 2004. Microfiltration and reverse osmosis for clarification and concentration of acerola juice. *Journal of Food Engineering,* 61**,** 477-482.

MCCORMACK, R. & NIBLOCK, G. 1998. Build and operate a clathrate desalination pilot plant. *US Bureau of Reclamation Water Treatment Technology Program Report,* 31.

MCCORMACK, R. A. & ANDERSEN, R. K. 1995. Clathrate desalination plant preliminary research study. Water treatment technology program report No. 5 (Final). Thermal Energy Storage, Inc., San Diego, CA (United States).

MCCORMACK, R. A. & NIBLOCK, G. A. 2000. *Investigation of high freezing temperature, zero ozone, and zero global warming potential, clathrate formers for desalination*, US Department of the Interior, Bureau of Reclamation, Technical Service.

MCEWEN, C. 1967. Tables for estimating sedimentation through linear concentration gradients of sucrose solution. *Analytical Biochemistry,* 20**,** 114-149.

MCHUNU, S. 2019. SA's sugar industry declining for the past 19 years. *BUSINESS REPORT*.

MIYAWAKI, O., GUNATHILAKE, M., OMOTE, C., KOYANAGI, T., SASAKI, T., TAKE, H., MATSUDA, A., ISHISAKI, K., MIWA, S. & KITANO, S. 2016. Progressive freeze-concentration of apple juice and its application to produce a new type apple wine. *journal of Food Engineering,* 171**,** 153-158.

MOHAMMADI, A., MANTEGHIAN, M., HAGHTALAB, A., MOHAMMADI, A. H. & RAHMATI-ABKENAR, M. 2014. Kinetic study of carbon dioxide hydrate formation in presence of silver nanoparticles and SDS. *Chemical Engineering Journal,* 237**,** 387-395.

MOHAMMADI, A., PAKZAD, M., MOHAMMADI, A. H. & JAHANGIRI, A. 2018. Kinetics of $(TBAF + CO_2)$ semi-clathrate hydrate formation in the presence and absence of SDS. *Petroleum Science,* 15**,** 375-384.

MOHAMMADI, A. H., ANDERSON, R. & TOHIDI, B. 2005. Carbon monoxide clathrate hydrates: equilibrium data and thermodynamic modeling. *AIChE Journal,* 51**,** 2825-2833.

MOHAMMADI, A. H. & RICHON, D. 2008. Thermodynamic model for predicting liquid water−hydrate equilibrium of the water− hydrocarbon system. *Industrial & Engineering Chemistry Research,* 47**,** 1346-1350.

MOHAMMADI, A. H., TOHIDI, B. & BURGASS, R. W. 2003. Equilibrium data and thermodynamic modeling of nitrogen, oxygen, and air clathrate hydrates. *Journal of Chemical & Engineering Data,* 48**,** 612-616.

MOOIJER-VAN DEN HEUVEL, M., SAWIRJO, N. & PETERS, C. 2006. Influence of fluoroalkanes on the phase behaviour of methane gas hydrate systems. *Fluid Phase Equilibria,* 241**,** 124-137.

MORADI, S., HAGHTALAB, A. & FAZLALI, A. 2013. Prediction of hydrate formation conditions in the solutions containing electrolyte and alcohol inhibitors and their mixtures using UNIQUAC-NRF models. *Fluid Phase Equilibria,* 349**,** 61-66.

MUNCK, J., SKJOLD-JØRGENSEN, S. & RASMUSSEN, P. 1988. Computations of the formation of gas hydrates. *Chemical Engineering Science,* 43**,** 2661-2672.

NENE, S., KAUR, S., SUMOD, K., JOSHI, B. & RAGHAVARAO, K. 2002. Membrane distillation for the concentration of raw cane-sugar syrup and membrane clarified sugarcane juice. *Desalination,* 147**,** 157-160.

NGEMA, P., NELSON, W., NAIDOO, P., RAMJUGERNATH, D. & RICHON, D. 2014a. Isothermal method for hydrate studies using a transparent variable volume cell. *Review of Scientific Instruments,* 85**,** 045123.

NGEMA, P. T., PETTICREW, C., NAIDOO, P., MOHAMMADI, A. H. & RAMJUGERNATH, D. 2014b. Experimental measurements and thermodynamic modeling of the dissociation conditions of clathrate hydrates for (refrigerant+ NaCl+ water) systems. *Journal of Chemical & Engineering Data,* 59**,** 466-475.

NOWAK, J., POPLEWSKA, I., ANTOS, D. & SEIDEL-MORGENSTERN, A. 2009. Adsorption behaviour of sugars versus their activity in single and multicomponent liquid solutions. *Journal of Chromatography A,* 1216**,** 8697-8704.

ONSEKIZOGLU, P., BAHCECI, K. S. & ACAR, M. J. 2010. Clarification and the concentration of apple juice using membrane processes: A comparative quality assessment. *Journal of Membrane Science,* 352**,** 160-165.

OSFOURI, S., AZIN, R., GHOLAMI, R. & IZADPANAH, A. A. 2015. Modeling hydrate formation conditions in the presence of electrolytes and polar inhibitor solutions. *The Journal of Chemical Thermodynamics,* 89**,** 251-263.

PAP, N., KERTÉSZ, S., PONGRÁCZ, E., MYLLYKOSKI, L., KEISKI, R. L., VATAI, G., LÁSZLÓ, Z., BESZÉDES, S. & HODÚR, C. 2009. Concentration of blackcurrant juice by reverse osmosis. *Desalination,* 241**,** 256-264.

PAP, N., PONGRÁCZ, E., JAAKKOLA, M., TOLONEN, T., VIRTANEN, V., TURKKI, A., HORVÁTH-HOVORKA, Z., VATAI, G. & KEISKI, R. L. 2010. The effect of pre-treatment on the anthocyanin and flavonol content of black currant juice (Ribes nigrum L.) in concentration by reverse osmosis. *Journal of Food Engineering,* 98**,** 429-436.

PARK, K.-N., HONG, S. Y., LEE, J. W., KANG, K. C., LEE, Y. C., HA, M.-G. & LEE, J. D. 2011. A new apparatus for seawater desalination by gas hydrate process and removal characteristics of dissolved minerals (Na^+, Mg^{2+}, Ca^{2+}, K^+, B^{3+}). *Desalination,* 274**,** 91-96.

PARRISH, W. R. & PRAUSNITZ, J. M. 1972. Dissociation pressures of gas hydrates formed by gas mixtures. *Industrial & Engineering Chemistry Process Design and Development,* 11**,** 26-35.

PARTOON, B. & JAVANMARDI, J. 2013. Effect of mixed thermodynamic and kinetic hydrate promoters on methane hydrate phase boundary and formation kinetics. *Journal of Chemical & Engineering Data,* 58**,** 501-509.

PATEL, N. C. & TEJA, A. S. 1982. A new cubic equation of state for fluids and fluid mixtures. *Chemical Engineering Science,* 37**,** 463-473.

PENG, D.-Y. & ROBINSON, D. B. 1976. A new two-constant equation of state. *Industrial & Engineering Chemistry Fundamentals,* 15**,** 59-64.

PETROTOS, K. B., QUANTICK, P. & PETROPAKIS, H. 1998. A study of the direct osmotic concentration of tomato juice in tubular membrane–module configuration. I. The effect of certain basic process parameters on the process performance. *Journal of Membrane Science,* 150**,** 99-110.

POLING, B. E., PRAUSNITZ, J. M. & O'CONNELL, J. P. 2001. *The properties of gases and liquids*, New York: Mcgraw-hill.

POLYDERA, A., STOFOROS, N. & TAOUKIS, P. 2005. Quality degradation kinetics of pasteurised and high pressure processed fresh navel orange juice: nutritional parameters and shelf life. *Innovative Food Science & Emerging Technologies,* 6**,** 1-9.

PUNDA, I., PRIKHODKO, D., DUVALL, CLARKE & MERLIN 2009. *Agribusiness Handbook: Sugar beet white sugar*.

PURWANTO, Y. A., OSHITA, S., SEO, Y. & KAWAGOE, Y. 2001. Concentration of liquid foods by the use of gas hydrate. *Journal of Food Engineering,* 47**,** 133-138.

PURWANTO, Y. A., OSHITA, S., SEO, Y. & KAWAGOE, Y. 2014. Separation process of nonpolar gas hydrate in food solution under high pressure apparatus. *International Journal of Chemical Engineering,* 2014.

PW POEL, HM SCHIWECK & SCHWARTZ, T. 1998. *Sugar technology. Beet and cane sugar manufacture*.

QIN, F., CHEN, X. D., RAMACHANDRA, S. & FREE, K. 2006. Heat transfer and power consumption in a scraped-surface heat exchanger while freezing aqueous solutions. *Separation and Purification Technology,* 48**,** 150-158.

RAAL, J. & MÜHLBAUER, A. 1998. *Phase equilibria: measurement and computation*, Washington, D.C: Taylor and Francious.

RANE, M. V. & JABADE, S. K. 2005. Freeze concentration of sugarcane juice in a jaggery making process. *Applied Thermal Engineering,* 25**,** 2122-2137.

RAVENTÓS, M., HERNÁNDEZ, E., AULEDA, J. & IBARZ, A. 2007. Concentration of aqueous sugar solutions in a multi-plate cryoconcentrator. *Journal of Food Engineering,* 79**,** 577-585.

REKTOR, A., VATAI, G. & BÉKÁSSY-MOLNÁR, E. 2006. Multi-step membrane processes for the concentration of grape juice. *Desalination,* 191**,** 446-453.

RENON, H. & PRAUSNITZ, J. M. 1968. Local compositions in thermodynamic excess functions for liquid mixtures. *AIChE journal,* 14**,** 135-144.

RICHON, D. 1996. New experimental developments for phase equilibrium measurements. *Fluid Phase Equilibria,* 116**,** 421-428.

RICHON, D. & LOOS, T. W. D. 2005. 6 Vapour—liquid equilibrium at high pressure. *In:* WEIR, R. D. & DE LOOS, T. W. (eds.) *Experimental Thermodynamics.* Elsevier.

SABIL, K. M., DUARTE, A. R. C., ZEVENBERGEN, J., AHMAD, M. M., YUSUP, S., OMAR, A. A. & PETERS, C. J. 2010. Kinetic of formation for single carbon dioxide and mixed carbon dioxide and tetrahydrofuran hydrates in water and sodium chloride aqueous solution. *International Journal of Greenhouse Gas Control,* 4**,** 798-805.

SAHASRABUDHE, A. B., DESAI, R. R. & JABADE, S. K. Modeling and simulation of a freeze concentration technique for sugarcane juice concentration. Applied Mechanics and Materials, 2012. Trans Tech Publ, 2768-2773.

SÁNCHEZ, J., RUIZ, Y., AULEDA, J., HERNÁNDEZ, E. & RAVENTÓS, M. 2009. Freeze concentration in the fruit juices industry. *Food Science and Technology International,* 15**,** 303-315.

SASA. 2019. *Sugar Industry Statistical Information* [Online]. Available: https://sasa.org.za/facts-and-figures/ [Accessed].

SEO, Y.-T., LEE, H. & YOON, J.-H. 2001. Hydrate phase equilibria of the carbon dioxide, methane, and water system. *Journal of Chemical & Engineering Data,* 46**,** 381-384.

SHIMADA, W., EBINUMA, T., OYAMA, H., KAMATA, Y., TAKEYA, S., UCHIDA, T., NAGAO, J. & NARITA, H. 2003. Separation of gas molecule using tetra-n-butyl ammonium bromide semi-clathrate hydrate crystals. *Japanese Journal of Applied Physics,* 42**,** L129.

SIKUKA, W. 2019. *South African Sugar Production Forecast to Grow Despite Revenue Pressures* [Online]. Available: https://gain.fas.usda.gov/Recent%20GAIN%20Publications/Sugar%20Annual_Pretoria_South%20Africa%20-%20Republic%20of_4-15-2019.pdf [Accessed].

SKOVBORG, P. & RASMUSSEN, P. 1994. A mass transport limited model for the growth of methane and ethane gas hydrates. *Chemical Engineering Science,* 49**,** 1131-1143.

SLOAN, E. D. & KOH, C. A. 2008. Clathrate hydrates of natural gases third edition. *CHEMICAL INDUSTRIES-NEW YORK THEN BOCA RATON-MARCEL DEKKER THEN CRC PRESS-,* 119.

SLOAN JR, E. D. & KOH, C. 2007. *Clathrate hydrates of natural gases*, CRC press.

SMITH, A. 2015. *Phase Equilibria of Refrigerant Gas Hydrate Systems in the Presence of Sucrose.* University of KwaZulu-Natal, Durban.

SMITH, A., BABAEE, S., MOHAMMADI, A. H., NAIDOO, P. & RAMJUGERNATH, D. 2016. Clathrate hydrate dissociation conditions for refrigerant+ sucrose aqueous solution: experimental measurement and thermodynamic modelling. *Fluid Phase Equilibria,* 413**,** 99-109.

SMITH, J., VAN NESS, H. & ABBOTT, M. 2005. *Vapor/liquid equilibrium: introduction. introduction to chemical engineering thermodynamics*, Singapore: McGraw Hill. p.

SOAVE, G. 1972. Equilibrium constants from a modified Redlich-Kwong equation of state. *Chemical Engineering Science,* 27**,** 1197-1203.

SOTOFT, L. F., CHRISTENSEN, K. V., ANDRÉSEN, R. & NORDDAHL, B. 2012. Full scale plant with membrane based concentration of blackcurrant juice on the basis of laboratory and pilot scale tests. *Chemical Engineering and Processing: Process Intensification,* 54**,** 12-21.

STOPOREV, A. S., SEMENOV, A. P., MEDVEDEV, V. I., SIZIKOV, A. A., GUSHCHIN, P. A., VINOKUROV, V. A. & MANAKOV, A. Y. 2018. Visual observation of gas hydrates nucleation and growth at a water–organic liquid interface. *Journal of Crystal Growth,* 485**,** 54-68.

STRYJEK, R. & VERA, J. 1986. PRSV: An improved Peng—Robinson equation of state for pure compounds and mixtures. *The Canadian Journal of Chemical Engineering,* 64**,** 334-340.

SUGAHARA, T., MURAYAMA, S., HASHIMOTO, S. & OHGAKI, K. 2005. Phase equilibria for $H_2+CO_2+H_2O$ system containing gas hydrates. *Fluid Phase Equilibria,* 233**,** 190-193.

TAJIMA, H. 2011. Gas hydrate formation kinetics in semi-batch flow reactor equipped with static mixer. *Hydrodynamics-Optimizing Methods and Tools.* IntechOpen.

TAJIMA, H., YAMASAKI, A. & KIYONO, F. 2004. Continuous formation of CO_2 hydrate via a kenics-type static mixer. *Energy & Fuels,* 18**,** 1451-1456.

TAN, Z., LI, S., SHEN, Y., LIU, D. & FAN, L. 2014. Phase equilibria of carbon dioxide, propane hydrate in the presence of glucose and fructose. *Applied Mechanics & Materials,* 521**,** 650-653.

TAYLOR, B. N. & KUYATT, C. E. 1994. Guidelines for evaluating and expressing the uncertainty of NIST measurement results. *NIST Technical Note***,** 1297.

TOHIDI, B., DANESH, A. & TODD, A. 1995. Modeling single and mixed electrolyte-solutions and its applications to gas hydrates. *Chemical Engineering Research & Design,* 73**,** 464-472.

TREBBLE, M. & BISHNOI, P. 1988. Thermodynamic property predictions with the Trebble-Bishnoi equation of state. *Fluid Phase Equilibria,* 39**,** 111-128.

TUMBA, K., HASHEMI, H., NAIDOO, P., MOHAMMADI, A. H. & RAMJUGERNATH, D. 2013. Dissociation data and thermodynamic modeling of clathrate hydrates of ethene, ethyne, and propene. *Journal of Chemical & Engineering Data,* 58**,** 3259-3264.

VALDERRAMA, J. O. 1990. A generalized Patel-Teja equation of state for polar and nonpolar fluids and their mixtures. *Journal of Chemical Engineering of Japan,* 23**,** 87-91.

VALDÉS, H., ROMERO, J., SAAVEDRA, A., PLAZA, A. & BUBNOVICH, V. 2009. Concentration of noni juice by means of osmotic distillation. *Journal of Membrane Science,* 330**,** 205-213.

VAN DER WAALS, J. H. & PLATTEEUW, J. C. 1959. *Clathrate Solutions, Advances in Chemical Physics,* 2**,** 1-57.

VYSNIAUSKAS, A. & BISHNOI, P. 1983. A kinetic study of methane hydrate formation. *Chemical Engineering Science,* 38**,** 1061-1072.

WAKISAKA, M., SHIRAI, Y. & SAKASHITA, S. 2001. Ice crystallization in a pilot-scale freeze wastewater treatment system. *Chemical Engineering and Processing: Process Intensification,* 40**,** 201-208.

WARCZOK, J., FERRANDO, M., LOPEZ, F. & GÜELL, C. 2004. Concentration of apple and pear juices by nanofiltration at low pressures. *Journal of Food Engineering,* 63**,** 63-70.

WARCZOK, J., GIERSZEWSKA, M., KUJAWSKI, W. & GÜELL, C. 2007. Application of osmotic membrane distillation for reconcentration of sugar solutions from osmotic dehydration. *Separation and Purification Technology,* 57**,** 425-429.

WARRIER, P., NAVEED KHAN, M., CARREON, M. A., PETERS, C. J. & KOH, C. A. 2018. Integrated gas hydrate-membrane system for natural gas purification. *Journal of Renewable and Sustainable Energy,* 10**,** 034701.

WENDLAND, M., HASSE, H. & MAURER, G. 1999. Experimental pressure− temperature data on three-and four-phase equilibria of fluid, hydrate, and ice phases in the system carbon dioxide− water. *Journal of Chemical & Engineering Data,* 44**,** 901-906.

YA, P., OSHITA, S., SEO, Y. & KAWAGOE, Y. 1998. Concentration of liquid foods by the use of gas hydrate. *JOURNAL of the JAPANESE SOCIETY of AGRICULTURAL MACHINERY,* 60**,** 171-172.

ZAMBRA, C., ROMERO, J., PINO, L., SAAVEDRA, A. & SANCHEZ, J. 2015. Concentration of cranberry juice by osmotic distillation process. *Journal of Food Engineering,* 144**,** 58-65.

ZHANG, C. S., FAN, S. S., LIANG, D. Q. & GUO, K. H. 2004. Effect of additives on formation of natural gas hydrate. *Fuel,* 83**,** 2115-2121.

Appendices

Appendix A: Thermodynamic modelling results

The comparative study and statistical analysis on the modelling approaches developed in this study are presented in tables A-1 (CO_2 + water), A-2 (CO_2 + sucrose solution) and A-3 (CO_2 + fructose solution). A summary of the best modelling combinations was presented in chapter 6.5.3 and table 6-12. As shown in Table 6.7, the models used included a combination of approaches and empirical equations.

Table 6-7. A summary of the thermodynamic model approaches used in this study.

Gas-liquid interaction	Activity coefficient in the liquid phase	Fugacity in the hydrate phase
Kihara potential (K-P) (Kihara, 1953)	- UNIQUAC (Abrams and Prausnitz, 1975)	Chemical potential (C-P) (Mohammadi et al., 2005)
Parrish – Prausnitz (P-P) (Parrish and Prausnitz, 1972) Munck-Skjold-Rasmussen (M-S-R) (Munck et al., 1988)	- UNIFAC (Fredenslund et al., 1975) - NRTL (Renon and Prausnitz, 1968)	Empty hydrate (E-H) (Mohammadi and Richon, 2008)

Table A-1. Result of modelling for the CO_2 + water at the temperature and pressure ranges of (276.6 - 282.6) K and (1.80 – 3.92) MPa.

Model	AAD(P) %
(P-P) and (C-P)	0.09
(P-P) and (E-H)	0.10
(M-S-R) and (C-P)	0.10
(M-S-R) and (E-H)	0.11
(K-P) and (C-P) [*]	0.03
(K-P) and (E-H)	0.05

[*] Best modelling combination

Table A-2. Result of modelling for the CO_2 + sucrose solution (20, 30, 35 and 40 ºBrix) at the temperature and pressure ranges of (276.4 - 281.4) K and (1.94 – 4.10) MPa.

Model	AAD(P) %
(P-P), UNIFAC (C-P)	1.00
(P-P), UNIFAC, (E-H)	1.17
(M-S-R), UNIFAC, (C-P)	0.98
(M-S-R), UNIFAC, (E-H)	1.59
(K-P), UNIFAC, (C-P)	1.95
(K-P), UNIFAC, (E-H)	1.93
(P-P), UNIQUAC, (C-P)	1.01
(P-P), UNQUAC, (E-H)	1.46
(M-S-R), UNQUAC, (C-P)	0.97
(M-S-R), UNQUAC, (E-H)	1.85
(K-P), UNQUAC, (C-P)	2.49
(K-P), UNQUAC, (E-H)	1.94
(P-P), NRTL, (C-P)	1.02

Table A-2 continued

Model	AAD(P) %
(P-P), NRTL, (E-H)	1.46
(M-S-R), NRTL, (C-P) [*]	0.96
(M-S-R), NRTL, (E-H)	1.85
(K-P), NRTL, (C-P)	2.66
(K-P), NRTL, (E-H)	1.94

[*] Best modelling combination

Table A-3. Result of modelling for the CO_2 + fructose solution (15, 20 and 30 ºBrix) at the temperature and pressure ranges of (274.3 – 280.8) K and (1.93 – 3.73) MPa.

Model	AAD(P) %
(P-P), UNIFAC (C-P)	1.27
(P-P), UNIFAC, (E-H)	1.05
(M-S-R), UNIFAC, (C-P) [*]	0.75
(M-S-R), UNIFAC, (E-H)	1.02
(K-P), UNIFAC, (C-P)	0.97
(K-P), UNIFAC, (E-H)	1.27
(P-P), UNIQUAC, (C-P)	0.98
(P-P), UNQUAC, (E-H)	1.23
(M-S-R), UNQUAC, (C-P)	0.88
(M-S-R), UNQUAC, (E-H)	1.04
(K-P), UNQUAC, (C-P)	1.63
(K-P), UNQUAC, (E-H)	1.38
(P-P), NRTL, (C-P)	0.90
(P-P), NRTL, (E-H)	1.05
(M-S-R), NRTL, (C-P)	0.88
(M-S-R), NRTL, (E-H)	1.03
(K-P), NRTL, (C-P)	1.69
(K-P), NRTL, (E-H)	1.47

[*] Best modelling combination

Appendix B: Kinetic results of CO_2 + water system

B.1 Induction time

The induction time is the time required for the hydrate crystal to create a stable nucleus and grow. Thee sample is kept at constant temperature and pressure inside the hydrate stability region in order to measure the induction time and expect the formation of a significant volume of the hydrated crystal. Figure B-1 shows the induction time for the formation of CO_2 hydrates at temperatures of 275.65 K and 2.70 MPa.
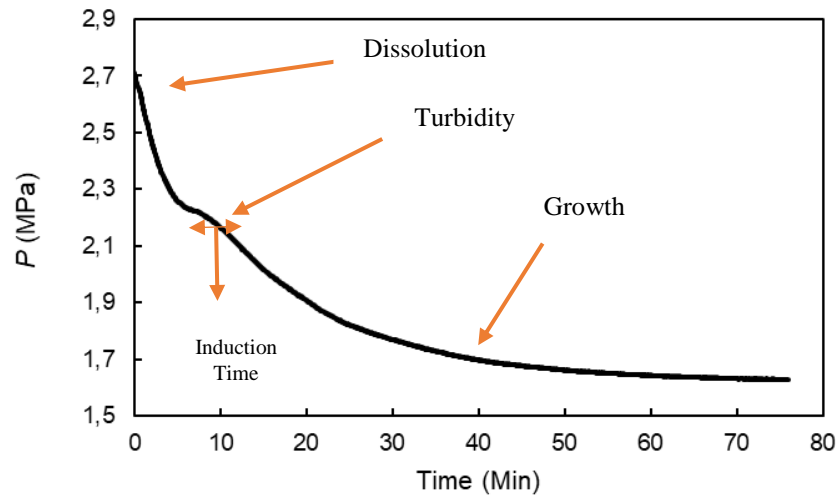

Figure B-1. Hydrate kinetic measurements of CO_2 + Water (this work).

As shown in Figure B-1, during the formation of carbon dioxide hydrates, three distinct regions can be determined. The first region is the stage of dissolution. During this period, some of the gas in the vapour phase is released to the vapour-liquid level and dissolved in the liquid phase. During the second period or induction period, carbon dioxide hydrate crystals are formed and decomposed until a stable nucleus is created and grown as detectable. The cloud point in Figure B-1 shows the beginning of the growth stage, which corresponds to the last period shown in Figure B-1. At the growth stage, CO_2 molecules are encapsulated into the cavities formed, and the system pressure is reduced to a constant value.

Figure B-2 shows the induction time of carbon dioxide hydrate at a constant temperature of 275.65 K and three initial pressures of 2.70, 2.90 and 3.10 MPa. The induction time at a constant temperature of 275.65 K and pressure of 2.70, 2.90, and 3.10 MPa are 16.23, 12.54 and 10.48 minutes, respectively. It is evident that with increasing the initial pressure at a constant temperature, the induction time decreases. Similar results are obtained by reducing the initial temperature at a constant

pressure which is shown in figure B-3. Thus, at first temperatures of 275.15 K and 276.15 K, and the constant pressure of 3.00 MPa, the induction time was 11.20 and 12.20 minutes, respectively. Table B-1 summarises the induction time obtained from these kinetic measurements.
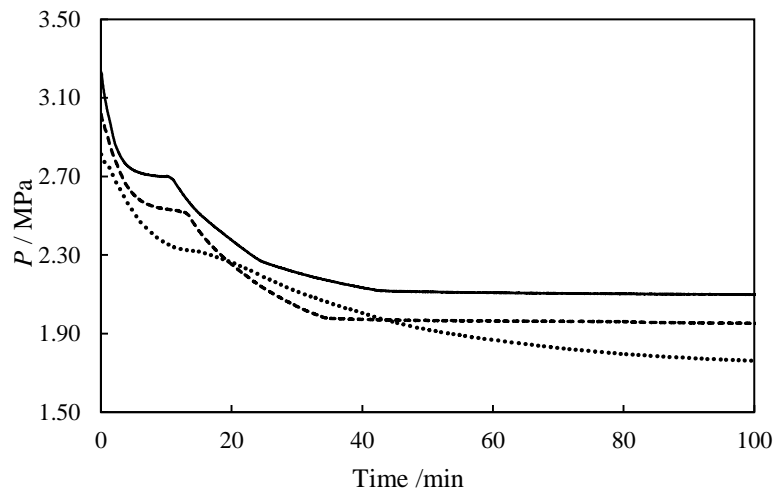

Figure B-2. Hydrate kinetic measurements of CO_2 + Water at 275.65 K; … 2.70, --- 2.90 and —— 3.10 MPa.
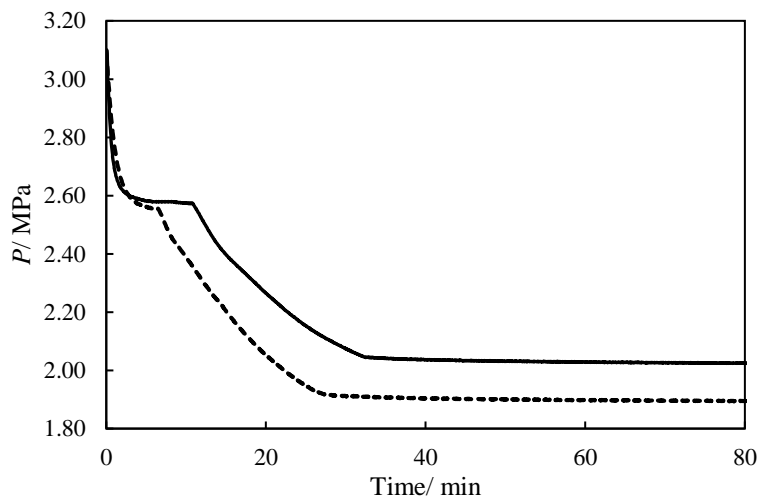

Figure B-3. Hydrate kinetic measurements of CO_2 + Water at 3.00 MPa; --- 275.15 and —— 276.15 K.

Table B-1. The induction time for CO_2 + water system at different temperatures and pressures.

Initial Temperature (K)	Initial Pressure (MPa)	Induction time (min)
275.65	2.70	16.23
275.65	2.90	12.54
275.65	3.10	10.48
275.15	3.00	11.20
276.15	3.00	12.21

$U(P) = 0.01$ MPa, $U(T) = 0.1$ K.

B.2 Gas consumption

The model proposed by (Englezos et al., 1987) was used to estimate the number of gas molecules intake during the formation of hydrates (presented in chapter 3). Figure B-4 shows CO_2 consumption an initial temperature of 275.65 K and pressure of 2.70 MPa. Gas consumption during the hydrate formation is divided into four regions. During the first region or induction time, gas consumption was almost zero as the hydrate crystals were not formed. CO_2 hydrate was then rapidly formed in the growth region (second region). During this period, CO_2 molecules were encapsulated within the hydrate cavities. The hydrate formation rate (HFR), was then reduced due to water consumption during hydrate formation and the effect of mass and heat transfer. In the fourth zone, the consumption of CO_2 became a constant value, and the formation of hydrate was complete.
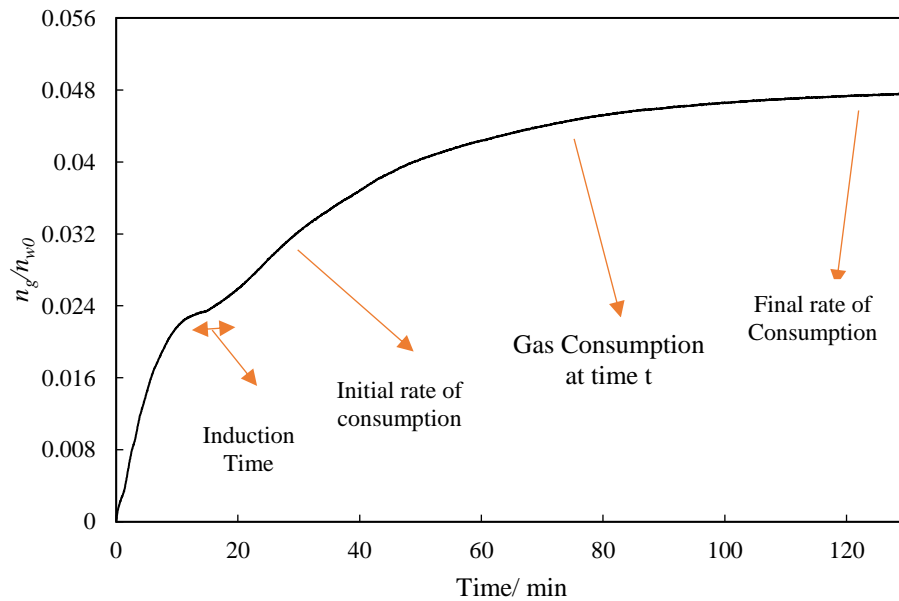
Figure B-4. CO_2 consumption per mole of water during the hydrate formation (this work).

In Figure B-5 the use of carbon dioxide in hydrate during hydrate formation was shown at a primary temperature of 275.65 K and various pressures of 2.70, 2.90 and 3. 10 MPa. By increasing the initial pressure at a constant temperature, CO_2 gas intake was increased. Figure B-6 shows the consumption of carbon dioxide during hydrate formation at an initial pressure of 3.00 MPa and two different temperatures of 275.15 and 276.15 k. It is evident that CO_2 consumption decreases with increasing the initial temperature at constant pressure.
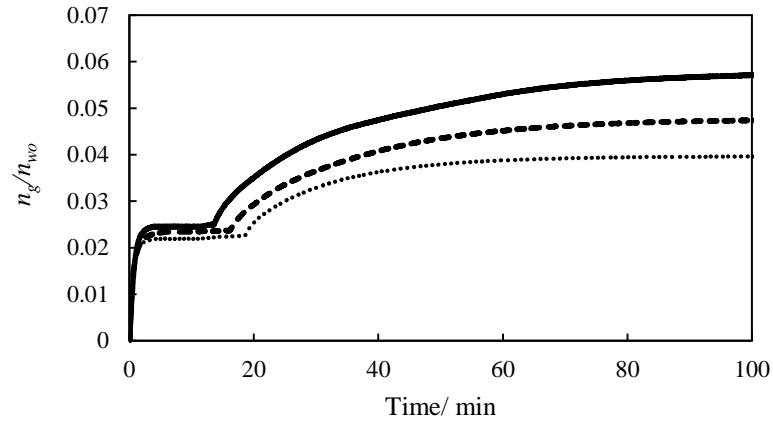
Figure B-5. Number of moles of CO_2 consumed per mole of water during the hydrate formation at an initial temperature of 275.65 K and different pressures (… 2.70, --- 2.90 and — 3.10 MPa)
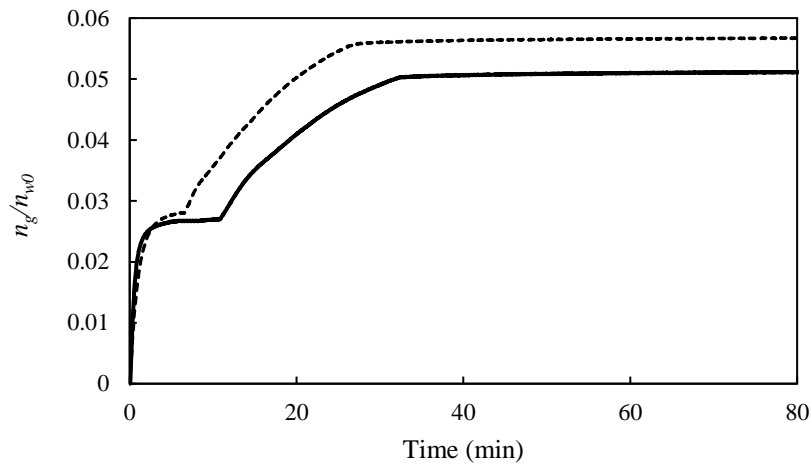

Figure B-6. Number of moles of CO_2 consumed per mole of water during the hydrate formation at an initial pressure of 3.00 MPa and two initial temperatures (--- 275.15 and — 276.15 K).

B.3 Storage capacity (SC)

The storage capacity (SC) of the gas hydrates are expressed as the volume of stored gas in the volume of gas hydrates under STP conditions (standard temperature). Figure B-7 shows the storage capacity at an initial temperature of 275.65 K and three initial pressures of 2.70, 2.90 and 3.10 MPa. The storage capacity increases with increasing the initial pressure.
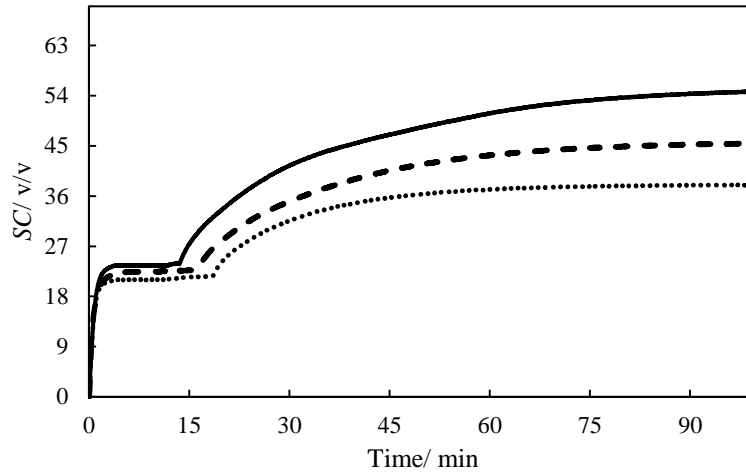
Figure B-7. SC of CO_2 during hydrate formation at an initial temperature of 275.65 K and different pressures (… 2.70, --- 2.90, and — 3.10 MPa).

Figure B-8 shows the SC at an initial pressure of 3.00 MPa and temperatures of 275.15 and 276.15 K. It is evident from the results that the SC decreases with increasing the initial temperature.
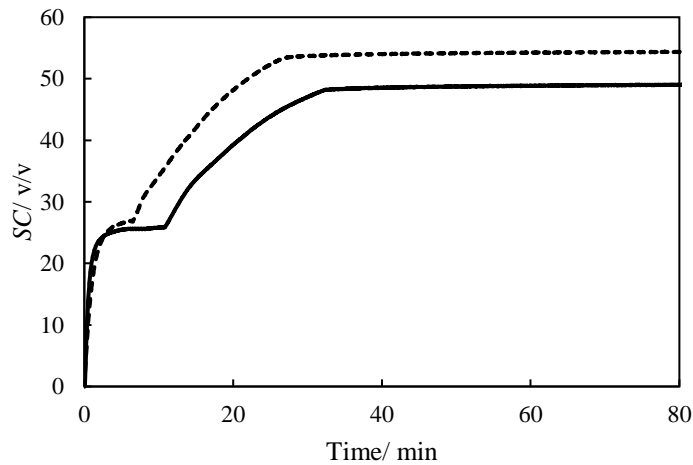

Figure B-8. SC of CO_2 during hydrate formation at an initial pressure of 3.00 MPa and different temperatures (--- 275.15 and — 276.15 K).

B.4 Hydrate formation rate (HFR)

The hydrate formation consists of three steps. In the first step, the gas molecules are moved from the vapour phase to the liquid. In the second step, the molecules of the gas are released to the boundary and eventually, in the third stage, the molecules of the gas are encapsulated into the hydrate holes (Sloan and Koh, 2008). The growth rate in each particle is obtained using the differences between the fugacity of the gas molecule in the bulk liquid and the fluid in the hydrate interface. The growth rate of CO_2 hydrates was modelled in this study. The hydrate formation rate is shown in Figures B-9 and B-10, with the highest peak rate obtained at 3.10 MPa (at a constant temperature of 275.65 K).
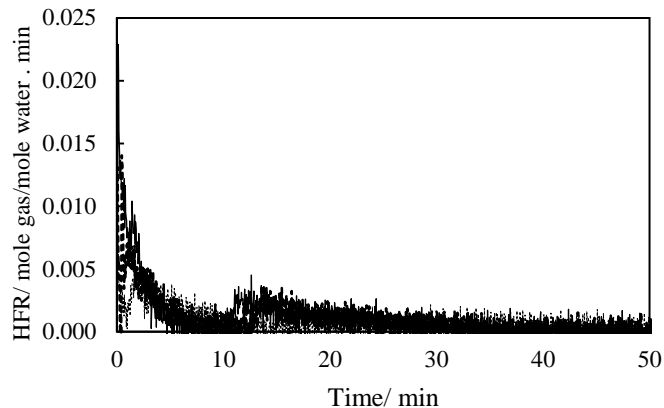
Figure B-9. HFR at an initial temperature of 275.65 K and different pressures (… 2.70, **---** 2.90 and —
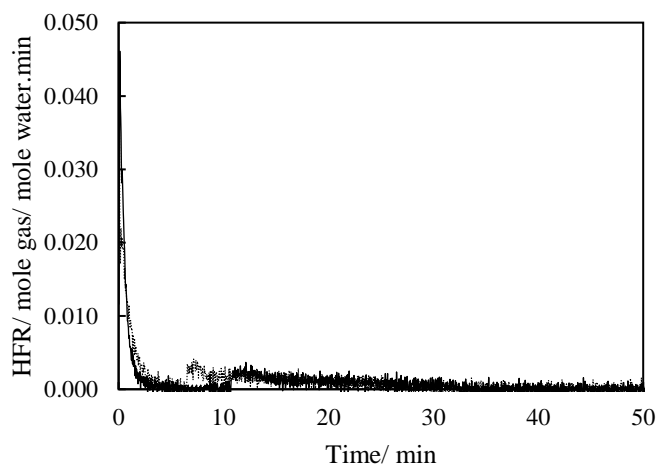3.10 MPa).

Figure B-10. HFR at an initial pressure of 3.00 MPa and different temperatures (… 275.15 and —
276.15 K).

B.5 Apparent rate constant (K_{app})

The apparent rate constant was measured at a constant temperature of 275.65 K and different pressure 2.70, 2.90, and 3.10 MPa. The maximum K_{app} at induction time is presented in figure B-11. With increasing the initial pressure, the rate constant was increased. Figure B-12 presents the maximum K_{app} for CO_2 + water system at a constant pressure of 3.00 MPa and temperatures of 275.15 and 276.15 K. It is evident from the figure that by increasing the temperature in constant pressure, the rate constant was decreased.
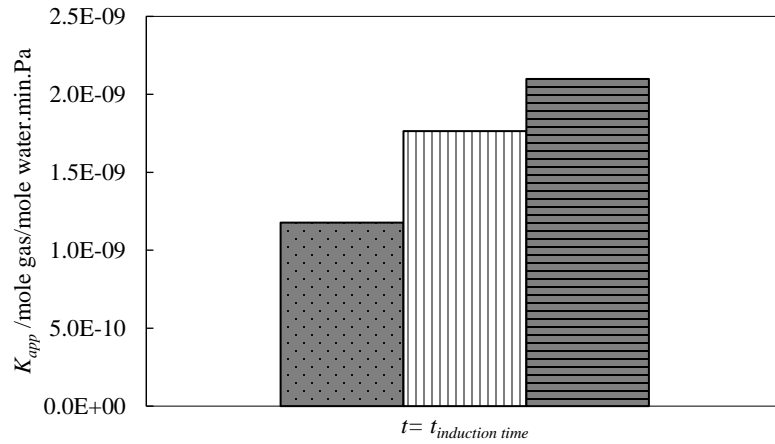
Figure B-11. Maximum K_{app} for CO_2 + water at constant temperature (275.65 K) and three different pressures; ▨ 2.70, ⦀ 2.90, and ▤ 3.10 MPa.
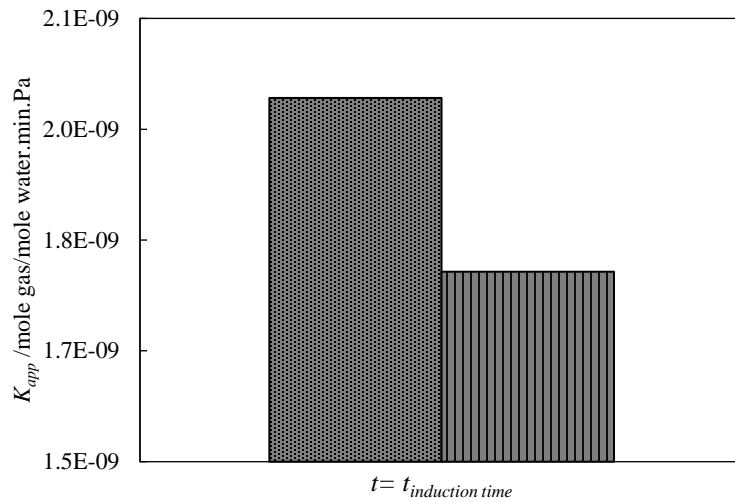

Figure B-12. Maximum K_{app} for CO_2 + water at constant pressure (3.00 MPa) and two different temperatures; ▨ 275.15 and ⦀ 276.15 K.